JETP Letters, Vol. 72, No. 10, 2000, pp. 481–485. From Pis'ma v Zhurnal Éksperimental'noĭ i Teoreticheskoĭ Fiziki, Vol. 72, No. 10, 2000, pp. 691–697.

A New Mechanism for Single-Spin Asymmetries in Strong Interactions[1]

N. I. Kochelev

Bogolyubov Laboratory of Theoretical Physics, Joint Institute for Nuclear Research, Dubna, Moscow region, 141980 Russia

Received October 9, 2000

It is shown that the contribution of instantons to the fragmentation of quarks leads to the appearance of an imaginary part in diagrams of quark–quark scattering at large transferred momentum. The imaginary part comes from the analytical continuation of the instanton amplitudes from Euclidean to Minkowsky space–time and reflects the quasiclassical origin of the instanton solution of QCD equations of motion. This phenomenon and instanton-induced quark spin-flip give a new nonperturbative mechanism for the observed anomalous single-spin asymmetries in hadron–hadron and lepton–hadron interactions. © *2000 MAIK "Nauka/Interperiodica".*

PACS numbers: 12.39.-x; 13.60.Hb; 14.65.-q; 14.70.Dj

1. INTRODUCTION

The explanation of the large observed single-spin asymmetries (SSA) at large energies and transferred momenta in many inclusive and exclusive processes is one of the most longstanding and outstanding problems in QCD [1, 2]. From a naive point of view, one can expect that with increasing energy and transferred momentum the role of quark spin in strong interactions should become smaller. At the same time, the experimental data on spin-dependent cross sections reveal the opposite tendency: the spin asymmetries do not disappear at large energy, showing in fact an anomalous growth with increasing transferred momentum.

Apart from our understanding of the origin of the large spin effects in QCD, the investigation of the fundamental mechanism which is responsible for SSA is also very important in view of future spin measurements at Brookhaven (RHIC-Spin Collaboration), CERN (COMPASS), and DESY (HERA-N).

Within leading order of perturbative QCD, it is impossible to obtain large SSA, because their values should be proportional to the current quark masses and should decrease with energy and momentum transfer [3]. Additional suppression factors are those related to the loop integration generating the imaginary part of the amplitude and an extra power of α_s.

Several attempts to explain the observed SSA have been undertaken. In [4], it was mentioned that the twist-3 contribution can be important to explain this puzzle. Recently in [5], the convolution formula for single-spin asymmetry which includes a twist-3 quark–gluon correlation function has been obtained and the single-spin asymmetries for the pion production have been estimated. The main problem of this approach is unknown spin-dependent twist-3 distribution functions, which in general are the functions of two variables and present the nonperturbative part of the convolution formula, together with rather well-known twist-2 distribution functions of the partons in nonpolarized nucleons. These twist-3 distribution functions should be either extracted from other experiments or calculated within some nonperturbative approach.

There are several phenomenological approaches which also take into account the nonperturbative effects on single-spin asymmetries [6]. Some of them use assumptions about quark transverse momenta in the distribution function (Sivers effect [7]) or in the quark fragmentation function (Collins effect [8]). In [9], an attempt to combine these two mechanisms for SSA was made.

However, all of these approaches are based on the phenomenological ways of introducing nonperturbative effects into the SSA problem. The most of the parameters of these models were obtained from the fit of the available SSA experimental data; therefore the predictable power of such models is rather low.

In this Letter, a new mechanism for single-spin asymmetries in strong interactions is suggested.

This mechanism is based on the existence, in the QCD vacuum, of the strong nonperturbative fluctuations of gluon fields, so-called instantons (see recent review [10]). The instanton model of QCD vacuum not only describes very well the main properties of the vacuum state, e.g., the values of the different quark and gluon condensates, but it is also rather successful in the description of hadron spectroscopy (see recent review [10] and references therein). Recent results of the lat-

[1] This article was submitted by the author in English.

tice QCD [11] confirm the importance of the instantons in QCD vacuum.

The importance of instantons for spin physics is related to their specific role in the chiral structure of QCD vacuum. Thus, the instantons describe subbarrier transitions between various classical minima of the QCD potential, which correspond to different values of the axial vector charge. The changing of the value of the axial vector charge due to instanton transition leads simultaneously to the quark chirality flip. In [12], it was mentioned that the quark chirality flip induced by instantons may give a natural explanation of the anomalous spin effects in strong interactions. In particular, the instanton solution of the famous "spin crisis" [13] was suggested [14].

We will show below that the instanton leads to a precise behavior of effective quark–instanton vertices as functions of the incoming quark virtualities, which will be responsible for the magnitude of the SSA. More specifically, an imaginary part arises for timelike virtualities of the quark in the diagrams induced by instantons, which is not suppressed at high energy and whose contribution significantly enhances the SSA.

2. SINGLE-SPIN ASYMMETRIES IN π-MESON PRODUCTION AND INSTANTONS

Let us estimate the instanton contribution to the SSA for hadron production in quark–quark scattering. For definiteness, we study π^+-meson production in the scattering of two *u*-quarks, one of them transversely polarized. Our goal is to explain the large SSA in the fragmentation region of the polarized quark at high energies. In this kinematic regime, only the diagrams of Fig. 1 can contribute significantly.[2] The method for calculating these diagrams is standard (see, for example, [15]). The single-spin asymmetry can be written in the following form [16]:

$$A = \frac{2Im(\Phi_5^*(\Phi_1 + \Phi_3))}{|\Phi_1|^2 + |\Phi_3|^2 + 4|\Phi_5|^2}, \quad (1)$$

where we neglected the contribution coming from double spin-flip amplitudes Φ_2 and Φ_4, which are suppressed by the factor $(m_q/\sqrt{S})$ with respect to the leading contributions; m_q is the quark mass and $S = (p_1 + p_2)^2$. The helicity amplitudes entering Eq. (1) are

$$\Phi_1 = M_{+,+;+,+}, \quad \Phi_3 = M_{+,-;+,-}, \quad \Phi_5 = M_{++;-+}. \quad (2)$$

By using for the gluon polarization tensor in Fig. 1 its high-energy limit [15]

$$D^{\mu\nu} = g_\perp^{\mu\nu} + \frac{2}{S}(p_1^\mu p_2^\nu + p_1^\nu p_2^\mu) \approx \frac{2}{S}(p_1^\mu p_2^\nu + p_1^\nu p_2^\mu), \quad (3)$$

the matrix element of the reaction

$$u(p_1)^\uparrow + u(p_2) \longrightarrow d(p_1') + u(p_2') + \pi^+(l) \quad (4)$$

is given by

$$\tilde{M} = \frac{2g_s^2 g_{\pi^+qq}}{Sq^2}\bar{u}(p_2')\hat{p}_1 t^a u(p_2)\bar{u}(p_1')p_2^\mu O_\mu u(p_1), \quad (5)$$

where g_s is the strong-coupling constant, g_{π^+qq} is the π^--quark coupling constant due to the instanton, and

$$Q_\mu = \gamma_5\left(\frac{\hat{l}\gamma_\mu}{d_1}F(k_1^2) - \frac{\gamma_\mu\hat{l}}{d_2}F(k_2^2)\right). \quad (6)$$

In order to obtain Eq. (6), the equations of motion are used. In Eq. (6), $F(k^2)$ is a form factor related to the finite size of the instanton and $d_{1,2}$ are quark propagators in Fig. 1, namely,

$$d_1 = (p_1' + l)^2 - m_q^2, \quad d_2 = (p_1 - l)^2 - m_q^2. \quad (7)$$

In principle, Eq. (5) should include an integral of the density of instantons $n(\rho)$ over the instanton size ρ. However, for estimating the SSA, here we use the simple version of the instanton liquid model, $n(\rho) = n_0\delta(\rho - \rho_c)$, with fixed instanton size $\rho_c = 1.6$ GeV^{-1}. This model gives a good description of the hadronic properties and is very suitable for obtaining estimates [10]. In Eq. (1), the density of the instantons is in the numerator and the denominator. Therefore, in the ratio it cancels. The structure in color space of all the helicity amplitudes in Eq. (1) is the same. Therefore, we can omit all global factors of Eq. (5) in the ratio as well. Thus, it is enough to consider the matrix element

$$M = \frac{1}{Sq^2}\bar{u}(p_2')\hat{p}_1 u(p_2)\bar{u}(p_1')p_2^\mu Q_\mu u(p_1). \quad (8)$$

In the high-energy limit, it is very suitable to use Sudakov variables

$$\begin{aligned} l &= x_F\tilde{p}_1 + \beta_l\tilde{p}_2 + l_\perp, \\ p_1' &= (1 - x_F)\tilde{p}_1 + \beta_1\tilde{p}_2 + p_{1\perp}', \\ q &= \alpha\tilde{p}_2 + \beta_q\tilde{p}_1 + q_\perp, \end{aligned} \quad (9)$$

where

$$\tilde{p}_1 = p_1^\mu - \frac{m_q^2}{S}p_2^\mu, \quad \tilde{p}_2 = p_2^\mu - \frac{m_q^2}{S}p_1^\mu, \quad (10)$$

and $\tilde{p}_1^2 = \tilde{p}_2^2 \longrightarrow 0$ at $S \gg m_q^2$. In this limit, in the bottom part of the diagrams in Fig. 1, due to Eq. (8), we have conservation of quark helicity

$$\{\bar{u}(p_2')\hat{p}_1 u(p_2)\}_{\lambda\lambda'} \approx \delta_{\lambda_2\lambda_2'}S \quad (11)$$

[2] We assume that the instanton-induced quark–quark interaction determines the strength of the πqq vertex. This is one of the important consequences of the instanton model (see [10] and references therein).

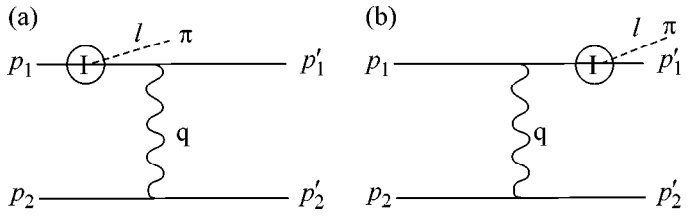

Fig. 1. The contribution of the instanton to the amplitude for π^+ production in the fragmentation region of the polarized quark in the scattering of two *u*-quarks. The label *I* denotes instanton.

and, therefore, for the helicity amplitude we have

$$M_{\{\lambda_1,\lambda_2;\lambda_1',\lambda_2'\}} = -\delta_{\lambda_2\lambda_2'}\frac{1}{q^2\beta_q}\{\bar{u}(p_1')q_\perp^\mu O_\mu u(p_1)\}_{\lambda_1,\lambda_1'}, \tag{12}$$

where the current conservation condition for the quark current in the top line in Fig. 1, $q.J^1 = 0$, is used and

$$\beta_q = \frac{m_q^2 x_F^2 + l_\perp^2 + x_F(q_\perp^2 - 2l_\perp.q_\perp)}{Sx_F(1-x_F)}. \tag{13}$$

By using the on-shell conditions for outcoming quarks, $p_1'^2 = p_2'^2 = m_q^2$, and neglecting the mass of the pion, $l^2 = 0$, one can easily obtain the following expressions for the quark propagators, $d_{1,2}$, and quark virtualities in the intermediate states, $k_{1,2}$, of Fig. 1:

$$d_1 = \frac{m_q^2 x_F^2 + (x_F q_\perp - l_\perp)^2}{x_F(1-x_F)}, \quad d_2 = -\frac{m_q^2 x_F^2 + l_\perp^2}{x_F}, \tag{14}$$

$$k_1^2 = \frac{m_q^2 x_F + (x_F q_\perp - l_\perp)^2}{x_F(1-x_F)}, \qquad k_2^2 = -\frac{l_\perp^2 - x_F(1-x_F)m_q^2}{x_F}. \tag{15}$$

By using the identity

$$\gamma_\nu\gamma_\mu = g_{\mu\nu} + i\sigma_{\mu\nu}, \tag{16}$$

one can write

$$\bar{u}(p_1')\gamma_5\hat{l}\hat{q}_\perp = -(q_\perp.l_\perp)\bar{u}(p_1')\gamma_5 u(p_1) + l_\nu q_\perp^\mu \bar{u}(p_1')i\gamma_5\sigma_{\mu\nu}u(p_1). \tag{17}$$

The matrix elements of operators in Eq. (17) for the different helicity states at high energy are known:

$$[\bar{u}\gamma_5 u]_{\lambda_1\lambda_1'} \approx \delta_{\lambda_1\lambda_1'}2m_q + \delta_{\lambda_1,-\lambda_1'}|q_\perp - l_\perp|,$$
$$[\bar{u}i\gamma_5 l_\nu q_\perp^\mu u]_{\lambda_1\lambda_1'} \approx -\delta_{\lambda_1,-\lambda_1'}\frac{l_\perp^2|q_\perp|}{2x_F}. \tag{18}$$

Therefore, the final result for helicity amplitudes in Eq. (1) is

$$\Phi_{\lambda_1,\lambda_1';\lambda_2,\lambda_2'} = \frac{\delta_{\lambda_2,\lambda_2'}}{q^2\beta_q}\Bigg\{\delta_{\lambda_1,-\lambda_1'}\Bigg[(q_\perp.l_\perp)|q_\perp - l_\perp|\left(\frac{F(k_1^2)}{d_1} - \frac{F(k_2^2)}{d_2}\right) + \frac{l_\perp^2|q_\perp|}{2x_F}\left(\frac{F(k_1^2)}{d_1} + \frac{F(k_2^2)}{d_2}\right)\Bigg] + \delta_{\lambda_1,\lambda_1'}2m_q(q_\perp.l_\perp)\left(\frac{F(k_1^2)}{d_1} - \frac{F(k_2^2)}{d_2}\right)\Bigg\}. \tag{19}$$

The main feature of the instanton-induced form factor $F(k^2)$ in Eq. (19) is its nontrivial dependence on the virtualities of the incoming quarks into the instanton vertex. In the general case of the on-shell pion and off-shell quarks with virtualities k_1^2 and k_2^2, the effective quark–pion vertex has the following form[3]:

$$g_{\pi qq}(k_1^2, k_2^2) = g_{\pi qq}F(k_1^2)F(k^2), \tag{20}$$

where $F(k_i^2)$ is related to the Fourier transform of the quark zero-mode in the instanton field in a singular gauge (see [10]),

$$F(k^2) = -x\frac{d}{dx}\{I_0(x)K_0(x) - I_1(x)K_1(x)\}, \tag{21}$$

where $x = \rho\sqrt{k^2}/2$.

The instanton is a classical solution of the QCD equations of motion in *Euclidean space–time*, which is characterized by its size ρ in *this* space–time. Therefore to obtain the result for the cross section, the analytical continuation of instanton amplitudes to the *physical* Minkowsky space–time should be done. This continuation should be performed in a careful way, because the instanton-induced amplitudes have a cut at the quark virtuality $k^2 = 0$ (see below). It is this cut which is responsible for the appearance of the imaginary part which is needed for SSA.

[3] The origin of the effective quark–pion vertex within the instanton model is the famous t'Hooft's four-quark interaction related to the quark zero-modes in instanton field [17].

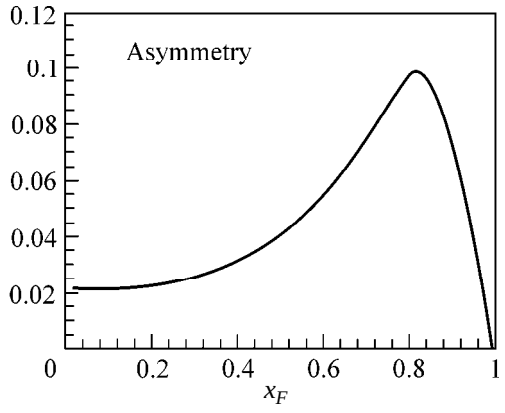

Fig. 2. The instanton contribution to the single-spin asymmetry for pion production as a function of x_F.

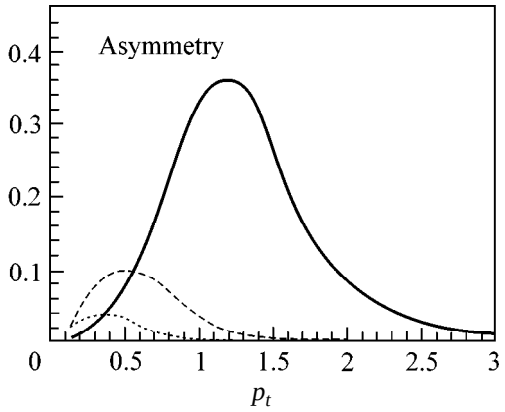

Fig. 3. The instanton contribution to the single-spin asymmetry for pion production as a function of x_F and $p_t = |l_\perp|$. Solid line is for $x_F = 0.9$, dashed line is for $x_F = 0.6$, and dotted line is for $x_F = 0.3$.

To eliminate the imaginary part, it is more suitable to use a good approximation for this form factor, which gives the correct behavior for the quark zero-mode at $k^2 \longrightarrow \infty$:

$$F(k^2) \approx \frac{1}{1 + \rho^3(\sqrt{k^2})^3/6}. \quad (22)$$

For a spacelike value of the quark virtuality in the intermediate state in Fig. 1a, we have $k_2^2 < 0$ and, therefore, in *Minkowsky* space–time, the form factor becomes

$$F(k_2^2) \approx \frac{1}{1 + \rho^3(\sqrt{|k_2|^2})^3/6}. \quad (23)$$

At the same time, for timelike virtuality in Fig. 1b, $k_1^2 > 0$ in *Minkowsky* space–time, one obtains an *imaginary* part in the form factor:

$$F(k_1^2) \approx \frac{1}{1 + i\rho^3(\sqrt{|k_1|^2})^3/6}. \quad (24)$$

It is well known that, to get significant single-spin asymmetry, one must have both quark-spin flip and a large imaginary part in the amplitude.[4] Equations (19) and (24) show that the instanton-induced diagrams have both these components. The SSA is proportional to the interference of the diagrams in Fig. 1. One can interpret the contribution from the first diagram (Fig. 1a) as a Sivers effect [7] in the quark distribution function and the contribution from the second diagram (Fig. 1b) as a contribution to the quark fragmentation function, the so-called Collins effect [8].

To obtain the final result for the asymmetry, one should integrate in Eq. (1) the numerator and the denominator over $q_\perp$ and regularize, in some way, the gluon propagator at small q^2. The usual procedure (see, for example, [15]) is to substitute in the gluon propagator, $q^2 \longrightarrow -(q_\perp^2 + \mu^2)$, where we use for the infrared regulator $\mu \approx \Lambda_{QCD} \approx m_q \approx 0.35$ GeV. The value of $m_q = 0.35$ GeV is the constituent quark mass within the instanton liquid model [10].

The result of the calculation of the SSA is presented in Fig. 2 as a function of x_F and in Fig. 3 as a function of both x_F and $p_\perp$. The value of the asymmetry is rather large, $A \approx 30\%$, in the large x_F and $p_\perp$ region. The magnitude and sign of the asymmetry of π^+-mesons is in qualitative agreement with the experimental data [1]. At the same time, the negative and smaller polarization of *d*-quark in comparison with *u*-quark polarization in protons should lead to the negative and small positive SSA for the π^-- and π^0-meson production, respectively. This feature also was observed by the E704 Collaboration. For a more detailed comparison with the total set of data, one should include in the calculation the *u*- and *d*-quark distribution functions in the polarized and unpolarized nucleon and take the modern result for the density of instantons from lattice calculations [11]. This will be the subject of a forthcoming paper.

We should stress that the instantons give large SSA at *large* transferred momentum. The scale of the transferred momentum, where one can expect the large SSA in the instanton approach, is determined by the average size of the instanton in QCD vacuum. This size is much smaller than the confinement size. Therefore, the topical values of the transferred momentum in instanton-induced quark fragmentation to hadrons are substantially larger than the usual value $p_\perp \approx 0.2$ GeV related to the confinement scale. It is this p_t dependence of SSA

[4] It is interesting that only the nonspin-flip amplitude in Eq. (19) is proportional to the quark mass. In the pQCD approach [3], we have the opposite situation, e.g., the spin-flip amplitude is proportional to the quark mass. The difference comes from the additional quark spin-flip at the quark–pion vertex in Fig. 1.

that poses one of the main problems in most attempts to explain the phenomena. One can also easily understand the origin of the observed enhancement of the SSA in large x_F region. Indeed, the value of SSA is determined by a product of the imaginary part of the diagram in Fig. 1b and the real part of the diagram in Fig. 1a. The imaginary part of diagram in Fig. 1b is proportional to the actuality of the quark in Fig. 1b coming into the instanton vertex (24). This virtuality is $k_1^2 \approx p_\perp^2/x_F(1-x_F)$. At the same time, the real part of the diagram in Fig. 1a is small at low x_F due to form factor $F(k_2^2)$, where $k_2^2 \approx -p_\perp^2/x_F$. As a result, the instanton approach predicts a large SSA only in large x_F region. This prediction is confirmed by the data [1].

It should be mentioned that the instanton (anti-instanton) transition defines the particular time direction[5] and, therefore, the possible connection of the instanton mechanism of the SSA with T-odd fragmentation functions [18] should be clarified. Recently, a large azimuthal asymmetry in semi-inclusive polarized electroproduction of pions was observed at HERMES [19]. It can be shown that the instanton mechanism for single-spin asymmetries suggested in our paper allows the explanation of these data [20] as well.

In summary, the instanton-induced contribution to the quark–quark-scattering amplitude leads to a large quark single-spin asymmetry at high energy and large transferred momentum. The origin of SSA is in the large imaginary part of the instanton-induced amplitudes in the timelike region of quark virtuality. This is related to the quasiclassical origin of the instanton, which stems from the fact that it is a solitonlike solution of the QCD classical equation of motion in *Euclidean* space–time. We should also emphasize that the appearance of the imaginary part in the quark–quark-scattering amplitudes, which include the quark lines with time-like momenta, is the common feature of the instanton-induced processes. The consideration of the different manifestations of this phenomenon in polarized and unpolarized lepton–hadron and hadron–hadron interactions will be the subject of forthcoming papers.

[5] The instanton describes the subbarrier transition in time from $-\infty$ to $+\infty$, while the anti-instanton is the transition in the opposite direction.

I am thankful to M. Anselmino, A. De Roeck, A.E. Dorokhov, S.B. Gerasimov, E.A. Kuraev, A.V. Efremov, E. Leader, M.G. Ryskin, and V. Vento for helpful discussions. I also very grateful to Prof. A. Di Giacomo for warm hospitality at Pisa University, where this paper was started. This work was supported in part by the Heisenberg–Landau and INFN–BLTP JINR exchange programs.

REFERENCES

1. D. L. Adams *et al.*, Phys. Lett. B **264**, 7 (1991); Phys. Rev. Lett. **77**, 2626 (1996).
2. A. D. Krisch, in *Proceedings of the 9th International Symposium on High Energy Spin Physics, Bonn, 1990*, p. 20; G. Bunce *et al.*, Part. World **3**, 1 (1992).
3. G. L. Kane, J. Pumplin, and W. Repko, Phys. Rev. Lett. **41**, 1689 (1978).
4. A. V. Efremov and O. V. Teryaev, Yad. Fiz. **39**, 1517 (1984) [Sov. J. Nucl. Phys. **39**, 962 (1984)].
5. J. W. Qiu and G. Sterman, Nucl. Phys. B **353**, 137 (1991); Phys. Rev. D **59**, 014004 (1999).
6. S. M. Troshin and N. E. Tyurin, Phys. Rev. D **54**, 838 (1996); C. Boros, Z.-T. Liang, T.-C. Meng, and R. Rittel, J. Phys. G **24**, 75 (1998).
7. D. Sivers, Phys. Rev. D **43**, 261 (1991).
8. J. C. Collins, Nucl. Phys. B **396**, 161 (1993).
9. M. Anselmino and F. Murgia, hep-ph/9901442.
10. T. Schäfer and E. V. Shuryak, Rev. Mod. Phys. **70**, 323 (1998).
11. D. A. Smith and M. J. Teper, Phys. Rev. D **58**, 014505 (1998).
12. A. E. Dorokhov, N. I. Kochelev, and Yu. A. Zubov, Int. J. Mod. Phys. A **8**, 603 (1993) and references therein.
13. M. Anselmino, A. Efremov, and E. Leader, Phys. Rep. **261**, 1 (1995).
14. N. I. Kochelev, Phys. Rev. D **57**, 5539 (1998).
15. A. Ahmedov, I. V. Akushevich, E. A. Kuraev, and P. G. Ratcliffe, hep-ph/9902418.
16. C. Bourrely, J. Soffer, and E. Leader, Phys. Rep. **59**, 95 (1980).
17. G. t'Hooft, Phys. Rev. D **14**, 3432 (1976).
18. D. Boer and P. J. Mulders, Phys. Rev. D **57**, 5780 (1998); D. Boer, R. Jakob, and P. J. Mulders, Phys. Lett. B **424**, 143 (1998).
19. H. Avakian, hep-ph/9908490.
20. N. I. Kochelev, A. V. Vinnikov, and T. Morii, to be published.

JETP Letters, Vol. 72, No. 10, 2000, pp. 486–489. Translated from Pis'ma v Zhurnal Éksperimental'noĭ i Teoreticheskoĭ Fiziki, Vol. 72, No. 10, 2000, pp. 698–703.

Observation of a Narrow Feature at 1545 MeV in the System of Two K_S Mesons

V. V. Vladimirskiĭ, V. K. Grigor'ev, O. N. Erofeeva, Yu. V. Katinov, V. I. Lisin, V. N. Luzin, V. N. Nozdrachev, V. V. Sokolovskiĭ*, G. D. Tikhomirov, E. A. Fadeeva, and Yu. P. Shkurenko

Institute of Theoretical and Experimental Physics, ul. Bol'shaya Cheremushkinskaya 25, Moscow, 117259 Russia

** e-mail: sokolovsky@vxitep.itep.ru*

Received October 17, 2000

Preliminary results of examining the system of two K_S mesons in the region of comparatively high transferred momenta are reported. The events were observed in the $\pi^- p$ interactions at an energy of 40 GeV on the ITEP 6-m magnetic spectrometer with a neutral trigger. At transferred momenta $|t| > 0.5$ GeV^2, a maximum with width $\Gamma \simeq 10$ MeV was observed in the $K_S K_S$ system at a mass of 1545 MeV with statistical significance of no less than 6 standard deviations. This phenomenon can be interpreted as the manifestation of a resonance with the indicated parameters. © *2000 MAIK "Nauka/Interperiodica".*

PACS numbers: 14.40.Ev

The overwhelming majority of the known mesons are quark–antiquark ($q\bar{q}$) bound states fitting neatly into the SU(3) multiplets. However, the modern theory of strong interactions (QCD) also predicts the existence of mesons whose structure is inconsistent with the $q\bar{q}$ composition. These particles, with evidently exotic combinations of quantum numbers such as the charge Q, the strangeness S, and the isospin I or the spin S, the parity P, and the charge parity C, are referred to as exotic states of the first and the second kind, respectively. To the third-kind exotic states, one refers those mesons whose quantum numbers are consistent with the $q\bar{q}$ composition but which have some properties that are different from the properties of ordinary mesons: nonstandard proportion between the decay channels, anomalously small widths, unusual formation mechanism, etc.

The $X(1545)$ resonance, whose observation is reported in this work, has a width of ~10 MeV and is produced at rather large transferred momenta. This feature was found in studies of the mass spectrum of the $K_S K_S$ system. Experimental data were obtained in 1985–1990 on the ITEP 6-m spectrometer mounted in a 40-GeV beam from the IHEP U-70 accelerator (Protvino, Russia). In the exposures whose data are examined in this study, a liquid hydrogen target was used. The system of two K_S mesons was mainly produced in the reaction

$$\pi^- p \longrightarrow K_S K_S n. \qquad (1)$$

The 6-m spectrometer was described in detail in [1, 2]. The spectrometer detects, with high efficiency, forward flying K_S mesons that decay into two charged π mesons. A large magnetic-field volume filled with track detectors makes it possible to measure the $K_S K_S$ mass with an accuracy of several megaelectronvolts. Reaction (1) was identified by a trigger device, whose basic elements were veto counters surrounding the liquid hydrogen target. The counters formed a double protective layer around the target. To suppress gamma quanta emitted from the target, lead converters were placed between the counters.

Because of the imperfect trigger operation, the setup detected a fraction of events from the reactions

$$\pi^- p \longrightarrow K_S K_S + (n + m\pi^0, p + \pi^-, \ldots). \qquad (2)$$

The majority of such events can easily be omitted by analyzing the missing mass of the system of two K_S mesons. However, in this study, the events from both reactions (1) and (2) were taken into account, because the feature under discussion was produced in both processes.

In the identification of narrow resonances (with a width of the order of several megaelectronvolts), both the instrumental resolution and the method of data processing are important. Fitting of the parameters measured for the K_S-meson forks considerably improves the accuracy of calculation of various physical quantities, including the $K_S K_S$ effective mass.

The fitting was carried out independently for each of the two forks. The following requirements were imposed: the effective mass of two pions forming the fork must be equal to the tabular mass of the K_S meson, and their tracks must intersect at a single point. Figure 1 illustrates the effect of this procedure on the refinement of the measured quantities (minimum distance between

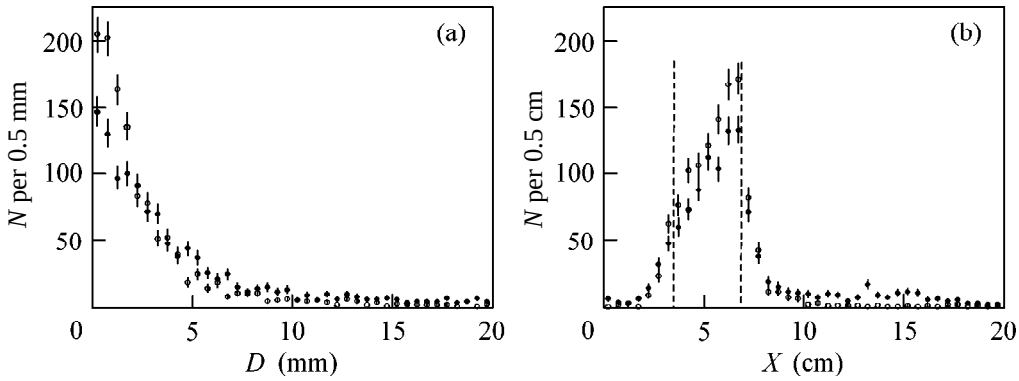

Fig. 1. The distributions of events (a) in minimal distance D between the trajectories of K_S mesons and (b) in the X coordinate of the vertices. Vertical dashed lines are the boundaries of the target. Light and dark circles are the fitted and the unfitted events, respectively.

the kaon trajectories and the distribution in the X coordinate of reaction vertices) of the system of two K_S mesons. The X axis is aligned with the momentum of the beam π meson, the Z axis is aligned with the magnetic field of the spectrometer, and the Y axis forms a right-handed system with these two axes.

The distribution of events in distance D between the trajectories of K_S mesons at the point of their closest approach is shown in Fig. 1a. The dark and light circles are the data obtained before and after fitting, respectively. It is seen that the distribution width reduces after fitting by a factor of about 1.5. For one-half of the events, the distance between the trajectories of K_S mesons is $\leq$1.5 mm. Knowledge of the dispersion of the D value allows one to obtain the upper estimate for the error in measuring the effective mass of the K_SK_S system. Indeed, the D value is a sum of two factors: spatial displacement of the trajectories and their rotation. However, only the rotation influences the error of effective mass. That is why this estimate provides only the upper limit for the error in measuring the angle between the momenta of the K_S mesons. To a first approximation, the angular error is proportional to the parameter D divided by the distance from the fork vertex to the midpoint of the measured part of the trajectory. In our case, the corresponding value is ~0.2 mrad. When recalculated to the effective mass of two K_S mesons, this yields an error no greater than 5 MeV, in agreement with the estimate obtained from the dispersion of the distributions of effective masses of the π^+ and π^- mesons, into which the K_S mesons decay. Note that these estimates are also not at variance with the widths of narrow features observed previously on the 6-m spectrometer (see, e.g. [3–5]).

As a result of fitting, the X coordinate of event vertices is also refined. The distribution of events in the X coordinate is shown in Fig. 1b. The coordinates of the beginning and the end of the target region are equal to 35 and 75 cm, respectively. The nonuniformity of the distribution over the target length is caused by the fact that the detection efficiency for events occurring in the beginning part of the target is suppressed by the neutral trigger more strongly than for the events occurring in the end part of the target. Data fitting results in a 25% increase in the number of events occurring within the target region.

Figure 2 demonstrates a portion of the mass spectrum at 1485–1610 MeV before (Fig. 2a) and after (Fig. 2b) the K_S-meson fork fitting. Note that in both cases the sampling criteria were identical (see below). The curves are the approximations of the experimental data by a constant and a Breit–Wigner function. One can see that the fitting procedure reduces the width of the resonance feature by approximately one half.

Figure 3 shows the distributions of events over the effective mass of two K_S mesons with a step of 20 MeV (a) without sampling of the modulus of the 4-momentum t transferred from a beam π^- meson to two K_S mesons and (b) with $|t| > 0.5$ GeV^2 sampling. These events were obtained by the following standard samplings: the effective mass of the forks (465–530 MeV) and the X, Y, and Z coordinates of the event vertex. For the 40-cm-long liquid hydrogen target, the sampling interval for the X coordinate was 60 cm. The sampling of the Y and Z coordinates cuts a 1.2×3.2-cm rectangle corresponding to the profile of a beam focused onto the target region. After this sampling, up to 40% of events were omitted. The sampling of the missing mass was rather mild: $-0.7 < MM^2 < 12$ GeV^2. After this sampling, the fraction of events of reactions (2) was ~30%.

A statistically significant signal (44 events against the expected background level of 16 events) is seen in Fig. 3b near 1550 MeV. This signal is shown in Fig. 2 in a smaller mass scale.

In order to determine the parameters of the observed resonance feature and its statistical significance, the experimental data were fitted by the maximum likeli-

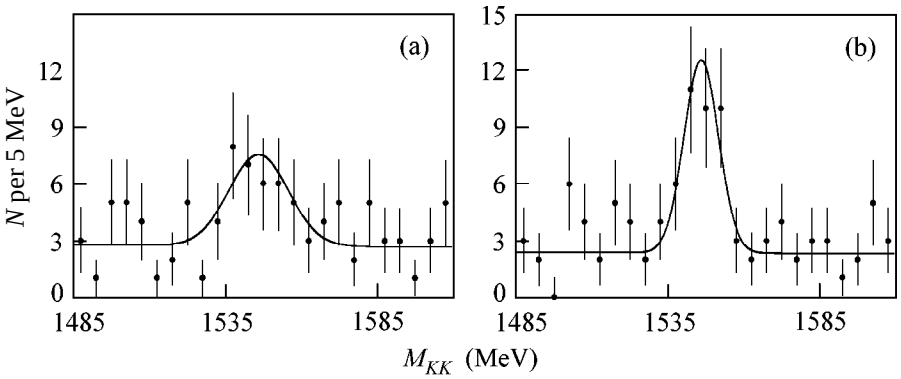

Fig. 2. Mass spectrum of the K_SK_S system in the interval 1485–1610 MeV for the $|t| > 0.5$ GeV^2 sampling of the transferred momentum with a step of 5 MeV: (a) unfitted and (b) fitted events.

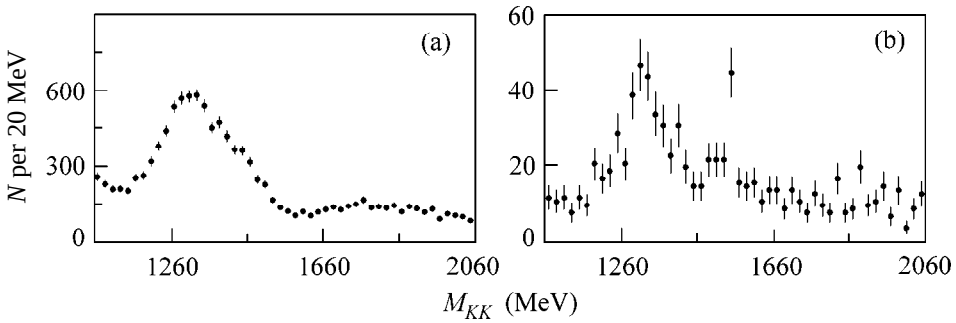

Fig. 3. The distributions of events over the effective mass of the K_SK_S system with a step of 20 MeV: (a) all events and (b) events with the $|t| > 0.5$ GeV^2 sampling of the transferred momentum.

hood method (MLM) in the K_SK_S mass interval 1400–1700 MeV. There are 189 events in this interval. The main advantage of the MLM, as compared to the histogram method, is that the mass and angles are not averaged over the bin width in the fitting procedure and the result is independent of the choice of reference point and number of steps into which the mass interval is divided.

Experimental data are described using the probability density function $F(P; \Omega)$, where P are the parameters and the elements of phase space Ω are the effective mass of two K_S mesons, the cosine of the Gottfried–Jackson angle θ, and the Treiman–Yang angle ϕ. These angles are defined in the rest frame of two K_S mesons (θ is the angle between the momenta of one of the K_S mesons and of a beam π^- meson, and ϕ is the angle between the normal to the production plane and the normal to the decay plane of two K_S mesons). The mass dependence is specified by a second-degree polynomial and a relativistic Breit–Wigner function. The angular dependences are expressed through the squares of the S-, D_0-, D_+-, G_0-, and G_+-wave amplitudes and have the form

$$S^2 = 1/4\pi, \tag{3}$$

$$D_0^2 = 5(3\cos^2\theta - 1)^2/16\pi, \tag{4}$$

$$D_+^2 = 15(\sin 2\theta \sin\phi)^2/4\pi, \tag{5}$$

$$G_0^2 = 9(35\cos^4\theta - 30\cos^2\theta + 3)^2/256\pi, \tag{6}$$

$$G_+^2 = 45\sin^2\theta\cos^2\theta(7\cos^2\theta - 3)^2\sin^2\phi/32\pi. \tag{7}$$

Then the functional

$$\int_\Omega \epsilon F(P; \Omega) d\Omega - \ln L \tag{8}$$

is minimized, where $L = \prod_{i=1}^{N} F(P; \Omega_i)$, ϵ is the detection efficiency, and N is the number of events. In the indicated mass interval, the efficiency depends only on the cosine of the Gottfried–Jackson angle θ. The χ^2 value is calculated by formula

$$\chi^2 = -2\ln L + \text{const}. \tag{9}$$

The constant is chosen so that the χ^2 value obtained without inclusion of the Breit–Wigner function is equal to 100. The angular distributions of the background are

Table

	Background waves, N_{events}			Resonance waves, N_{events}				Resonance parameters, MeV		$\chi^2 - N_{df}$
	S	D_0	D_+	S	D_0	D_+	G_-	$M \pm \Delta M$	$\Gamma \pm \Delta\Gamma$	
1	62	49	82	–	–	–	–	–	–	100
2	51	38	70	12	8	14	–	1544.6 ± 3.5	10.4 ± 3.3	77
3	60	47	51	–	–	37	–	1544.7 ± 3.0	10.3 ± 3.0	56
4	66	37	58	–	–	–	32	1545.8 ± 3.0	10.0 ± 3.0	60
5	68	39	47	–	–	23	16	1545.1 ± 3.1	11.0 ± 3.0	52

described using only the S, D_0, and D_+ waves. The contribution from the other waves is negligibly small.

The minimization showed that, of the studied waves, only two, D_+ and G_+, contributed to the χ^2 value by at least 20 units less than did any other wave. The results of five minimization variants are presented in the table, where the following data are given: the number of events from each wave of the background and resonance and the central values of mass and resonance width. The last column gives the χ^2 values with regard to the number of degrees of freedom N_{df}.

It follows from the table that the statistical significance of observation of the $X(1545)$ resonance with the indicated parameters is no less than six standard deviations. Another indirect corroboration of the fact that this feature is not a statistical outlier is that it was observed in all three runs in which the experimental data were collected.

The χ^2 values obtained upon data fitting by the D_- wave (third variant of minimization) and G_+ wave (fourth variant) are so close to each other that neither of them may be preferred. At the same time, the description of the resonance feature by the sum of these two waves (fifth variant) does not provide any substantial advantage over the D_+ wave: the inclusion of the G_+ wave changes the χ^2 value by only four units. The approximation of the angular distribution by the set of background waves (second variant) yields a χ^2 value that is considerably worse than that given by the variants with D_+ or G_+ waves.

The product $\sigma \cdot \mathrm{BR}(K_S K_S)$ of the cross section for production of the $X(1545)$ resonance into the branching ratio is estimated at ~6 nb.

The results of this study are the following. With a statistical significance of no less than six standard deviations, evidence is obtained of the existence of a 1545-MeV feature with a width of ≃10 MeV. Because this resonance decays into two identical bosons, its angular momentum and parity can only be the following: $J^P = 0^+, 2^+, 4^+, 6^+ \ldots$. The values 0^+ and 6^+ can be omitted with a high degree of certainty. Note that the resonance cannot be described by the set of waves that is appropriate for the neighboring mass regions. The restricted available statistics gives no way of deciding between the 2^+ or 4^+ states. The spin projection of the resonance onto the quantization axis is ±1.

We are grateful to the staff of the IHEP U-70 accelerator and the personnel of the ITEP 6-m spectrometer for collecting the statistical data. This work was supported by the Russian Foundation for Basic Research, project no. 99-02-18540.

REFERENCES

1. B. V. Bolonkin, O. N. Baloshin, A. M. Blagorodov, *et al.*, Preprint No. 86, ITÉF (Institute of Theoretical and Experimental Physics, Moscow, 1973).
2. B. V. Bolonkin, V. V. Vladimirskiĭ, A. P. Grishin, *et al.*, Preprint No. 154, ITÉF (Institute of Theoretical and Experimental Physics, Moscow, 1981).
3. V. K. Grigor'ev, O. N. Baloshin, B. P. Barkov, *et al.*, Yad. Fiz. **59**, 2187 (1996) [Phys. At. Nucl. **59**, 2105 (1996)].
4. B. P. Barkov, V. V. Vladimirskiĭ, V. K. Grigor'ev, *et al.*, Pis'ma Zh. Éksp. Teor. Fiz. **70**, 242 (1999) [JETP Lett. **70**, 248 (1999)].
5. V. K. Grigor'ev, B. P. Barkov, O. N. Baloshin, *et al.*, Yad. Fiz. **62**, 513 (1999) [Phys. At. Nucl. **62**, 470 (1999)].

Translated by R. Tyapaev

JETP Letters, Vol. 72, No. 10, 2000, pp. 490–494. Translated from Pis'ma v Zhurnal Éksperimental'noĭ i Teoreticheskoĭ Fiziki, Vol. 72, No. 10, 2000, pp. 704–710.

On the Spectral and Statistical Properties of Rayleigh–Taylor Mixing

A. M. Oparin*, N. A. Inogamov, and A. Yu. Dem'yanov*****

** Institute of Automatic Design, Russian Academy of Sciences, Moscow, 123056 Russia*

*** Landau Institute for Theoretical Physics, Russian Academy of Sciences, Chernogolovka, Moscow region, 142432 Russia*

**** Moscow Institute of Physics and Technology, Institutskiĭ per. 9, Dolgoprudnyĭ, Moscow region, 141700 Russia*

Received September 28, 2000

Dynamics of turbulent mixing due to the Rayleigh–Taylor instability is considered. The mixing layer consists of a single horizontal array of large-scale structures. The characteristics of these structures are studied by the spectral and statistical methods. Mixing stimulation by long-wavelength noise is studied. It is demonstrated that, for typical homogeneous unscaled noise, self-similarity $h \propto t^2$ is retained. The threshold amplitude of random broadband noise is determined, below which this noise can be ignored. The mixing deceleration by the side boundaries is studied. The stimulation and deceleration effects sizably influence the mixing coefficient α_+, increasing and decreasing it, respectively. © *2000 MAIK "Nauka/Interperiodica".*

PACS numbers: 47.20.Bp; 47.20.Ma; 47.27.Eq

In this work, the instability of an interface between a heavy substance and a light substance positioned underneath (Rayleigh–Taylor instability; see reviews [1–5]) is considered. The instability is of importance in astrophysics, e.g., in the problem of supernova fragmentation [6], in high energy density physics in the problems of pulsed magnetohydrodynamic generators [5], inertial fusion [2, 4], etc. The results of the theoretical analysis of numerous computing experiments "tracking" turbulence development on detailed computational grids are presented. A great body of calculations are analyzed, in which the grid sizes $N_x \times N_z$, the density ratio $\mu = \rho_l/\rho_h$ of the contacting light and heavy substances, the initial conditions, the Mach number, and other parameters influencing the mixing process were varied. The computing experiment is based on the mathematical model of a compressible nonviscous multicomponent medium. The conservation laws (complete set of Euler equations) are modeled [7–10]. The computations are carried out using the large-particle method [7, 8] and the quasi-monotonic hybrid grid-characteristics method [8–10], which are traditionally invoked for modeling hydrodynamic instabilities.

The topical problem of turbulent mixing is investigated in a series of works [11–22]. As a rule, prime attention has been given to the vertical profile $\bar{\rho}(z) = \langle\rho\rangle_\perp$ averaged over the transverse coordinates ($\perp$ sign). It is used to determine the mixing coefficient α_+ and the asymmetry coefficient $\mathrm{As} = \alpha_+/\alpha_-$.[1] The transverse averaging nullifies the important numerical information about the dominant structures that are responsible for the mixing dynamics. The authors of the works devoted to the spectra and the transverse structure restrict themselves, first, to the statement that these structures enlarge[2] and, second, to the study of the small-scale asymptotic behavior of the spectrum. In the present state of the art, qualitative statements are not sufficient. In this work, first, a new approach is suggested which allows the qualitative description of the structure enlargement. It amounts to the use of numerical data for constructing the spectra of quantities $f = \{\rho, u, w, p\}$ in the self-similar variables $\tilde{f}_{\hat{n}}$, where ρ, u, w, and p are the density, the horizontal and vertical velocities, and the pressure, respectively. Second, the study of small-

[1] A mixing layer in an incompressible medium quiescent at infinity is bounded from above and below by the mixing fronts or boundaries that spread in the heavy and light fluids, respectively. Full thickness h of the layer is the sum $h_+ + h_-$ of displacements of the upper (+) and lower (–) fronts from the plane of the unperturbed interface. In the self-similarity case, one has $h_\pm = \alpha_\pm \mathrm{A}t g t^2$, where $\mathrm{At} = (1 - \mu)/(1 + \mu)$ and g is the acceleration. This defines the coefficients α_+ and As.

[2] This phenomenon was theoretically predicted in [13, 23]. In [23], the self-similarity formula $\bar{\lambda} \sim t^2$ was deduced for the transverse length scale of the dominant structures governing the acceleration of the upper front.

0021-3640/00/7210-0490$20.00

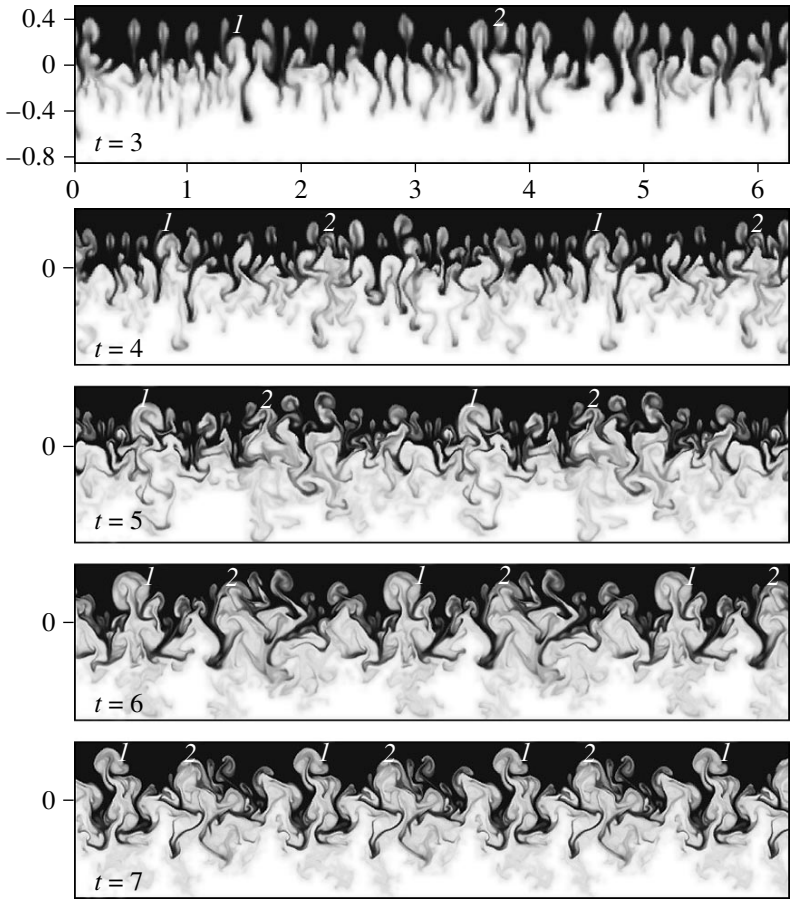

Fig. 1. Typical structures (density) of a mixing layer for different instants of time. Black color corresponds to the heavy substance and white color, to the light substance. Gravitational force is directed downward.

scale asymptotic behavior, which is essential for elucidating the problems of mixing fineness (dispersivity) and Kolmogorov dissipation, is complemented by studying the long-wavelength domain. This is a very important problem, because it is the long-wavelength amplitudes which determine the spreading rate of the mixing layer and, hence, the $\alpha_{\pm}$ coefficients.

The mixing layer has a well-defined horizontal structure (Fig. 1). The neighboring columns of heavy and light substances (spikes and bubbles) are seen. The heavy columns are darker. The extent of grayness is proportional to the density. The direction of movement is, for the most part, vertical. The heavy substance mainly goes down, while the light substance floats up.

In the variant shown in Fig. 1, the grid consists of $N_x \times N_y = 600 \times 1500$ points and square meshes. The length of the calculated domain $L_\perp = 2\pi$, the acceleration $g = 1$, and the density ratio $\mu = 0.1$. The small-scale perturbation was specified at $t = 0$ in the form of a near-surface velocity field:

$$\mathbf{v} = -\nabla\varphi, \quad \varphi = \sum \varphi_n,$$
$$\varphi_n = \mathrm{sgn}z(a_n^0 \cos nx + b_n^0 \sin nx)\exp(-n|z|)/n, \tag{1}$$

where n is the number of the harmonic (n = 50–100). The transient stage is completed at $t = 2\text{–}3/\sqrt{\mathrm{At}}$ and gives way to the self-similarity regime. The presence of the transient stage is caused by the non-self-similarity of the initial conditions.

In the self-similarity regime, both vertical and horizontal sizes are proportional to t^2 and change in a similar way. The photographs in Fig. 1 are scaled with regard to this similarity. For this reason, the structures in all pictures in Fig. 1 have approximately the same geometric sizes. This allows one to leave aside the mesh enlargement and concentrate on the revelation of the typical meshes and their substructure. The phase component is renewed from photograph to photograph, because the structure sizes increase substantially in the corresponding time interval. The upper picture in Fig. 1 ($t = 3$) is taken as the starting point. For each instant of time (i.e., each picture), the h_+ value is determined from the bubble top with the greatest vertical coordinate. Next, the sizes of each subsequent picture of the computational field at $t = k$ (k = 4, 5, 6, 7) are demagnified by a factor of $h_+(t = k)/h_+(t = 3)$. Second, each computational domain is repeated along the horizontal axis

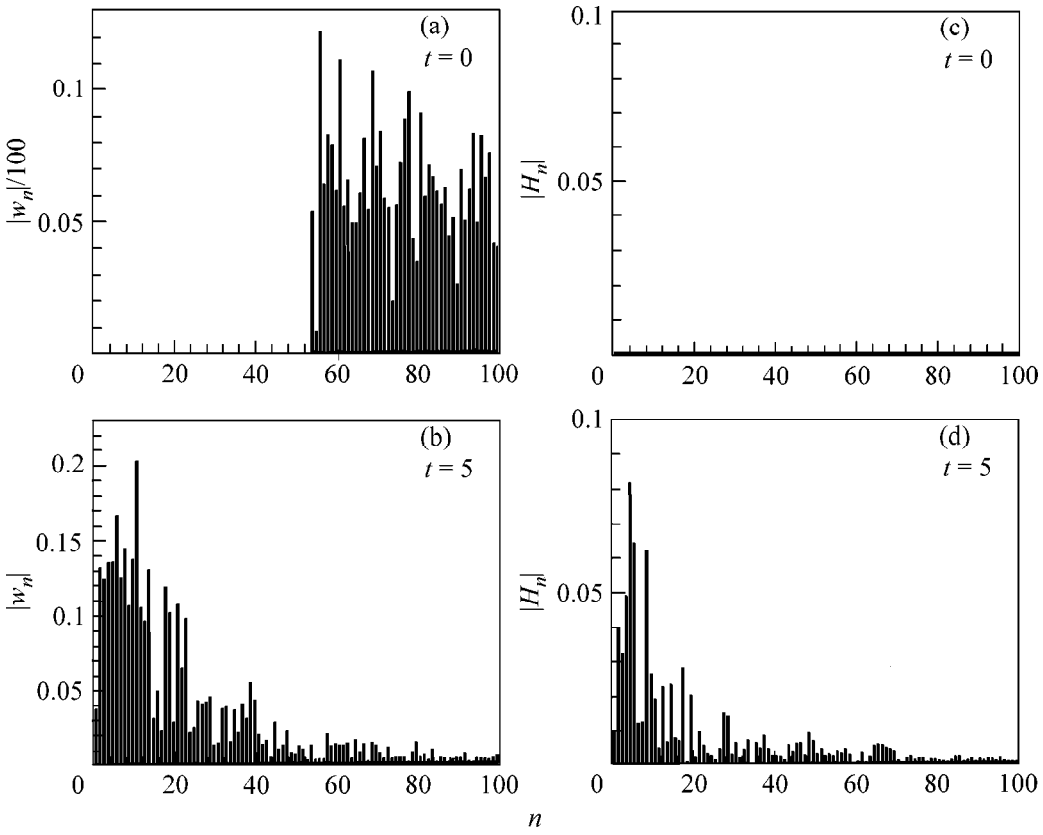

Fig. 2. The spectra of (a, b) $|w_n|$ and (c, d) $|H_n|$ for the initial perturbation and at time $t = 5$.

many times so as to make the horizontal dimensions of the pictures identical.[3]

A structure comprising several bubbles and spikes is rather typical. This is ordinarily a block or a cluster of several relatively small bubbles and spikes and a rather large bubble. In Fig. 1, the evolution is traced for two bubbles (indicated by numbers) that grow to the largest size to the end of the simulation.

Figure 2 shows the spectra of the vertical velocity $w(x, z = 0, t = 5)$ and the mass $H(x, t = 5)$ of the column. For an arbitrary function $f(x, \ldots)$, its spectrum $f_n(\ldots)$ is calculated as

$$f_n = \sqrt{a_n^2 + b_n^2}, \quad a_n = \pi^{-1}\int_0^{2\pi} f\cos nx\,dx,$$

$$b_n = \pi^{-1}\int_0^{2\pi} f\sin nx\,dx,$$

$$f(x, \ldots) = \sum (a_n\cos nx + b_n\sin nx).$$

[3] On the side boundaries of the computational domain, the periodic boundary conditions were used, and the impenetrability conditions were used on the upper and lower boundaries.

$H(x, t) = \int \rho(x, z, t)\,dz/(\rho_h - \rho_l)$ is the mass of a vertical column, where the integration goes from the "bottom" $z = -h_{\text{down}}$ to the "top" $z = h_{\text{top}}$ of the box. Since the initial perturbation applies only to the velocity, $|H_n| = 0$ at $t = 0$. With time, the dominant structures grow, resulting in a gradual shift of the spectral distribution toward the left of the wavenumber axis.

An example of a self-similar spectrum calculated for the vertical velocity component at the $z = 0$ section is presented in Fig. 3. The self-similar spectrum is calculated by expressions of the form

$$\tilde{\rho}_{\hat{n}}(\hat{z}) = \frac{\rho_n(z, t)}{\rho_h t}, \quad \tilde{w}_{\hat{n}}(\hat{z}) = \frac{w_n(z, t)}{t^2},$$
$$\tilde{p}_{\hat{n}}(\hat{z}) = \frac{p_n(z, t)}{\rho_h t^3}, \quad \tilde{H}_{\hat{n}} = \frac{H_n(t)}{t^3}. \qquad (2)$$

One may say that these expressions are obtained from the formulas of self-similar substitution in the coordinate representation via division by $\sqrt{\bar{n}}$, with $\bar{n} \propto 1/t^2$. This is caused by the delta correlation of the Fourier transforms of the modeled functions (their computer representations are discrete) and by the special procedure used for the integration of such delta-correlated functions (replacement of the linear differential dk by

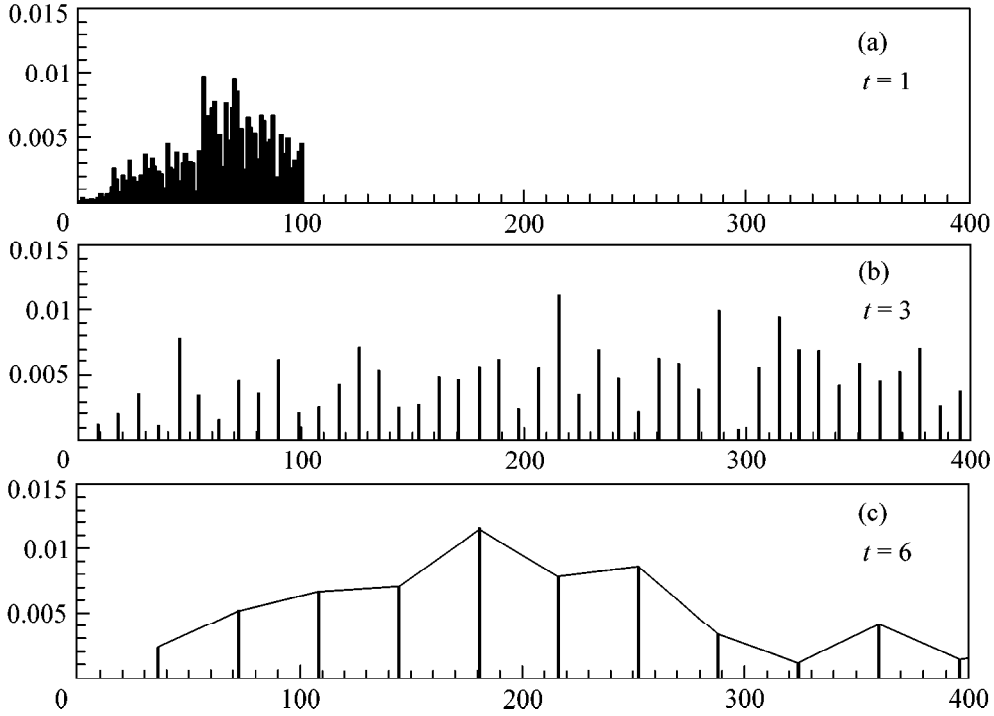

Fig. 3. Self-similar spectra of $|\tilde{w}_{\hat{n}}|$ at times t = (a) 1, (b) 3, and (c) 6.

its root $\sqrt{dk}$; see [3, 4]). Relationships (2) are quite important. For instance, they lead to the nontrivial conclusion that the maximum spectral amplitude of pressure fluctuations grows in proportion to t^3. In representation (2), the spectra are universal at the self-similarity stage of evolution.[4] Recall that the self-similarity stage is established at $t = 2–3/\sqrt{\mathrm{At}}$ (for the grid density chosen), while the deceleration becomes noticeable after $t = 6–7/\sqrt{\mathrm{At}}$ (weakly depends on the grid point spacing). Figures 3b and 3c refer to the self-similarity stage of evolution. The shapes (maxima and widths) of the corresponding spectra are stationary in the self-similar variables, and the number of harmonics in the self-similar distribution decreases with time. Figure 3a corresponds to the (earlier) instant of time of the transient evolution. The corresponding spectrum is shifted to the longer wavelengths, as compared to the self-similar spectrum.

The calculations of a great many variants were used to study mixing stimulation by the long-wavelength perturbations.[5] The initial perturbation was applied to the velocity and had the form of a sum of small-scale and broadband perturbations. The broadband perturbation, being uniform in wavenumber, does not introduce any characteristic scale and, hence, retains quadratic self-similarity (probably, with different coefficients $\alpha_{\pm}$). Let us also represent the initial broadband perturbation as harmonic expansion (1). Let

$$a_n^0 = (w_{sat})_n \xi_n \varepsilon_{wb}, \quad b_n^0 = (w_{sat})_n \xi'_n \varepsilon_{wb}, \qquad (3)$$

where ξ_n and ξ'_n are independent random numbers uniformly distributed in the interval [–1, 1]. The initial field (1) and (3) is specified by three factors. First, the saturation velocity $(w_{sat})_n = F\sqrt{(1-\mu)g/n}$, where $F \approx 0.6$ for the two-dimensional case and is of the order of 1 for three dimensions (see [24]); second, the random multipliers; and, third, the dimensionless parameter ε_{wb}. This perturbation does not define any characteristic scale. It is specified by a single parameter, namely, by the amplitude ε_{wb} of the random broadband noise. Figure 4 is a compilation of the computational results obtained for different ε_{wb} values. One can see that the stimulation can tangibly enhance the mixing coefficient α_{-}. These calculations give evidence for the occurrence of a threshold $(\varepsilon_{wb})_{thr}$ of about 10‰. At below-threshold amplitudes, the mixing occurs spontaneously and the noise effect can be ignored. At above-threshold amplitudes, the flow undergoes reconstruction. The spectral hump shifts to the long-wavelength side. This reflects the strengthening of subharmonics. The strengthening of the long-wavelength wing implies mixing intensification, which manifests itself as an

[4] The results presented in Figs. 1–3 are obtained by the quasi-monotonic hybrid grid-characteristics method [10]. Notice that the alternative numerical approach (large-particle method) gives the same universal spectrum.

[5] These calculations were carried out by A.Yu. Dem'yanov using the large-particle method [7].

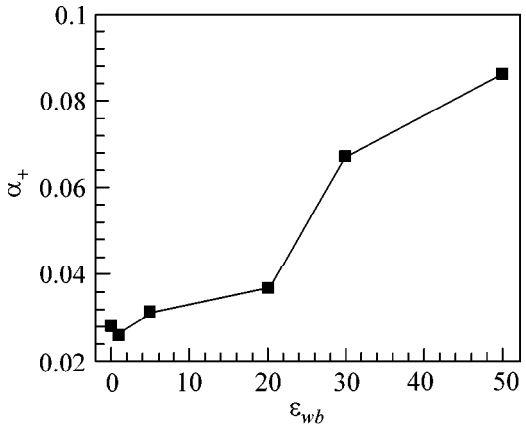

Fig. 4. Mixing coefficient $\alpha_+(t = 5)$ as a function of amplitude ε_{wb} in %.

increase in the coefficient α_-. Whereas the subharmonics in the spontaneous process are genetically associated with the central hump in the spectrum, a portion of subharmonics in the stimulation is "borrowed" from the broadband noise that is present from the outset. The threshold amplitude is appreciable and is of practical importance. For instance, it would make no sense to reduce the noise amplitude below its threshold level by virtue of any expensive technological manipulations (e.g., polishing).

The side boundaries of the computational domain limit the horizontal size of large structures (clusters) and hamper mixing and thereby reduce the coefficient of turbulent mixing. In our computations, this "constraint" effect is particularly pronounced when modeling the evolution of small-scale perturbations after achieving time $t = 6–7/\sqrt{\mathrm{At}}$. One of us (N.A.I.) analytically solved the problem of asymptotic long-time behavior of the Rayleigh–Taylor mixing in the extended computational domains. The constrained asymptotic expression was found to be $h_+ \propto t^{2/5}$ instead of its free form $h_+ \propto t^2$. We assume that the time $t = 6–7/\sqrt{\mathrm{At}}$ in our computations characterizes the onset of deceleration by the side boundaries and the flow reconstruction from the free to the constrained asymptotic regime.

We are grateful to S.I. Anisimov and O.M. Belotserkovskiĭ for helpful discussions. This work was supported by the Russian Foundation for Basic Research, project nos. 99-02-16666 and 00-01-00250.

REFERENCES

1. D. H. Sharp, Physica D (Amsterdam) **12**, 3 (1984).
2. H.-J. Kull, Phys. Rep. **206**, 197 (1991).
3. N. A. Inogamov, Astrophys. Space Phys. Rev. **10** (2), 1 (1999).
4. N. A. Inogamov, A. Yu. Dem'yanov, and É. E. Son, *Hydrodynamics of Mixing* (Mosk. Fiz.-Tekh. Inst., Moscow, 1999).
5. É. I. Asinovskiĭ, V. A. Zeĭgarnik, E. F. Lebedev, *et al.*, *Pulsed MHD Transformers of Chemical Energy into Electrical Power*, Ed. by A. E. Sheĭndlin and V. E. Fortov (Énergoatomizdat, Moscow, 1997).
6. J. Kane, D. Arnett, B. A. Remington, *et al.*, Phys. Plasmas **6** (5), 2065 (1999).
7. O. M. Belotserkovskiĭ, *Numerical Simulation in Mechanics of Continuous Media* (Fizmatgiz, Moscow, 1994, 2nd ed.).
8. O. M. Belotserkovskiĭ and A. M. Oparin, *Numerical Experiment in Turbulence: From Order to Chaos* (Nauka, Moscow, 2000, 2nd ed.).
9. O. M. Belotserkovskiĭ, V. A. Gushchin, and V. N. Kon'shin, Zh. Vychisl. Mat. Mat. Fiz. **27**, 594 (1987).
10. A. M. Oparin, in *New in Numerical Simulation: Algorithms, Computing Experiments, Results*, Ed. by A. S. Kholodov (Nauka, Moscow, 2000), p. 63.
11. S. Z. Belen'kiĭ and E. S. Fradkin, Tr. Fiz. Inst. Akad. Nauk SSSR **29**, 207 (1965).
12. V. E. Neuvazhaev, Prikl. Mekh. Tekh. Fiz., No. 6, 82 (1976).
13. N. A. Inogamov, Pis'ma Zh. Tekh. Fiz. **4**, 743 (1978) [Sov. Tech. Phys. Lett. **4**, 299 (1978)].
14. M. B. Schneider, G. Dimonte, and B. Remington, Phys. Rev. Lett. **80**, 3507 (1998).
15. D. L. Youngs, Phys. Fluids A **3**, 1312 (1991).
16. K. I. Read, Physica D (Amsterdam) **12**, 45 (1984).
17. Yu. V. Yanilkin, Vopr. At. Nauki Tekh., Ser.: Mat. Mod. Fiz. Protsessov, No. 4, 88 (1999).
18. J. Glimm, J. W. Grove, X.-L. Li, *et al.*, SIAM J. Sci. Comput. (USA) **19**, 703 (1998).
19. N. N. Anuchina, N. S. Es'kov, A. V. Polionov, *et al.*, in *Proceedings of the 6th International Workshop on the Physics of Compressible Turbulent Mixing* (Imprimerie Caractere, Marseille, 1997).
20. M. D. Kamchibekov, E. E. Meshkov, N. V. Nevmerzhitskiĭ, and E. A. Sotskov, *Turbulent Mixing at the Cylindrical Gas–Liquid Interface*, Preprint No. 46-96, VNIIÉF, RFYaTs (All-Russia Research Institute of Experimental Physics, Russian Federal Nuclear Center, Sarov, 1996).
21. U. Alon, J. Hecht, D. Ofer, and D. Shvarts, Phys. Rev. Lett. **74**, 534 (1995).
22. D. Ofer, U. Alon, D. Shvarts, *et al.*, Phys. Plasmas **3**, 3073 (1996).
23. S. I. Anisimov, Ya. B. Zel'dovich, N. A. Inogamov, and M. F. Ivanov, in *Shock Waves, Explosions and Detonation*, Ed. by J. R. Bowen, J.-C. Leyer, and R. I. Soloukhin (AIAA, Washington, DC, 1983); Prog. Astronaut. Aeronaut. **87**, 218 (1983).
24. N. A. Inogamov and A. M. Oparin, Zh. Éksp. Teor. Fiz. **116**, 908 (1999) [JETP **89**, 481 (1999)].

Translated by V. Sakun

JETP Letters, Vol. 72, No. 10, 2000, pp. 495–498. Translated from Pis'ma v Zhurnal Éksperimental'noĭ i Teoreticheskoĭ Fiziki, Vol. 72, No. 10, 2000, pp. 711–716.

Ultranarrow Optical Beams in Quadratically Nonlinear Media

A. V. Pimenov*, A. P. Sukhorukov*, and L. Torner**

** Moscow State University, Vorob'evy gory, Moscow, 119899 Russia*

*** Universitat Politecnica de Catalunya, Department of Signal Theory and Communications, Barcelona, ES 08034, Spain*

Received October 16, 2000

The vector Maxwell equations for the first- and second-harmonic planar beams are solved with allowance made for the nonlinear diffraction that weakens quadratic nonlinearity. The structure of the transverse and longitudinal components of the electromagnetic field of a parametric soliton is calculated for different values of the wave vector and phase mismatch. Exact analytic expressions are obtained for the self-similar profiles of extremally narrow solitons, and it is shown that the width has a fundamental limit of the order of a wavelength in a linear medium. © *2000 MAIK "Nauka/Interperiodica".*

PACS numbers: 42.65.Tg

The purpose of this work was to develop the theory of spatial parametric solitons whose widths are comparable to the emission wavelength. Parametric solitons resulting from the three-wave interaction were predicted in [1] and, after the experimental proof of their existence in optics [2], have been much investigated in recent years [3–6]. Trapping of ultranarrow solitons allows one to achieve the highest possible degree of energy localization. Until recently, the theory of spatial solitons was mainly developed for wide beams within the framework of the nonlinear Schrödinger equations. Description of the properties of the narrow wave beams requires an alternative approach that is based on the rigorous solution of the Maxwell equations. Such a program was implemented in [7–9] in the analysis of diffraction in cubic media and, more recently, initiated for the case of ultranarrow beam trapping into a parametric soliton in a quadratic medium. For instance, the interaction between the first- and second-harmonic two-dimensional localized waves polarized in the diffraction plane was analyzed in [10] to demonstrate that the longitudinal components give rise to nonlinear diffraction that weakens the parametric self-action. In this work, one more type of interaction between the first-harmonic ordinary wave and the second-harmonic extraordinary wave is considered, with nonlinear diffraction being executed only by the first harmonic. In addition to the numerical calculations, we obtain the exact analytic expressions for the fundamental limiting widths and self-similar profiles of all components of parametric solitons. It is revealed that, on passing from paraxial to ultranarrow beams, the dispersion form changes and, simultaneously, weakening of the nonlinear coupling becomes operative.

Let us consider two waves propagating along the Z axis and undergoing two-dimensional diffraction in the (YZ) plane. The electric field of the waves can be written as

$$\mathbf{E}_j = \frac{1}{2}\sum \mathbf{E}_j(y, z)\exp(i\omega_j t) + \text{c.c.},$$

where ω_j (j = 1 and 2) is the frequency and $\omega_2 = 2\omega_1$. It follows from the Maxwell equations, as applied to the diffraction of a TE wave, that the transverse electric-field component E_{jx} normal to the diffraction plane obeys the equation

$$\frac{\partial^2 E_{jx}}{\partial y^2} + \frac{\partial^2 E_{jx}}{\partial z^2} + \frac{\omega_j^2}{c^2} D_{jx} = 0, \tag{1a}$$

while the transverse component D_{jy} of the electric displacement vector lying in the diffraction plane (TM wave) obeys the equation

$$\frac{1}{\varepsilon_{jl}}\frac{\partial^2 D_{jy}}{\partial y^2} + \frac{\partial^2 E_{jy}}{\partial z^2} + \frac{\omega_j^2}{c^2} D_{jy} = 0, \tag{1b}$$

where ε_{jl} is the dielectric constant of the linear medium. The electric displacement and electric field vectors are related by the quadratic susceptibility tensor as

$$\mathbf{D}_1 = \varepsilon_1 \mathbf{E}_1 + 4\pi\hat{\chi}_2 \mathbf{E}_1^* \mathbf{E}_2, \tag{2a}$$

$$\mathbf{D}_2 = \varepsilon_2 \mathbf{E}_2 + 2\pi\hat{\chi}_2 \mathbf{E}_1^2. \tag{2b}$$

Equation (1b) includes the second derivative of displacement D_j, which contains a nonlinear part [cf. Eqs. (2)]. As a result, the diffraction generally becomes nonlinear, which should manifest itself in ultranarrow beams.

Let us consider the interacting localized waves propagating in a crystal whose principal optical axis (X) is oriented normal to the waveguide plane. We seek the solution corresponding to the spatial solitons, i.e., cw beams with plane phase fronts,

$$\mathbf{E}_j = \mathbf{E}_j(y)\exp(-ik_j z). \quad (3)$$

In the phase-matching regime, one has for the nonlinear wave vectors $k_2 = 2k_1$. After inserting Eq. (3) into Eqs. (1) and replacing $E_1 = D_1/(\varepsilon_1 + 4\pi\chi_2 E_2)$, the nonlinear diffraction effects are concentrated in the terms allowing for the weakening of the interaction. The resultant equations for the envelopes of a parametric soliton are as follows:

$$\frac{d^2u}{dY^2} - u + \frac{uv}{1+bv} = 0,$$
$$\frac{d^2v}{dY^2} - \alpha v + \frac{u^2}{2(1+bv)^2} = 0, \quad (4)$$

where $u = 8\pi\sqrt{(1-b)}\,\chi_2 D_{1x}/b\varepsilon_1^2$ is the normalized electric displacement of the fundamental wave; $v = 4\pi\chi_2 E_{2y}/b\varepsilon_1$ is the normalized second-harmonic electric field; $Y = yk_{1l}\sqrt{b/(1-b)}$ is the dimensionless transverse coordinate; $k_{jl} = \sqrt{\varepsilon_{jl}}\,\omega/c$ is the wave number in the linear medium; $\alpha = (4k_1^2 - k_{2l}^2)/(k_1^2 - k_{1l}^2)$ is the parameter of relative phase mismatch (for the linear phase matching, $k_{2l} = 2k_{1l}$ and $\alpha = 4$); and $b = 1 - k_{1l}^2/k_1^2$ is the parameter responsible both for the nonlinear phase mismatch and for the weakening (saturation) of the interaction ($b > 0$). Set (4) is driven by the Hamiltonian

$$H = (du/dY)^2 + (dv/dY)^2 - u^2 - \alpha v^2 + u^2 v/(1+bv).$$

In the absence of a resonance with linear waves ($\alpha > 0$), we will seek the solution of Eqs. (4) in the form of bright solitons with symmetric bell-shaped profiles, by analogy with the low-intensity case [1]. Although such solutions can only be obtained numerically, one can use the self-focusing condition $u, v > 0$, the symmetry properties $u'(0) = v'(0) = 0$, and the fact that the curvatures of profiles are negative at their maxima $u''(0) = v''(0) < 0$ to arrive, for $H = 0$, at the following analytic estimate for the amplitude maxima $u_m = u(0)$ and $v_m = v(0)$:

$$1 < (1-b)v_m < 4(3b + \sqrt{1+8b})/(1+12b+\sqrt{1+8b}), \quad (5)$$
$$u_m = v_m\sqrt{\alpha(1+bv_m)/[v_m(1-b)-1]}.$$

It is seen from Eq. (5) that the soliton may exist if $b = 1 - k_{1l}^2/k_1^2 < 1$. This implies that the wave vector of the soliton $k_1 > k_{1l}$ and, hence, it moves slower than the linear wave. As the beam width decreases, the wave number k_1 increases and $b \longrightarrow 1$. For wide beams with $b \ll 1$, one has $1 < v_m < 2$ and $u_m > \sqrt{2\alpha}$ [6], and for the extremally narrow beams, one has $1 < (1-b)v_m < 3/2$ and $u_m > \sqrt{27\alpha/4}\,(1-b)^{-3/2}$.

The paraxial approximation for the weak fields of wide beams is realized in Eq. (4) by setting $b \ll 1$. In this limit, the saturation effect becomes insignificant, because, according to Eq. (5), $bv_m \ll 1$; i.e., $4\pi\chi_2 E_{2y} \ll \varepsilon_1$ and $D_{1x} \approx \varepsilon_1 E_{1x}$, and the soliton dispersion is greatly simplified because of a small nonlinear change in the wave vectors: $k_j^2 - k_{jl}^2 \cong 2k_{jl}(k_j - k_{jl})$, $k_1 \cong k_{1l}(1 + b/2)$, and $\alpha \cong 2(2k_1 - k_{2l})/(k_1 - k_{1l})$. In this approximation, Eq. (4) takes the standard form corresponding to the envelopes of spatial quadratic solitons [1]. In particular, the profiles of wide solitons have the form $u = \sqrt{2}\,v = \frac{3}{\sqrt{2}}\,\mathrm{sech}^2(Y/2)$ at $\alpha = 1$ [1]. The properties of such solitons were numerically analyzed in [5, 6].

In strong fields such as $4\pi\chi_2 E_{2x} \geq \varepsilon_1$, the nonlinearity weakens and a peculiar kind of saturation mechanism is switched on. As a result, the properties of the narrow beams differ from those of the wide beams. Let us consider the strong saturation regime $bv_m \gg 1$, which occurs, according to Eq. (5), if $b \longrightarrow 1$. In this case, Eqs. (4) for the soliton core take the form

$$u'' + (1-b)u - u/v = 0, \quad (6a)$$
$$v'' - \alpha v + u^2/2v^2 = 0. \quad (6b)$$

We will seek the asymptotic solution at $(1-b) \longrightarrow 0$ in the self-similar form. To first order in the small parameter, Eq. (6b) is replaced by the algebraic relationship $2\alpha v^3 = u^2$ (by analogy with the cascade nonlinearity), whereupon Eq. (6a) can easily be solved to yield the analytic expression for the core of an extremally narrow soliton localized in the $|k_{1l}y| < 3\pi/2$ region:

$$u = u_m\cos^3(k_{1l}/3), \quad v = v_m\cos^2(k_{1l}y/3), \quad (7)$$

where the peak amplitudes are $u_m = (1-b)^{-3/2}(27\alpha/4)^{1/2}$ and $v_m = \frac{3}{2}(1-b)^{-1}$ and $k_{1l}y = Y(1-b)^{1/2}b^{-1/2}$. Interestingly, the limiting profiles and their widths are independent of the phase-mismatch parameter α, whose value tends to 4 as $b \longrightarrow 1$. At $|k_{1l}y| < 3\pi/2$, the envelopes of the normalized transverse electric-field components of the fundamental harmonic in the soliton core are $E_{1y} = (u_m/v_m)\cos(k_{1y}y/3)$ and $H_{1x} = n_{1l}(1-b)^{-1/2}E_{1y}$. The Maxwell equations can be used to find the remaining components in the form $E_{1z} = iu_m\varepsilon_1^{-1}\cos^2(k_{1y}y/3)\sin(k_{1y}y/3)$, $H_{2y} = n_{2l}(1-b)^{-1/2}E_{2x}$, and $H_{2z} = in_{1l}u_m\sin(2k_{1y}y/3)$. The envelopes of the transverse components are bell-

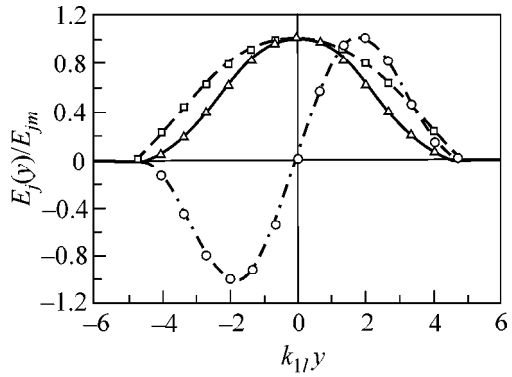

Fig. 1. Electric-field distribution over the cross section of an extremally narrow quadratic soliton with parameters $\alpha = 4$ and $b = 0.99$: (solid line) the transverse E_{1y} and (dash–dotted line) the longitudinal E_{1z} components of the fundamental wave and (dashed line) the transverse E_{2x} component of the second harmonic. The symbols △, ○, and □ denote the amplitudes of the self-similar profile calculated by Eq. (7).

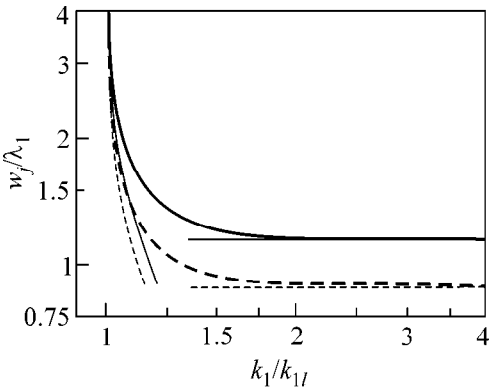

Fig. 2. Normalized (to the wavelength) widths of the envelopes calculated for the transverse electric-field components of (solid line) the fundamental wave E_{1y} and (dashed line) the second harmonic E_{2x} as functions of the nonlinear wave number for $\alpha = 4$. Thin lines indicate the asymptotic values corresponding to the (left) wide and (right) extremally narrow beams.

shaped, while the longitudinal components have a two-humped shape; the magnetic fields greatly exceed the electric fields.

Using Eq. (7), it is straightforward to find the following fundamental values for the smallest attainable soliton widths at the e^{-1} level of electric-field amplitude:

$$w_1 = 6k_{1l}^{-1}\arccos(e^{-1}) \approx 1.14\lambda_{1l},$$
$$w_2 = 6k_{1l}^{-1}\arccos(e^{-1/2}) \approx 0.878\lambda_{1l}. \quad (8)$$

Therefore, fundamental limit (8) for the full width of a spatial parametric soliton is on the order of a wavelength in the linear medium.

We solved the complete set of Eqs. (4) numerically by the relaxation method [11] for the phase-matching regime ($\alpha = 4$) and the normalized soliton wave numbers k_1/k_{1l} ranging from 1 to 10; this corresponds to the variation of the saturation parameter b in the range 0–0.99. The profiles of the transverse and longitudinal electric-field components of the extremally narrow soliton calculated numerically for $k_1/k_{1l} = 10$ ($b = 0.99$) and analytically by Eqs. (7) are presented in Fig. 1. Both profiles nicely coincide in the soliton core. A decrease in the soliton width with increasing wave number is illustrated in Fig. 2. The thin lines at the left of the figure indicate the transverse dimensions calculated within the framework of the classical theory of wide solitons [1–6]. The calculations were carried out upon setting $u = k_{1l}(k_1 - k_{1l})^{-1}(4\pi\chi_2 E_{1y}/\varepsilon_1)$, $v = k_{1l}(k_1 - k_{1l})^{-1}(2\pi\chi_2 E_{2x}/\varepsilon_1)$, $Y = y\sqrt{2k_{1l}(k_1 - k_{1l})}$, and $b = 0$ in Eqs. (4). Then the following expressions for the envelopes can be used: $u \approx 4.07\,\mathrm{sech}^p(Y/p)$ and $v \approx 1.68\,\mathrm{sech}^2(Y/p)$, where $p \approx 1.47$ [12]. A comparison of the curves in Fig. 2 shows that the paraxial approximation applies well to the wide spatial quadratic solitons up to $k_1 \approx 1.12k_{1l}$ or $b \approx 0.2$, where the width $w \approx 1.5\lambda_1$ and the amplitude $E_{2xm} \approx 0.4\varepsilon_2\chi_2^{-1}$. On further narrowing of the beam, the nonlinear diffraction mechanism becomes operative and the widths tend to their fundamental limits (8), which are indicated in Fig. 2 by the thin horizontal lines. The smallest width is, practically, established at $k_1 \approx 2k_{1l}$. The normalized peak amplitudes of the transverse and longitudinal components are shown in Fig. 3 as functions of the wave number. The departure from the paraxial approximation (thin lines) becomes appreciable slightly later than for the beam width (cf. Fig. 2), namely, at $k_1 \approx 1.3k_{1l}$ or $b \approx 0.4$. The longitudinal component is negligibly small for the wide beams but monotonically increases with the narrowing

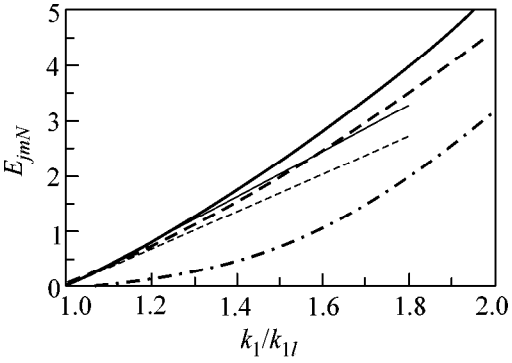

Fig. 3. Normalized peak amplitudes $E_{jmN} = 4\pi\chi_2 E_{jm}/\varepsilon_j$ of the three electric-field components of a quadratic soliton vs. the nonlinear wave number k_1/k_{1l} of the fundamental wave. Notations are as in Fig. 2.

of the soliton and becomes larger than the transverse components at $k_1/k_{1l} > 2.5$.

In summary, the theory of extremally narrow parametric solitons has been developed in this work. The equations derived for the envelopes of the transverse and longitudinal electric- and magnetic-field components of two harmonics allow for the weakening of the interaction by virtue of nonlinear diffraction. The soliton profiles are calculated for various phase-mismatch and saturation parameters. The transition from the paraxial approximation to the theory of ultranarrow beams is traced. Exact analytic solutions of the asymptotic equations are obtained for the extremally narrow solitons, and the fundamental limiting width is determined for a quadratic soliton.

This work was supported in part by the Russian Foundation for Basic Research (project no. 99-02-18161), the INTAS (grant no. 97-0581), and the programs "Leading Scientific Schools" (grant no. 00-15-96561) and "Russian Universities" (grant no. 99-2251).

REFERENCES

1. Yu. N. Karamzin and A. P. Sukhorukov, Pis'ma Zh. Éksp. Teor. Fiz. **20**, 734 (1974) [JETP Lett. **20**, 339 (1974)]; Zh. Éksp. Teor. Fiz. **68**, 834 (1975) [Sov. Phys. JETP **41**, 414 (1975)].
2. W. E. Torruellas, Z. Wang, D. J. Hagan, *et al.*, Phys. Rev. Lett. **74**, 5036 (1995); W. E. Torruellas, Z. Wang, L. Torner, *et al.*, Opt. Lett. **20**, 1949 (1995).
3. G. Stegeman, D. J. Hagan, and L. Torner, Opt. Quantum Electron. **28**, 1691 (1996); L. Torner, in *Beam Shaping and Control with Nonlinear Optics*, Ed. by F. Kajzer and R. Reinisch (Plenum, New York, 1998), p. 229.
4. *Advanced Photonics with Second-Order Nonlinear Processes*, Ed. by A. D. Boardman, L. Pavlov, and S. Tanev (Kluwer, Dordrecht, 1998).
5. A. V. Buryak and Yu. S. Kivshar, Phys. Lett. A **197**, 407 (1995).
6. L. Torner, Opt. Commun. **114**, 136 (1995).
7. E. Granot, S. Sternklar, Y. Isby, *et al.*, Opt. Lett. **22**, 1290 (1997); Opt. Commun. **178**, 431 (2000).
8. V. E. Semenov, N. N. Rozanov, and N. V. Vysotina, Zh. Éksp. Teor. Fiz. **116**, 458 (1999) [JETP **89**, 243 (1999)].
9. A. D. Boardman, K. Marinov, D. I. Pushkarov, *et al.*, Opt. Quantum Electron. **32**, 49 (2000).
10. A. D. Boardman, K. Marinov, D. I. Pushkarov, *et al.*, Phys. Rev. E **62**, 2871 (2000).
11. W. H. Press, B. P. Flannery, and S. A. Teukolsky, *Numerical Recipes* (Cambridge Univ. Press, Cambridge, 1987).
12. A. A. Sukhorukov, Phys. Rev. E **61**, 4530 (2000).

Translated by V. Sakun

JETP Letters, Vol. 72, No. 10, 2000, pp. 499–502. Translated from Pis'ma v Zhurnal Éksperimental'noĭ i Teoreticheskoĭ Fiziki, Vol. 72, No. 10, 2000, pp. 717–722.

Observation of Stimulated Raman Scattering in $Y_3Al_5O_{12}$ Single Crystals and Nanocrystalline Ceramics and in These Materials Activated with Laser Ions Nd^{3+} and Yb^{3+}

A. A. Kaminskiĭ[1,*], H. J. Eichler[2], K. Ueda[3,], S. N. Bagaev[4], G. M. A. Gad[2], J. Lu[3], T. Murai[3], H. Yagi[5], and T. Yanagitani[5]**

[1] *Shubnikov Institute of Crystallography, Russian Academy of Sciences, Leninskiĭ pr. 59, Moscow, 117333 Russia*
** e-mail: kaminalex@mail.ru*
[2] *Optical Institute, Technical University of Berlin, D-10623 Berlin, Germany*
[3] *Institute of Laser Science, University of Electrocommunications, 182-8585 Tokyo, Japan*
*** e-mail: ueda@ils.uec.ac.jp*
[4] *Institute of Laser Physics, Siberian Division, Russian Academy of Sciences, pr. Akademika Lavrent'eva 13/3, Novosibirsk, 630090 Russia*
[5] *Takuma Works, Konoshima Chemical Co. Ltd., 769-11 Kagawa, Japan*

Received October 18, 2000

High-order Raman parametric generation was excited in the visible and near-IR regions on the Stokes and anti-Stokes lines of $Y_3Al_5O_{12}$ single crystals and nanocrystalline ceramics. All generation components, as well as the $\chi^{(3)}$-active vibrational modes of these materials, were identified. In connection with the extensive use of the Nd^{3+}- and Yb^{3+}-doped $Y_3Al_5O_{12}$ crystals and, in recent years, nanocrystalline $Y_3Al_5O_{12} : Nd^{3+}$ ceramics in laser physics and quantum electronics, the applied aspect of the observed nonlinear properties of these materials is outlined. © *2000 MAIK "Nauka/Interperiodica".*

PACS numbers: 42.65.Dr; 42.70.-a

1. Crystal compounds with the garnet cubic structure (space group O_h^{10}-I*a*3*d*, no. 230) form the most representative class of active media among the known solid-state media generating stimulated emission. Among these, $Y_3Al_5O_{12} : Nd^{3+}$ crystals are most popular [1, 2]. On their base, world industry has developed to date more than a million various types of lasers for scientific, civil, and military purposes, as well as for medicine. The preparation of laser nanocrystalline $Y_3Al_5O_{12} : Nd^{3+}$ ceramics [3, 4] possessing a series of advantages over single crystals is one of the latest impressive advances in materials science and technology [5]. In spite of the fact that the spectroscopic, lasing, and other characteristics of these materials (in particular, crystals) have been extensively studied to date [6–9], their nonlinear optical properties associated with cubic nonlinear susceptibility $\chi^{(3)}$ have escaped the attention of researchers. In light of a wide and long-term use of pico- and femtosecond Nd^{3+}:$Y_3Al_5O_{12}$ and, in recent years, Yb^{3+}:$Y_3Al_5O_{12}$ lasers, this fact looked, in a way, like a curious phenomenon. In particular, intracavity ultrastrong light fields are, in principle, capable of self-modifying the spectroscopic purity of generation and making its mode structure more complex. Some other unwanted manifestations of the nonlinear interactions can also occur in these lasers [8]. At the same time, the $\chi^{(3)}$ processes in active media may be useful in developing powerful sources of coherent emission at new wavelengths (see, e.g., [10–12]).

2. In this work, we report the observation of stimulated Raman scattering (SRS) both in rated "pure" single crystals and nanocrystalline ceramics $Y_3Al_5O_{12}$ and in their analogues activated with laser ions Nd^{3+} and Yb^{3+}. We determined the type and energy of the SRS-active vibrational modes of these new $\chi^{(3)}$-nonlinear materials and identified all experimentally detected Stokes and anti-Stokes components of the parametrically excited generation.

3. Single crystals of yttrium aluminum garnet were grown by the usual Czochralski method in Pt crucibles. The SRS experiments were accomplished with rods 6–8 mm in diameter and up to 90 mm in length (along the crystallographic ⟨111⟩ direction) and with commercial (Litton–Aitron Inc.) $Y_3Al_5O_{12} : Nd^{3+}$ laser crystals ($C_{Nd} \approx 0.9$ at. %) ≈120 mm in length. Optically transparent nanocrystalline ceramics were prepared by the modified urea precipitation method using $(NH_4)_2SO_4$ urea and other additions that are necessary for this technique [4, 9]. The corresponding experimental samples were bars 40 mm in length with cross section

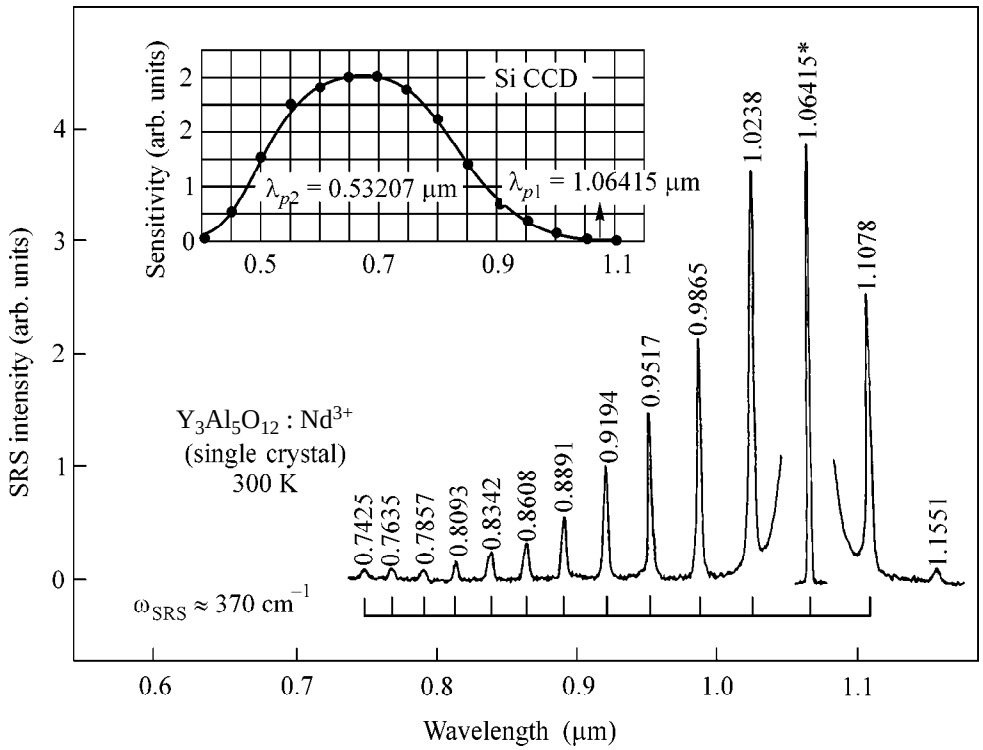

Fig. 1. Scheme of steady-state SRS in $Y_3Al_5O_{12}$: Nd^{3+} single crystal ($C_{Nd} \approx 1$ at. %, l = 50 mm) at 300 K. Pumping is at λ_{p1} = 1.06415 μm (the line is asterisked) and recording is along the crystallographic ⟨111⟩ direction; E-vector of the pump emission is oriented perpendicularly to ⟨111⟩. Line intensities are not recalculated to the spectral sensitivity of the Si-CCD detector (see inset) of the CSMA complex. The interrelation between the SRS-active lattice mode with frequency $\omega_{SRS} \approx 370$ cm^{-1} and the Stokes and anti-Stokes generation components is indicated by brackets. Line wavelengths are given in μm, and frequency spacings are in cm^{-1}.

10×10 mm. Electron microscopy suggested that the pore volume concentration in these samples was ≈1 ppm (≈10^{-4}%) and the average size of $Y_3Al_5O_{12}$ grains was about 1 μm. Scattering losses in the visible region were estimated at ≈0.009 cm^{-1}. Comparative measurements and the use of the well-known Rayleigh formula d^6/λ^4 for the scattering intensity (d and λ are the scatterer size and the emission wavelength, respectively) showed that the average size of grain faces in the ceramics was less than 1 μm. Note also that the plane-parallel (≈20″) ends of the single-crystal and the nanocrystalline samples were not coated with an antireflection layer at this step of measurements.

4. The SRS experiments were carried out using a cavity-free single-pass pump circuit and a powerful picosecond Nd^{3+}:$Y_3Al_5O_{12}$ laser with two amplifier stages. The laser was capable of generating pulses with a repetition rate of 1 Hz both on its fundamental $^4F_{3/2} \longrightarrow {}^4I_{11/2}$ transition with λ_{p1} = 1.06415 μm ($\tau_{p1} \approx$ 110 ps) and output of up to 10 mJ and using an external efficient (≈25%) frequency doubler ($KTiOPO_4$) with λ_{p2} = 0.53207 μm (τ_{p2} = 80 ps). Pump emission with Gaussian intensity distribution over the beam cross section was focused onto the sample by a lens with focal distance adjusted so that the SRS transformation was maximum. This was usually achieved when the diameter of the pump beam waist in the sample was 50–75 μm. Note, in advance, that these experimental conditions provided the steady-state regime for the SRS. The spectral composition of a multifrequency parametric generation excited at 300 K in the nanocrystalline $Y_3Al_5O_{12}$ and $Y_3Al_5O_{12}$: Nd^{3+} ($C_{Nd} \approx 1\%$) ceramics and the $Y_3Al_5O_{12}$, $Y_3Al_5O_{12}$: Nd^{3+} ($C_{Nd} \approx 1\%$), and $Y_3Al_5O_{12}$:Yb^{3+} ($C_{Yb} \approx$ 5%) single crystals was studied with a spectrometric CSMA complex based on a grating monochromator (McPherson-218, Czerny-Turner arrangement) and a Si-CCD matrix (Hamamatsu S3423-1024Q) with maximum sensitivity in the red spectral region (see inset in Fig. 1). Some of the SRS spectra, together with the results of identification of the Stokes and anti-Stokes components, are presented in Figs. 1 and 2. One can see that the frequencies of the SRS-active vibrational modes in the single crystal and the nanocrystalline ceramics, to experimental accuracy, coincide and are equal to $\omega_{SRS} \approx 370$ cm^{-1}.

5. The unit cell of $Y_3Al_5O_{12}$ contains eight formula units, with Al^{3+} cations occupying sites of two types with different oxygen coordination environments: 16

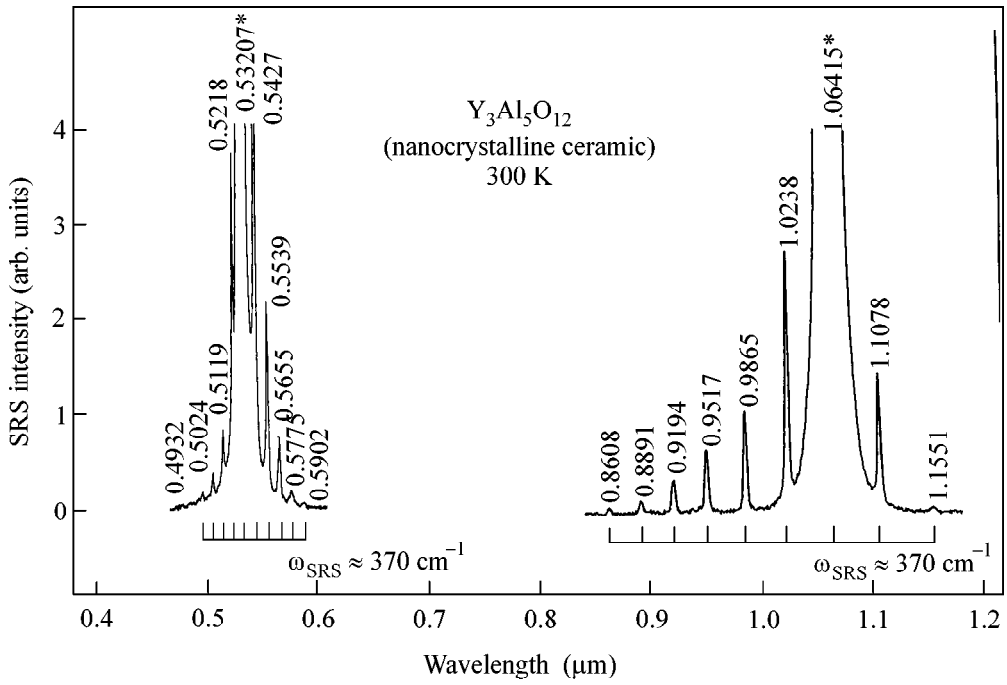

Fig. 2. Steady-state SRS spectra of the nanocrystalline ceramic of $Y_3Al_5O_{12}$ (l = 40 mm) recorded at 300 K upon pumping in the near-IR (λ_{p1} = 1.06415 μm) and visible (λ_{p2} = 0.53207 μm) regions. Notations as in Fig. 1. Pump line is asterisked.

a-octahedral (local symmetry C_{3i}) and 24 *d*-tetrahedral (S_4) sites. The Y^{3+} cations and their Nd^{3+} (Yb^{3+}) substituents are positioned in 24 dodecahedral *c* sites (D_2). The O^{2-} anions occupy 96 general positions *h* (C_1). Eighty atoms of the unit cell of $Y_3Al_5O_{12}$ have $3N = 240$ degrees of freedom, which, according to factor group analysis [3, 4] and symmetry degeneracy, give rise to 98 vibrational modes belonging to the following irreducible representations at $k = 0$ (center of Brillouin zone):

$$\Gamma_N = 3A_{1g} + 8E_g + 14F_{2g} + 5A_{1u} + 5A_{2u} + 5A_{2g} + 10E_u + 14F_{1g} + 16F_{2u} + 18F_{1u}.$$

Of these, the A_{1g}, E_g, and F_{2g} modes should appear in the spontaneous Raman (SR) spectrum and the F_{1u} mode should appear in the IR absorption and reflection spectra [15].

The SR spectra shown in Fig. 3 give an indication of the spectral distribution of optical modes in the media. They were recorded in the "back reflection" geometry using a Raman spectrometer based on an MD-1000 grating monochromator (Koken-Kogyo) equipped with a C5410 photon counter (Hamamatsu E1341). In these experiments, the SRS was excited by a high-stability cw Nd^{3+}:$Y_3Al_5O_{12}$ JUNO532-100S laser (second harmonic). An analysis of the SR spectra of the $Y_3Al_5O_{12}$ single crystals suggests (see, e.g., [13, 14]) that the line at ≈370 cm^{-1} may be due to the $A_{g1}(\nu_1)$ and $F_{2g}(\nu_3)$ internal vibrations whose frequencies coincide for the tetrahedral AlO_4^{5-} and octahedral AlO_6^{9-} ion groups. Considering that the spontaneous and the stimulated Raman spectra of single crystals and nanocrystalline ceramics of $Y_3Al_5O_{12}$ are virtually identical, as are also the other physical properties of these materials [3–5], we concluded that their SRS-active modes with frequency $\omega_{SRS} \approx 370$ cm^{-1} are of the same nature.

6. From comparative measurements with the known $\chi^{(3)}$- active $PbWO_4$ and $KY(WO_4)_2$ crystals [16], we have determined, with a satisfactory accuracy, the gain coefficient (g_{ss}) for the steady-state SRS in our $Y_3Al_5O_{12}$ materials. The steady-state $\chi^{(3)}$-generation regime was provided well by the experimental conditions, because, in all these media, $\tau_p \gg T_2 = 1/\pi\Delta\nu_R \approx 2$ ps, where T_2 and $\Delta\nu_R$ are the phonon relaxation time and the width of the corresponding spontaneous Raman line, respectively. We measured the peak pump (threshold) power P_{thr}, at which the generation of the first Stokes component (λ_{St1} = 1.1078 μm) began to be reliably detected. Next, by using the well-known approximate expression [17] for the gain increment $g_{ss}P_{thr}l_R \approx 30$ (l_R is the SRS-active length of a medium), we calculated the g_{ss} coefficient. For the $Y_3Al_5O_{12}$ crystals and ceramics, this value was found to be $g_{ss} = 0.1 \pm 0.05$ cm/GW. We also managed to estimate the total efficiency of the nonlinear $\chi^{(3)}$ transformation for one-micrometer picosecond pumping of all Stokes and anti-Stokes components in $Y_3Al_5O_{12}$. For instance, at a

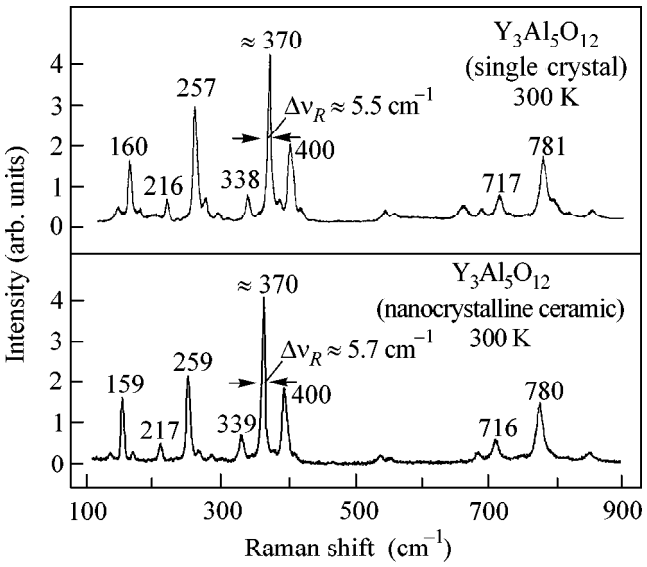

Fig. 3. SRS spectra of the single crystal and the nanocrystalline ceramic of $Y_3Al_5O_{12}$ at 300 K. Raman energies of the most intense lines are given in cm^{-1}. The spectra are recorded in the geometry close to the geometry of the SRS experiments with these media.

pump power density of about 1.5 GW/cm^2, this efficiency for the single crystals and the nanocrystalline ceramics was as high as 10%. It should also be noted that, for the pump power density close to its "breakdown" value, the $\chi^{(3)}$-generation spectra of the $Y_3Al_5O_{12}$ single crystals represented a broad continuum with the Stokes and anti-Stokes lines "superimposed" on it. We assign the onset of continuum generation to the formation of self-focusing fibers in the generating crystals. The bandwidth of the anti-Stokes continuum wing was as large as ≈6000 cm^{-1}.

7. In summary, we have discovered new $\chi^{(3)}$-nonlinear properties of the $Y_3Al_5O_{12}$-based crystalline materials that are most popular in laser physics and quantum electronics and excited the multifrequency SRS by picosecond pumping at 300 K. In spite of the relatively low Raman gain in these materials, one should consider this phenomenon as a possible stray effect when developing lasers for generating ultrashort pulses. At the same time, the observed SRS seems to be intense enough for developing new SRS lasers in themselves. Fabrication of fiber single-crystalline $Y_3Al_5O_{12}$ Raman laser-frequency converters also seems to be tempting.

8. The presented study was greatly promoted by the cooperation of the authors at the Joint Open Laboratory "Laser Crystals and Precision Laser Systems." This work was supported in part (A.A.K. and S.N.B.) by the Russian Foundation for Basic Research and the State Programs "Fundamental Metrology," "Fundamental Spectroscopy," and "Optics: Laser Physics."

REFERENCES

1. W. Koechner, *Solid-State-Laser Engineering* (Springer-Verlag, Berlin, 1976, 1980, 1991, 2000).
2. *Handbook of Laser Science and Technology*, Ed. by M. J. Weber (CRC Press, Boca Raton, 1982, 1991).
3. A. Ikesue and T. Kinoshita, J. Am. Ceram. Soc. **78**, 1033 (1995).
4. T. Yanagitani, H. Yagi, and Y. Hiro, Jpn. Patent No. 10-101411 (1998).
5. J. Lu, M. Prabhu, J. Song, *et al.*, Appl. Phys. B (in press).
6. A. A. Kaminskii, *Laser Crystals, Their Physics and Properties* (Springer-Verlag, Berlin, 1981, 1990).
7. A. A. Kaminskii, *Crystalline Lasers: Physical Processes and Operating Schemes* (CRC Press, Boca Raton, 1996).
8. C. Flytzanis, in *Encyclopedia of Applied Physics*, Ed. by G. L. Trigs (VCH, Berlin, 1995), Vol. 12.
9. M. Sekita, H. Haneda, T. Yanagitani, and S. Shiransaki, J. Appl. Phys. **67**, 453 (1990).
10. J. T. Murray, R. C. Powell, and N. Peyghambarian, J. Lumin. **66–67**, 89 (1995).
11. A. A. Kaminskii, S. N. Bagayev, J. Hulliger, *et al.*, Appl. Phys. B **67B**, 157 (1998).
12. P. G. Zverev, T. T. Basiev, V. V. Osiko, *et al.*, Opt. Mater. **11**, 315 (1999).
13. J. P. Hurrell, S. P. S. Porto, I. F. Chany, *et al.*, Phys. Rev. **173**, 851 (1968).
14. R. L. Rousseau, R. P. Baumann, and S. P. S. Porto, J. Raman Spectrosc. **10**, 253 (1981).
15. G. Mace, G. Schaack, T. Ng, *et al.*, Z. Phys. **230**, 391 (1970).
16. A. A. Kaminskii, C. L. McCray, H. R. Lee, *et al.*, Opt. Commun. **183**, 277 (2000).
17. Y. R. Shen, *The Principles of Nonlinear Optics* (Wiley, New York, 1984).

Translated by V. Sakun

JETP Letters, Vol. 72, No. 10, 2000, pp. 503–505. From Pis'ma v Zhurnal Éksperimental'noĭ i Teoreticheskoĭ Fiziki, Vol. 72, No. 10, 2000, pp. 723–726.

Some Exact Solutions for the Classical Hall Effect in an Inhomogeneous Magnetic Field[1]

A. V. Chaplik

Institute of Semiconductor Physics, Siberian Division, Russian Academy of Sciences, pr. Akademika Lavrent'eva 13, Novosibirsk, 630090 Russia

e-mail: chaplik@isp.nsc.ru

Received October 4, 2000

The classical Hall effect in inhomogeneous systems is considered for the case of one-dimensional inhomogeneity. For a certain geometry of the problem and for the magnetic field linearly depending on the coordinate, the distribution of current density corresponds to the skin-effect. © *2000 MAIK "Nauka/Interperiodica".*

PACS numbers: 72.15.Gd

The behavior of 2D electrons in a spatially nonuniform magnetic field is of interest in various aspects. The simplest situation is a one-dimensional inhomogeneity when the normal component of the magnetic field B_z varies in only one direction, say $B_z(y)$. Müller [1] considered the ballistic regime of a 2D electronic system for the special case $B_z(y) = B_0 ky$ and for the geometry when the current flows in the x direction perpendicularly to the magnetic-field gradient. Numerical solution of the Schrödinger equation carried out in [1] gives the current distribution in the y direction $j_x(y)$. Nonzero values of $j_x(y)$ (without electric field) arise because the Landau degeneracy is removed in the inhomogeneous magnetic field and the eigenstates become current-carrying. Of course, the total current $J = \int j_x(y)dy$ equals zero in the absence of the electric field (the case with electric field was not considered in [1]).

In the present paper, I will consider the classical magnetotransport, for which the local relation between the current density $\mathbf{j}$ and the electric field $\mathbf{E}$ is valid,

$$j_\alpha = \sigma_{\alpha\beta}(y)E_\beta, \tag{1}$$

where α, β label the Cartesian components of the magnetoconductivity tensor $\hat{\sigma}$. The inhomogeneity is assumed to be one-dimensional (in the y direction), but both possible geometries of the experiments ($\mathbf{j} \parallel y$ and $\mathbf{j} \perp y$) will be considered. In the geometry of [1] $\mathbf{j} \perp y$, the exact analytic (and quite simple) solution is possible for an arbitrary dependence $\hat{\sigma}(y)$, including the case of a nonuniform magnetic field. In the other geometry $\mathbf{j} \parallel y$, the exact analytic (and rather unexpected) result is obtained for the Müller model $B_z = B_0 ky$: there exists a specific static skin-effect when the current density exponentially depends on the transverse coordinate x.

In both cases, I will consider a specimen in the form of a strip of finite width and infinite length. The total current J is fixed (measured by ammeter), while the electric-field components E_x and E_y are to be found from Eqs. (1) and

$$\mathrm{div}\mathbf{j} = 0, \quad \mathrm{curl}\mathbf{E} = 0. \tag{2}$$

In such a positioning of the problem one does not need to solve the Poisson equation.

Current perpendicular to the direction of inhomogeneity. The system of Eqs. (1) and (2), written in the components, reads

$$\begin{gathered} j_x = \sigma_0 E_x + \sigma_1 E_y, \quad j_y = -\sigma_1 E_x + \sigma_0 E_y, \\ \frac{\partial j_x}{\partial x} + \frac{\partial j_y}{\partial y} = 0; \quad \frac{\partial E_x}{\partial y} - \frac{\partial E_y}{\partial x} = 0, \end{gathered} \tag{3}$$

where $\sigma_0 = \sigma_{xx} = \sigma_{yy}$, $\sigma_1 = \sigma_{xy}$.

Look for the solution with $j_y \equiv 0$. Strictly speaking, one needs the solution with $j_y(y = 0) = j_y(y = L) = 0$, where L is the width of the strip. However, due to the evident uniquity of the solution, the assumption made does not violate the generality. Then we have

$$\begin{gathered} E_y = \frac{\sigma_1}{\sigma_0}E_x = k(y)E_x, \quad j_x = \left(\sigma_0 + \frac{\sigma_1^2}{\sigma_0}\right)E_x = q(y)E_x, \\ k \equiv \frac{\sigma_1}{\sigma_0}, \quad q \equiv \frac{\sigma_0^2 + \sigma_1^2}{\sigma_0} = \frac{1}{\rho_0}, \end{gathered} \tag{4}$$

where $\rho_{\alpha\beta}$ is the magnetoresistance tensor $\rho_0 = \rho_{xx}$. Further,

$$\mathrm{div}\mathbf{j} = \frac{\partial j_x}{\partial x} = q(y)\frac{\partial E_x}{\partial x} = -q(y)\frac{\partial^2 \Phi}{\partial x^2} = 0, \tag{5}$$

[1] This article was submitted by the author in English.

with $\mathbf{E} = -\nabla\Phi(x, y)$.

The general solution of Eq. (5) has the form

$$\Phi = A(y)x + B(y). \quad (6)$$

It follows from Eq. (4) that

$$\frac{\partial A}{\partial y}x + \frac{\partial B}{\partial y} = k(y)A(y). \quad (7)$$

Hence,

$$A = \text{const}, \quad B = A\int_{y_0}^{y} k(y')dy'. \quad (8)$$

The fixed total current determines the value A:

$$J = \int_0^L j_x dy = -A\int_0^L q(y')dy', \quad (9)$$

and the problem is solved. The Hall voltage, defined as $\Phi(x, 0) - \Phi(x, L)$, equals

$$V_H = A\int_0^L k(y')dy' = -J\int_0^L k(y')dy' / \int_0^L q(y')dy', \quad (10)$$

and one gets the following expression for the *effective* Hall resistance:

$$\rho_1^{\text{eff}} = \left\langle \frac{\rho_1}{\rho_0} \right\rangle / \left\langle \frac{1}{\rho_0} \right\rangle, \quad (11)$$

where the brackets mean averaging over y:

$$\langle u \rangle \equiv \frac{1}{L}\int_0^L u(y)dy. \quad (12)$$

The diagonal component of $\rho_{\alpha\beta}^{\text{eff}}$ is

$$\rho_0^{\text{eff}} = \left\langle \frac{1}{\rho_0} \right\rangle^{-1}, \quad (13)$$

which simply corresponds to the parallel connection of the conducting filaments stretched along the current direction.

Equations (8) and (10) are valid for any kind of one-dimensional inhomogeneity (e.g., carrier concentration, magnetic field, and the density of scatterers). If the specimen is homogeneous and only the magnetic field depends on y, the following relations hold between σ_0 and σ_1:

$$\frac{\sigma_1}{\sigma_0} = \lambda B(y), \quad \lambda = \text{const}, \quad \frac{\sigma_0^2 + \sigma_1^2}{\sigma_0} \equiv \sigma = \text{const}, \quad (14)$$

following from the classical Drude kinetic theory; σ is the Drude conductivity for $B = 0$. Then $\rho_1^{\text{eff}} = \langle \rho_1 \rangle$, which corresponds to the sequential connection of the Hall voltages created by the magnetic field in each conducting filament parallel to Ox. Thus, in the geometry considered in this section, for a homogeneous specimen and inhomogeneous magnetic field, the results are quite trivial:

$$\rho_0^{\text{eff}} = \left\langle \frac{1}{\rho_0} \right\rangle^{-1}, \quad \rho_1^{\text{eff}} = \langle \rho_1 \rangle. \quad (15)$$

Note that for an inhomogeneous specimen, a more complicated result (8) is valid instead of the second relation of Eq. (15).

Current parallel to the magnetic field gradient. Consider now a strip parallel to y and look for the solution with $j_x(y) \equiv 0$. The specimen is assumed to be homogeneous, and the local values $\sigma_0(y)$ and $\sigma_1(y)$ are determined by the classical kinetic theory:

$$\sigma_0 = \frac{\sigma}{1 + (\lambda B)^2}, \quad \sigma_1 = \frac{\sigma\lambda B}{1 + (\lambda B)^2}, \quad B = B(y). \quad (16)$$

Then, from Eqs. (3) with $j_x = 0$, one can easily obtain

$$j_y = \sigma E_y, \quad \frac{\partial^2 \Phi}{\partial y^2} = 0, \quad E_x = -\lambda B(y)E_y, \quad (17)$$

where the last relation in Eq. (17) follows again from $j_x = 0$. Hence,

$$\Phi = C_1(x)y + C_2(x),$$
$$\frac{\partial C_1}{\partial x}y + \frac{\partial C_2}{\partial x} = -\lambda B(y)C_1(x), \quad (18)$$

and for the Müller model $B(y) = B_0 ky$ the solution has the form

$$C_1 = Ce^{-\lambda B_0 kx}, \quad C_2 \equiv 0, \quad \Phi = Cye^{-\lambda kx B_0}. \quad (19)$$

From Eq. (19) one obtains

$$E_x = C\lambda B_0 kye^{-\lambda B_0 kx}, \quad E_y = -Ce^{-\lambda B_0 kx},$$
$$j_y = -\sigma Ce^{-\lambda B_0 kx}, \quad (20)$$

where the constant C can be found via the total current

$$J = \int_0^L j_y dx = -\frac{\sigma C}{\lambda B_0 k}(1 - e^{-\lambda B_0 kL}). \quad (21)$$

The Hall voltage is

$$\Phi(x = 0, y) - \Phi(x = L, y) = y\frac{J\lambda B_0 k}{\sigma}, \quad (22)$$

and the Hall resistance at the point y is

$$\rho_H^{(y)} = \frac{\lambda B_0 ky}{\sigma} = \rho\omega_c(y)\tau, \quad (23)$$

where $\rho = 1/\sigma$, τ is the relaxation time, and $\omega_c(y)$ is the local value of the cyclotron frequency $\omega_c(y)\tau = \lambda B(y)$. The most remarkable feature of the obtained solution is the exponential distribution of the current density along

the x direction [see Eq. (20)]. This can be called the static skin-effect. Depending on the signs of J, B_0, and k, the current in the y direction is concentrated either at the left ($x = 0$) or at the right ($x = L$) edge of the strip. The depth of skin layer l_s is defined by the magnetic-field gradient: $l_s = 1/k\omega_{c0}\tau$, where ω_{c0} is the cyclotron frequency for $B = B_0$. The electric field also depends exponentially on the transverse coordinate. Hence, when measuring the Hall voltage V_H between the left edge of the strip $x = 0$ and some variable point x (for the same y) inside the strip, one will find the exponential dependence $V_H(x)$, which would be experimental evidence of the skin-effect.

Alternating electric field. The results obtained above can easily be extended to the case of finite frequency ω of the electric field, if $\omega \ll 1/\tau_M$, where τ_M is the Maxwell relaxation time. For the 3D situation, $1/\tau_M = 4\pi\sigma_{3D}$, and for 2D, $1/\tau_M = 2\pi\sigma_{2D}/L$. The parameter $\omega\tau$ can be of an arbitrary magnitude. By making use of the well-known formulas for $\sigma_{\alpha\beta}(B)$ allowing for the dispersion, one can easily see that it is necessary just to substitute

$$\sigma \longrightarrow \frac{\sigma}{1 - i\omega\tau}$$

in all preceeding formulas. For example, the Hall voltage between the points (o, y) and (x, y) reads

$$V_H(o, x; y) = CyR_e\left\{\left[1 - \exp\frac{(-kx)\omega_{c0}\tau(1 + i\omega\tau)}{1 + \omega^2\tau^2}\right]e^{-i\omega t}\right\}. \quad (24)$$

Thus, the voltage and the current density decay with oscillations when the distance from the strip edge increases.

How to realize the linearly nonuniform magnetic field. Here, I consider only the case of a 2D system. Since 2D electrons "feel" only the normal component of the magnetic field B_n, the inhomogeneity of B_n can be achieved for a thin conducting film bent to a proper shape and placed in a uniform field $\mathbf{B}(0, 0, B)$. The dependence $B_n(y) = B_0ky$ is realized for the cylindrical surface $z = F(y)$, where

$$F(y) = \pm\frac{1}{2k}[\sqrt{2ky(1 - 2ky)} + \arcsin\sqrt{2ky}], \quad 0 \le ky \le \frac{1}{2}. \quad (25)$$

In conclusion, the exact analytic solutions are obtained for the classical Hall effect in inhomogeneous systems. If the current flows perpendicularly to the inhomogeneity, the solution is possible in a quite general form. For parallel orientation of the current and magnetic-field gradient, the analytic solution is found for the linearly inhomogeneous magnetic field. In the latter case, the static skin-effect occurs for a specimen in the form of a long strip.

This work was supported by the Russian Foundation for Basic Research (project no. 99-02-17127) and by the NWO.

REFERENCES

1. J. E. Müller, Phys. Rev. Lett. **68**, 385 (1992).

JETP Letters, Vol. 72, No. 10, 2000, pp. 506–510. Translated from Pis'ma v Zhurnal Éksperimental'noĭ i Teoreticheskoĭ Fiziki, Vol. 72, No. 10, 2000, pp. 727–733.

Conductivity of 2D Systems: Role of the Correlation Effects

É. G. Batyev

Institute of Semiconductor Physics, Siberian Division, Russian Academy of Sciences, pr. Akademika Lavrent'eva 13, Novosibirsk, 630090 Russia

Received October 6, 2000

A description is proposed for a low-density 2D electron system in which, according to the experimental data, a metal–insulator transition occurs with varying carrier density. In such a system, the correlation effects due to the interaction between the charge carriers can play a significant role. The system is assumed to possess a short-wavelength soft mode, which models the effect of the aforementioned interaction. The conductivity of the system (the metallic state is considered) depends not only on the common impurity scattering of the charge carriers, but also on the scattering of the Bose excitations (the soft mode), which leads to an additional dissipation of the momentum of the system. The number of Bose excitations varies with temperature, which causes a temperature dependence of the conductivity. © *2000 MAIK "Nauka/Interperiodica".*

PACS numbers: 71.27.+a; 71.30.+h

Recent experiments revealed a kind of metal–insulator transition in 2D systems (electron or hole ones) in zero magnetic field. The effect was observed on high-mobility samples whose resistance was found to drop sharply with decreasing temperature when the carrier concentration exceeded some critical value, whereas samples with lower concentrations exhibited an increase in their resistance. This phenomenon was interpreted as the metal–insulator transition (see [1–3]).

The results of these studies contradict the well-known statement that, in disordered 2D systems, all single-particle (electron or hole) states are localized [4]; i.e., the metallic state in such systems is impossible.

At the same time, in a system with strong interaction between the charge carriers, the single-particle states are considerably distorted by this interaction and the aforementioned statements may fail. According to the estimates, for the concentrations used in the experiments, the Coulomb interaction between the carriers exceeds the Fermi energy and, hence, can strongly affect the properties of single-particle excitations. Therefore, the conclusions concerning the localization of the latter can be different.

Such an idea was put forward in a number of publications, which presented arguments in support of the existence of the metallic state in the case of strong interaction between the carriers (see, e.g., [3]). Leaving aside the fundamental justification and proceeding only from the fact that the experiments provide direct evidence in favor of this idea, I will investigate the cause of the sharp temperature dependence of the resistivity. Attempts were made to explain this effect on the basis of the single-particle approach (see, e.g., [5, 6]). Without denying the significance of various single-particle effects, it would be desirable to determine a single cause for both the metallic state and the temperature dependence of the resistivity observed in the experiment, i.e., the strong interaction and the correlation effects, so that no contributions of any other factors should be taken into account.

This paper presents a model in which a qualitatively new characteristic describing the role of the correlation effects is explicitly introduced. Namely, it is assumed that, in addition to the conventional Fermi excitations, a short-wavelength soft mode, which corresponds to Bose-type excitations with low energy and finite momenta, is present in the system.

The soft mode is a precursor of the phase transition. In the case of a crystallization-type transition, the corresponding feature should occur in the density–density correlator and the aforementioned Bose excitations should have a zero spin. Such an assumption was used in the theory of liquid–crystal transition in He^3 [7]. It is also possible that a similar feature occurs in the spin density–spin density correlator, as was assumed in the theory [8] developed for describing liquid He^3 with allowance made for the interaction between the Fermi excitations and the soft mode. In this case, one can consider Bose excitations with spin 1. In the cited paper [8], these excitations were strongly damped, because they were characterized by the momenta $< 2p_F$ (p_F is the Fermi momentum) and could decay into a pair of Fermi excitations (otherwise, they would be "good" quasiparticles). In both papers cited above [7, 8], the momenta corresponding to the soft mode were finite.

For the problems considered in this paper and for the approach used below, the origin of these Bose excitations and type of their spin are of no importance. However, they can be significant in studying other

0021-3640/00/7210-0506$20.00

properties (e.g., in a magnetic field). Let us consider more closely the type of soft mode.

In an ideal Fermi gas, correlations occur between the particles with identical spins because of the Pauli principle, whereas the particles with opposite spins do not correlate at all. Let us assume that a weak interaction (repulsion) occurs in the system. For simplicity, a short-range interaction of the delta-function type is considered. This interaction does not affect (to a first approximation) the correlations between the particles with identical spins, but it leads to the correlations between the particles with opposite spins. As a result, each particle tends to a position between the particles with opposite spins. As the repulsion grows stronger, this tendency is enhanced, and, in the case of a strong interaction (for a Coulomb interaction, one has the so-called Wigner liquid), every particle has particles with opposite spins as its nearest neighbors; i.e., an antiferromagnetic short-range order is formed in the system. As a result, the appearance of an antiferromagnetic-type soft mode is possible, which means the maximum spin susceptibility at low frequencies and finite momenta. This is the precursor of the transition to the state with a spin-density wave. Thus, apparently, the presence of an antiferromagnetic-type soft mode is not a specific feature of He^3, as one might infer from [8], but a general property of Fermi systems with a strong interaction.

The aforesaid is true for systems without spin polarization. In a completely spin-polarized system (in a magnetic field parallel to its plane), another type of soft mode is possible [7].

Let us now describe the model and the method of solving the problem under discussion. A 2D electron (hole) system with a strong interaction is considered. In addition to the conventional Fermi excitations, this system contains Bose-type excitations with the spectrum

$$\Omega_{\mathbf{q}}^2 = \Omega_0^2 + v_0^2(q - q_0)^2. \tag{1}$$

It is assumed that $\Omega_0 \ll \epsilon_F$, as it must be for the soft mode (ϵ_F is the Fermi energy), although, in systems with hole conductivity, this condition is presumably not fully satisfied. The velocity is $v_0 \sim v_F$ (v_F is the Fermi velocity). As for the momentum q_0 corresponding to the minimal energy of a Bose excitation (this excitation will be called a magnon, in accordance with the above considerations), one only can state that $q_0 \sim p_F$. In [8], it was assumed that $q_0 < 2p_F$, and, hence, this excitation was strongly damped. It is possible that, in the 2D case with a type of interaction other than in He^3, the situation will be different:

$$q_0 > 2p_F. \tag{2}$$

In any case, the latter assumption considerably simplifies the analysis. Therefore, it will be assumed that Eq. (2) is valid and one deals with good, weakly damped excitations with spin 1 (magnons).

Thus, the system under study contains two types of elementary excitations: Fermi excitations (called electrons) and Bose excitations (magnons). Both of them are scattered by the impurities, and the system loses its momentum through these two channels. One can assume that, at low temperatures, as usual, the contribution made by the electrons is temperature-independent. This is not the case with the magnons because of the dependence of their number on temperature (if for no other reason). It is the aim of this work to determine the magnon contribution to the friction of the system under study. This problem will be considered using its simplest possible formulation and some simplifications, which will be specified below.

The main simplification is as follows: it is assumed that the scattering by the impurities is sufficiently small for the two subsystems (electrons and magnons) to be in thermal equilibrium with each other at temperature T. Then, the state of the system is completely characterized by the velocity of its motion $\mathbf{u}$. In this case, the excitation energy varies in a known way; namely, for a magnon, one has

$$\Omega_{\mathbf{q}} \longrightarrow \Omega_{\mathbf{q}} + \mathbf{qu}. \tag{3}$$

This quantity will be involved in the energy conservation law. The equilibrium distribution function for the magnons, $N_{\mathbf{q}}$, has the form of the standard Bose distribution

$$N_{\mathbf{q}} = \frac{1}{\exp(\Omega_{\mathbf{q}}/T) - 1}. \tag{4}$$

To calculate the variation per unit time in the momentum of the system because of the magnon scattering, $(d\mathbf{P}/dt)_m$, the Fermi golden rule is used. As a result, one obtains

$$\left(\frac{d\mathbf{P}}{dt}\right)_m = 2\pi \sum_{\mathbf{q}, \mathbf{q}'} \overline{|W_{\mathbf{q}', \mathbf{q}}|^2} \delta(\Omega_{\mathbf{q}} + \mathbf{qu} - \Omega_{\mathbf{q}'} - \mathbf{q}'\mathbf{u}) \times N_{\mathbf{q}}(1 + N_{\mathbf{q}'})(\mathbf{q}' - \mathbf{q}). \tag{5}$$

Here, $W_{\mathbf{q}', \mathbf{q}}$ is the matrix element corresponding to the impurity scattering of a magnon from the state with the momentum $\mathbf{q}$ to the state with the momentum $\mathbf{q}'$. The bar over the squared absolute value of the matrix element means averaging over the impurity positions.

Here and below, for simplicity, all formulas are written as if there is a single nondegenerate soft mode (as for spin 0). Degeneracy (spin 1) would lead to changes in some constants, which, in the best case, are known within an order of magnitude. The dependences obtained for both cases are identical (for spinless impurities).

Let us analyze the right-hand side of Eq. (5). Because of the factor $(\mathbf{q}' - \mathbf{q})$, the contribution quadratic in the magnon filling factors disappears and the

linear contribution can be transformed by applying the substitution

$$N_{\mathbf{q}} \longrightarrow \frac{1}{2}(N_{\mathbf{q}} - N_{\mathbf{q}'}) \approx \frac{1}{2}\frac{dN_{\mathbf{q}}}{d\Omega_{\mathbf{q}}}(\mathbf{q}' - \mathbf{q})\mathbf{u}.$$

In the approximation linear in $\mathbf{u}$, one can neglect the terms with $\mathbf{u}$ involved in the argument of the delta function. Then, instead of Eq. (5), one obtains

$$\left(\frac{d\mathbf{P}}{dt}\right)_m \approx \pi\sum_{\mathbf{q},\,\mathbf{q}'}\overline{|W_{\mathbf{q}',\,\mathbf{q}}|^2}\delta(\Omega_{\mathbf{q}} - \Omega_{\mathbf{q}'}) \times \frac{dN_{\mathbf{q}}}{d\Omega_{\mathbf{q}}}(\mathbf{q}' - \mathbf{q})((\mathbf{q}' - \mathbf{q})\mathbf{u}). \tag{6}$$

Near the minimum of the spectrum, one has $q' \approx q \approx q_0$. Integrating with respect to the angles on the assumption that $\overline{|W_{\mathbf{q}',\,\mathbf{q}}|^2}$ is constant, one obtains the following expression instead of Eq. (6):

$$\left(\frac{d\mathbf{P}}{dt}\right)_m \approx \pi\sum_{\mathbf{q},\,\mathbf{q}'}\overline{|W_{\mathbf{q}',\,\mathbf{q}}|^2}\delta(\Omega_{\mathbf{q}} - \Omega_{\mathbf{q}'})\frac{dN_{\mathbf{q}}}{d\Omega_{\mathbf{q}}}q_0^2\mathbf{u}. \tag{7}$$

The interaction with impurities will be described in the simplest way by specifying the corresponding operator:

$$\hat{W} = \frac{g}{2V}\sum_{\mathbf{q},\,\mathbf{q}',\,\nu}\exp(i(\mathbf{q} - \mathbf{q}')\mathbf{R}_\nu)B_{\mathbf{q}}B_{-\mathbf{q}'}, \tag{8}$$

where the summation is over the impurities ($\mathbf{R}_\nu$ is the radius vector of the νth impurity) and over the momenta, and the operator $B_{\mathbf{q}}$ is determined as

$$B_{\mathbf{q}} = \frac{b_{\mathbf{q}} + b^+_{-\mathbf{q}}}{\sqrt{\Omega_{\mathbf{q}}}}. \tag{9}$$

Here, $b^+_{\mathbf{q}}(b_{\mathbf{q}})$ is the operator of the creation (annihilation) of a magnon with momentum $\mathbf{q}$ and g is the coupling constant ($g > 0$, which corresponds to the case of repulsion; otherwise, it would be necessary to take into account the bound magnon states at the impurities); this expression also involves a usual factor that contains the magnon energy (as in the case of an oscillator). Equation (9) corresponds to a magnon with a zero spin projection; evidently, for other projections, the results will be the same (spinless impurities). Note that, for a zero-spin excitation, one would also have a contribution linear in the operators.

The matrix element involved in Eq. (7) has the form

$$W_{\mathbf{q},\,\mathbf{q}'} = \frac{g}{V}\frac{1}{\sqrt{\Omega_{\mathbf{q}}\Omega_{\mathbf{q}'}}}\sum_\nu \exp(i(\mathbf{q} - \mathbf{q}')\mathbf{R}_\nu)$$

[see Eqs. (8) and (9)]. After averaging over the impurity positions, one obtains for the squared absolute value of the matrix element

$$\overline{|W_{\mathbf{q}',\,\mathbf{q}}|^2} = \frac{g^2}{V}\frac{1}{\Omega_{\mathbf{q}}\Omega_{\mathbf{q}'}}n_i,$$

where n_i is the impurity concentration.

Passing from sums to integrals in Eq. (7) and introducing the magnon relaxation time τ_m, instead of Eq. (7), one obtains the expression

$$\left(\frac{d\mathbf{P}}{dt}\right)_m = -\frac{1}{\tau_m}\mathbf{P}, \quad \frac{\mathbf{P}}{V} = nm\mathbf{u}, \tag{10}$$

where n and m are the concentration and the mass of carriers and τ_m is determined by the formula

$$\frac{1}{\tau_m} = -\frac{n_i}{n}\frac{q_0^4}{\pi m v_0^2}\int_{\Omega_0}^{\infty}\frac{|\tilde{g}(\Omega)|^2 d\Omega}{\Omega^2 - \Omega_0^2}\frac{dN}{d\Omega}. \tag{11}$$

Here, the quantity g is replaced by $\tilde{g}(\Omega)$, which corresponds to the renormalized interaction with impurities. The point is that, in the case under study, one cannot restrict oneself to the first order of perturbation theory because of the divergence of the integral at the lower limit; such a divergence and the need for renormalization occur because of the form of spectrum (1).

To determine $\tilde{g}(\Omega)$, it is necessary to consider the scattering by a single impurity and to perform the summation of the series of perturbation theory [the interaction with the impurities is determined by Eqs. (8) and (9)]. This can be done by applying the diagram technique. Here, the calculations are omitted; they can be found in the books on quantum mechanics (see, e.g., [9], §43, where the calculations are performed without using the diagrammatic technique). The result is

$$\tilde{g}(\Omega) = g\left[1 - \frac{2g}{V}\sum_{\mathbf{k}}\frac{1}{(\Omega + i\delta)^2 - \Omega_{\mathbf{k}}^2}\right]^{-1} \longrightarrow g\left[1 + ig\frac{q_0}{v_0}\frac{1}{\sqrt{\Omega^2 - \Omega_0^2}}\right]^{-1} \tag{12}$$

(δ determines the path around the pole, $\delta \longrightarrow +0$). From this expression, one can see that, for $\Omega \longrightarrow \Omega_0$, the corrections to the interaction are truly significant and the interaction becomes equal to zero, which eliminates the difficulty related to the divergence of the integral in Eq. (11).

For the analysis of Eq. (11), different variants are possible, depending on the value of g. Only one of them will be considered, which seems to be the most probable. The quantities q_0 and v_0 are of the same order of magnitude as the corresponding Fermi quantities [see note after Eq. (1)], whereas Ω and Ω_0 are much smaller than the Fermi energy. Therefore, if g is not too small

(on the same scale), one can neglect unity in the denominator in Eq. (12). Then, instead of Eq. (12), one obtains

$$\tilde{g}(\Omega) \approx -i\frac{v_0}{q_0}\sqrt{\Omega^2 - \Omega_0^2}. \quad (13)$$

In this limit, the constant g, which characterizes the interaction with the impurity, totally disappears.

Calculating the integral in Eq. (11) by using Eq. (13) for $\tilde{g}(\Omega)$, one gets

$$\frac{1}{\tau_m} \approx \frac{n_i}{n}\frac{q_0^2}{\pi m}N(\Omega_0), \quad (14)$$
$$N(\Omega_0) = [\exp(\Omega_0/T) - 1]^{-1}.$$

The conductivity σ is expressed through the relaxation time τ in the usual way:

$$\sigma = \frac{ne^2\tau}{m}, \quad \frac{1}{\tau} = \frac{1}{\tau_e} + \frac{1}{\tau_m}, \quad (15)$$

where τ_e is the electron relaxation time (which is assumed to be constant).

The resistivity $\rho = 1/\sigma$ at temperature $T < \Omega_0$ can be represented in the form

$$\rho \approx \rho_0 + \rho_1 \exp(-\Omega_0/T) \quad (16)$$

(the relation of ρ_0 and ρ_1 to the parameters of the model can be obtained from comparison with the expressions given above). In some experiments [10, 11], it is this type of temperature dependence that is obtained for sufficiently low temperatures. In terms of the model under consideration, one can reveal the meaning of the constant T_0 involved in the experimental dependence [10, 11] [instead of Ω_0 in Eq. (16)]: T_0 corresponds to the minimal magnon energy Ω_0. The experiments [10, 11] show that this quantity decreases as the density becomes lower, which is quite natural for such a quantity: the role of the correlation effects increases with decreasing density, and this leads to softening of the soft mode. However, at high temperatures, one obtains a dependence that is not likely to be observed in reality:

$$\rho \approx \rho_0 + \rho_1\frac{T}{\Omega_0} \quad (T \gg \Omega_0).$$

Possibly, this can be explained by the temperature dependence of spectrum (1) (such a dependence was not considered in this paper): since, with increasing temperature, one seemingly moves away from the transition, one should expect that Ω_0^2 increases according to the law

$$\Omega_0^2 \longrightarrow \Omega_0^2 + \alpha T^2,$$

as it must near the minimum (α is a constant factor). Then, with increasing temperature, the resistivity should tend to saturation, which qualitatively agrees with the experiment. However, currently there are no computational results in support of this hypothesis. An alternative explanation is as follows: for the aforementioned experiments [10, 11], the condition $T \gg \Omega_0$ means that the temperature becomes of the order of the Fermi energy, and, in this case, there is little of the soft mode left.

In closing, it should be noted that the origin of the observed metal–insulator transition is still not determined. In connection with the main idea described above, one may present the following considerations. Even for repulsive impurities, a bound magnon state at the system of impurities, or, more precisely, at the fluctuations of the impurity concentration, is possible in the regions where the local impurity concentration is below its average value. Because of the specific properties of the magnon spectrum, such a bound state is possible for an attractive potential as low as one likes, and this effective attraction occurs just in this kind of region. It is also possible that, with a decrease in Ω_0, i.e., with a decrease in the carrier concentration, the energy of the bound state (with allowance for the positive Ω_0) can approach zero (or even become negative). Then, at the absolute zero of temperature, this state will be filled, not with a single magnon but with a finite number of magnons (as far as the anharmonicities allow); i.e., a kind of local Bose condensate of magnons will be formed. In other words, in the attraction region, a small crystallite of a different phase—the phase with the spin density wave—can be formed. One can expect that such regions should noticeably affect the conductivity of the system, namely, lead to its decrease. At finite temperatures, the Bose condensate fails (one can say that the crystallites melt), which can lead to an increase in the conductivity. This effect was observed on the insulator side of the transition in the systems under study. Thus, the mechanism responsible for the transition from the metallic state to the insulating one can be the formation of crystalline fragments in the metallic phase. All this (and the question concerning the effect of the bound states on the conductivity in the metallic phase) requires special consideration.

I am grateful to A.V. Chaplik and M.V. Éntin for useful discussions. The work was supported in part by the Russian Foundation for Basic Research (project no. 00-15-96800) and the State Program of the Russian Federation “Physics of Solid Nanostructures.”

REFERENCES

1. S. V. Kravchenko, G. V. Kravchenko, J. E. Furneaux, *et al.*, Phys. Rev. B **50**, 8039 (1994); S. V. Kravchenko, Whitney E. Mason, and G. E. Bowker, Phys. Rev. B **51**, 7038 (1995); S. V. Kravchenko, D. Simonian, and M. P. Sarachik, Phys. Rev. Lett. **77**, 4938 (1996).
2. *Proceedings of the 13th International Conference on the Electronic Properties of Two-Dimensional Systems, Ottawa, Canada, 1999.*

3. Jongsoo Yoon, C. C. Li, D. C. Tsui, and M. Shayegan, Phys. Rev. Lett. **84**, 4421 (2000); S. C. Dultz and H. W. Jiang, Phys. Rev. Lett. **84**, 4689 (2000).
4. E. Abrahams, P. W. Anderson, D. C. Licciardello, and T. V. Ramakrishnan, Phys. Rev. Lett. **42**, 673 (1979).
5. V. M. Pudalov, Pis'ma Zh. Éksp. Teor. Fiz. **66**, 168 (1997) [JETP Lett. **66**, 175 (1997)].
6. B. L. Altshuler and D. L. Maslov, Phys. Rev. Lett. **82**, 145 (1999).
7. É. G. Batyev, Zh. Éksp. Teor. Fiz. **70**, 578 (1976) [Sov. Phys. JETP **43**, 300 (1976)].
8. A. M. Dyugaev, Zh. Éksp. Teor. Fiz. **70**, 2390 (1976) [Sov. Phys. JETP **43**, 1247 (1976)].
9. L. D. Landau and E. M. Lifshitz, *Course of Theoretical Physics*, Vol. 3: *Quantum Mechanics: Non-Relativistic Theory* (Nauka, Moscow, 1989, 4th ed.; Pergamon, New York, 1977, 3rd ed.).
10. Y. Hanein, U. Meirav, D. Shahar, *et al.*, Phys. Rev. Lett. **80**, 1288 (1998).
11. S. J. Papadakis and M. Shayegan, Phys. Rev. B **57**, R15068 (1998).

Translated by E. Golyamina

JETP Letters, Vol. 72, No. 10, 2000, pp. 511–515. Translated from Pis'ma v Zhurnal Éksperimental'noĭ i Teoreticheskoĭ Fiziki, Vol. 72, No. 10, 2000, pp. 734–739.

Coexistence of the Superconducting Condensate and the Quasi-stationary States of Hole Pairs

V. I. Belyavskiĭ* and Yu. V. Kopaev**

** State Pedagogical University, Voronezh, 394043 Russia*

*** Lebedev Institute of Physics, Russian Academy of Sciences, Leninskiĭ pr. 53, Moscow, 117924 Russia*

e-mail: kopaev@sci.lebedev.ru

Received October 6, 2000

The formation of bound states in the case of a direct Coulomb repulsion between two holes whose reciprocal effective mass tensor has principal values of opposite signs is considered as a possible mechanism of high-T_C superconductivity. The study of the specific features of the scattering amplitude shows that, under certain conditions, in addition to the quasi-stationary states, states with a negative attenuation are possible, which corresponds to the tendency toward the formation of a hole pair condensate. The coexistence of the quasi-stationary states and the condensate qualitatively agrees with the phase diagram of *p*-type doped high-T_C superconducting cuprates. © *2000 MAIK "Nauka/Interperiodica".*

PACS numbers: 74.20.-z

The specific features of the electronic structure of *p*-type doped high-T_C superconducting compounds, such as the quasi-two-dimensional character of electronic states, the Fermi contour with nesting features, and the presence of a saddle point of the electronic dispersion law near the Fermi level [1], provide the possibility for the formation of bound states of quasiparticle (electron or hole) pairs with a quasi-momentum $\mathbf{K} \neq 0$ [2]. The Fermi contour (or its considerable part) belongs to the *k*-space region with a hyperbolic metric: in the vicinity of the saddle point, the principal values of the 2D tensor of the reciprocal effective masses have opposite signs. As a result, the character of the electron interaction, which contributes to the correlation energy, is changed: the actual repulsion of like charges can give way to an effective attraction [3, 4]. The filling of the states inside the Fermi contour leads to the following situation: for each quasi-momentum of a pair, there exists a certain 2D Brillouin zone region to which the quasi-momenta $\mathbf{k}_\pm = \mathbf{K}/2 \pm \mathbf{k}$ of the two quasiparticles forming the pair belong (here, $\mathbf{k}$ is the quasi-momentum of the relative motion). This accounts for the weakening of the correlations in the electron subsystem of a metal. Therefore, the interaction energy for two quasiparticles can be approximately represented as $\Xi_\mathbf{K} a^2 \cdot \tilde{U}(\mathbf{k})$ [2], where $\Xi_\mathbf{K}$ is the area of the region of the quasi-momenta $\mathbf{k}_\pm$, a is the interatomic distance, and $\tilde{U}(\mathbf{k}) = 4\pi e^2(k^2 + k_0^2)^{-1}$ is the Fourier transform of the energy of the screened Coulomb interaction with the screening parameter $k_0^2 = 4\pi e^2 g_F$; here, g_F is the density of states at the Fermi level. Figure 1a shows the Fermi contour typical of *p*-doped high-T_C superconducting compounds. The contour exhibits a nesting feature in the [100] direction; the Fermi momentum along this direction is denoted by k_F. The region $\Xi_\mathbf{K}$ for the vector $K < 2k_F$, which is also directed along [100], is shown in Fig. 1a by hatching. One can see that the region $\Xi_\mathbf{K}$ consists of two parts: the inner part ($\Xi_\mathbf{K}^{(e)}$) corresponding to the electron pairs and the outer part ($\Xi_\mathbf{K}^{(h)}$) corresponding to the hole pairs, as shown in Fig. 1b (if $K > 2k_F$, the whole region $\Xi_\mathbf{K}$ corresponds to the hole-type excitations). Because of the specific features of the electronic spectrum of high-T_C cuprates in the vicinity of the saddle point (the flat-band extended saddle point [1]), the region with a hyperbolic metric occupies a considerable part of the 2D Brillouin zone. An increase in the *p*-type doping level causes the Fermi level to approach the saddle points, whereas, in the case of *n*-type doping (the hole concentration is below the half-filling), an increase in the electron concentration causes the Fermi contour to move away from the saddle points. This fact (and the related asymmetry in the determination of $\Xi_\mathbf{K}^{(e)}$ and $\Xi_\mathbf{K}^{(h)}$) can be one of the factors responsible for the electron–hole asymmetry observed in high-T_C cuprates [1].

To perform a qualitative study of the correlation effects which may give rise to the formation of the bound states of quasiparticle pairs, we can use the effective-mass approximation by representing the

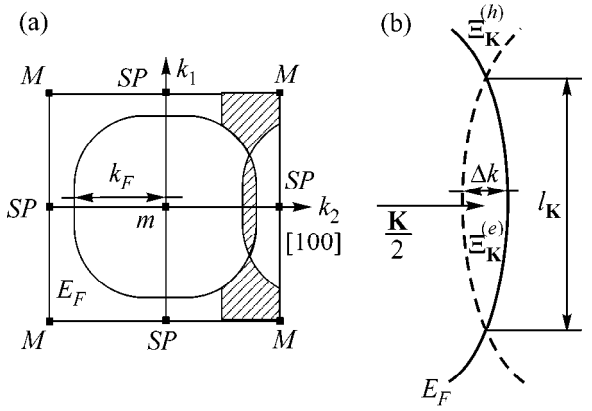

Fig. 1. Fermi contour (E_F) typical of *p*-type doped high-T_C cuprates. The 2D Brillouin zone is centered at the point (π, π) corresponding to the minimum (*m*) of the hole band; the maximum of the hole band is denoted by *M*, and the saddle points are denoted by *SP*. The region $\Xi_{\mathbf{K}}$ corresponding to the vector $K < 2k_F$ along the [100] nesting direction is shown (a) by hatching and (b) separately with its components $\Xi_{\mathbf{K}}^{(e)}$ and $\Xi_{\mathbf{K}}^{(h)}$ corresponding to the electron-type and hole-type excitations.

equivalent Hamiltonian of the relative pair motion in the form [2]

$$\hat{H}_{\mathbf{K}} = \frac{\hbar^2}{2m}(\nu k_1^2 - k_2^2) + \Xi_{\mathbf{K}} a^2 \cdot \tilde{U}(\mathbf{k}_1, \mathbf{k}_2). \qquad (1)$$

Here, the pair energy is measured relative to the value $2\varepsilon(\mathbf{K}/2)$; *m* is the dimensional parameter of mass; and the dimensionless coefficient $\nu \ll 1$, which characterizes the degree of anisotropy of the dispersion law near the point $\mathbf{K}/2$ and, on average, takes into account the deviations of the constant-energy lines from the ideal nesting direction within the region $\Xi_{\mathbf{K}}$, can be estimated as $\nu \approx (\Delta k/l_{\mathbf{K}})^2$, where $l_{\mathbf{K}}$ and Δk are the length and the width of the region $\Xi_{\mathbf{K}}^{(e)}$, respectively, (Fig. 1). Thus, the effective hole mass along the direction of the vector $\mathbf{K}$ (the k_2 axis) is negative, whereas, in the direction perpendicular to $\mathbf{K}$ (the k_1 axis), it is positive and large due to nesting.

All eigenfunctions of Hamiltonian (1) belong to a continuum spectrum. Therefore, it would be natural to seek them in the form of the sum of the incident wave with quasi-momentum $\mathbf{q}$ and the scattered wave $\tilde{\chi}_{\mathbf{Kq}}(\mathbf{k})$ representing the solution to the integral equation [5]

$$\frac{\hbar^2}{2m}(\omega - k^2)\tilde{\chi}_{\mathbf{Kq}}(\mathbf{k}) = \Xi_{\mathbf{K}} a^2 \cdot \tilde{U}(\mathbf{k} - \mathbf{q}) + \int_{(\Xi_{\mathbf{K}})} \Xi_{\mathbf{K}} a^2 \cdot \tilde{U}(\mathbf{k} - \mathbf{k}')\tilde{\chi}_{\mathbf{Kq}}(\mathbf{k}')\frac{d^2k'}{(2\pi)^2}. \qquad (2)$$

Here, $\omega = q^2$ and $k^2 = \nu k_1^2 - k_2^2$. The zero-current state is described by a linear combination of such wave functions with the crystallographically equivalent vectors $\mathbf{K}$ which transform according to one of the irreducible representations of the crystal symmetry group [2]. Note that Eq. (2) coincides with the equation for the *t*-matrix considered in [6] in connection with the problem of instability of the normal state with respect to the formation of bound states of electron pairs. Since the integration in Eq. (2) goes over the region $\Xi_{\mathbf{K}}$, which is small compared to the Brillouin zone, the integral term can be estimated by setting $\tilde{U}(\mathbf{k} - \mathbf{k}') \approx \tilde{U}(0)$. In this case, the solution to Eq. (2) takes the form [2]

$$\tilde{\chi}_{\mathbf{Kq}}(\mathbf{k}) = \frac{-w_{\mathbf{K}}}{1 + w_{\mathbf{K}} B_{\mathbf{K}}(\omega)} \frac{1}{k^2 - \omega - i0 \cdot \operatorname{sgn}\omega}, \qquad (3)$$

where $w_{\mathbf{K}} = (4\pi/k_0 a^*)\Xi_{\mathbf{K}} a^2$, $a^* = \hbar^2/me^2$, and the signum function provides the condition that is necessary for solution (3) to represent a diverging wave. The function $B_{\mathbf{K}}(\omega)$ is determined by the expression

$$B_{\mathbf{K}}(\omega) = \int_{(\Xi_{\mathbf{K}})} \frac{1}{k^2 - \omega - i0 \cdot \operatorname{sgn}\omega} \frac{d^2k}{(2\pi)^2} \equiv B_{\mathbf{K}1}(\omega) + iB_{\mathbf{K}2}(\omega). \qquad (4)$$

For real values of ω, the functions $B_{\mathbf{K}1}(\omega)$ and $B_{\mathbf{K}2}(\omega)$ have the form

$$B_{\mathbf{K}1}(\omega) = p.v. \int_{(\Xi_{\mathbf{K}})} \frac{1}{k^2 - \omega} \frac{d^2k}{(2\pi)^2},$$
$$B_{\mathbf{K}2}(\omega) = \pi \int_{(\Xi_{\mathbf{K}})} \delta(k^2 - \omega) \frac{d^2k}{(2\pi)^2}. \qquad (5)$$

If we assume that $\omega = \omega_{\mathbf{K}}^{(0)} - i\Gamma_{\mathbf{K}}$ is the solution to the equation $1 + w_{\mathbf{K}} B_{\mathbf{K}}(\omega) = 0$ and that $\Gamma_{\mathbf{K}} \ll \omega_{\mathbf{K}}^{(0)}$, then, for $\Gamma_{\mathbf{K}} > 0$, the quantity $\omega_{\mathbf{K}}^{(0)}$ can be considered [7] as the energy of a quasi-stationary state (QSS) that is determined as the solution to the equation

$$1 + w_{\mathbf{K}} B_{\mathbf{K}1}(\omega) = 0. \qquad (6)$$

The attenuation of the QSS has the form $\Gamma_{\mathbf{K}} = w_{\mathbf{K}} B_{\mathbf{K}2}(\omega_{\mathbf{K}}^{(0)})/B'_{\mathbf{K}1}(\omega_{\mathbf{K}}^{(0)})$, where $B'_{\mathbf{K}1} \equiv dB_{\mathbf{K}1}/d\omega$.

Assuming that the region $\Xi_{\mathbf{K}}$ has approximately the form of a rectangular strip with length $l_{\mathbf{K}}$ along the k_1

axis and width Δk along the k_2 axis, for $B_{\mathbf{K}2}(\omega)$ we obtain the expression

$$B_{\mathbf{K}2}(\omega) = \frac{1}{2\pi\sqrt{\nu}}\ln\left|\frac{\sqrt{\omega^*}+\sqrt{\omega^*+\omega}}{\sqrt{\omega_*}+\sqrt{\omega_*+\omega}}\right|, \quad -\omega_{-1} \le \omega \le \omega_1, \tag{7}$$

where $\omega_* = \max\{-\omega; 0\}$, $\omega^* = \min\{\omega_1 - \omega; \omega_{-1}\}$, $\omega_{-1} = (\Delta k/2)^2$, and $\omega_1 = \nu l_{\mathbf{K}}^2/4$; with allowance made for the relation $\nu \approx (\Delta k/l_{\mathbf{K}})^2$, we have $\omega_{-1} = \omega_1$. For $\omega \le -\omega_{-1}$ and $\omega \ge \omega_1$, we have $B_{\mathbf{K}2}(\omega) = 0$. The plot of function (7) is shown in Fig. 2.

The function $B_{\mathbf{K}1}(\omega)$ in the same approximation is determined by the integral

$$B_{\mathbf{K}1}(\omega) = \frac{-\mathrm{sgn}\,\omega}{2\pi\sqrt{\nu}}\int_0^{\omega_1^{1/2}} \ln\left|\frac{\omega_1^{1/2}+(k+\omega\,\mathrm{sgn}\,\omega)^{1/2}}{\omega_1^{1/2}-(k^2+\omega\,\mathrm{sgn}\,\omega)^{1/2}}\right| \times \frac{dk}{(k^2+\omega\,\mathrm{sgn}\,\omega)^{1/2}}, \tag{8}$$

for which the expression through the tabulated special functions is unknown. The plot of function (8) is schematically represented in Fig. 2. At the points $\omega = \pm\omega_1$, the function $B_{\mathbf{K}1}(\omega)$ has logarithmic singularities, and at $\omega = 0$ it has a first-order discontinuity. For $\nu \ll 1$, we have $B_{\mathbf{K}1}(+0) \approx -1/4\sqrt{\nu}$ and $B_{\mathbf{K}1}(-0) \approx 1/\pi^2\sqrt{\nu}$. When $|\omega| \longrightarrow \infty$, the asymptotic behavior of function (8) has the form $B_{\mathbf{K}1}(\omega) \sim -\Xi_{\mathbf{K}}/4\pi^2\omega$. Since $B_{\mathbf{K}1}(\omega) = 0$ at $\Delta k = 0$, the quasi-momentum of a pair, $\mathbf{K}$, cannot be equal to $2k_F$.

It should be noted that, in a Cooper pairing channel ($K = 0$), the energy of the relative motion of a pair is totally insensitive to the signs of the effective masses for small Δk: the approximation linear in $k - k_F$ proves to be sufficient, so that the pair energy is determined by the quasiparticle velocity ν_F at the Fermi contour rather than by the effective masses. For a Cooper channel, the function $B_{\mathbf{K}1}(\omega)$ has the form

$$B_{\mathbf{K}1}(\omega) = \frac{1}{8\pi}\ln\left|\frac{\omega_c-\omega}{\omega_c+\omega}\right|, \tag{9}$$

where $\omega_c = 2k_F\Delta k$; the role of the region Ξ_0 is in this case played by the zone of width Δk adjacent to the whole closed Fermi contour, independently of its shape (for simplicity, in Eq. (9), the Fermi contour is assumed to be circular). In the BCS theory [8], the quantity ω_c plays the role of the cutoff parameter, because the width Δk of the zone within which the states with opposite quasi-momenta are characterized by effective attraction is determined from the condition that the energy difference $\varepsilon(k_F + \Delta k) - \varepsilon(k_F)$ is of the same order as the characteristic phonon energy. When the quasi-momentum of a pair is nonzero, the Cooper channel is suppressed

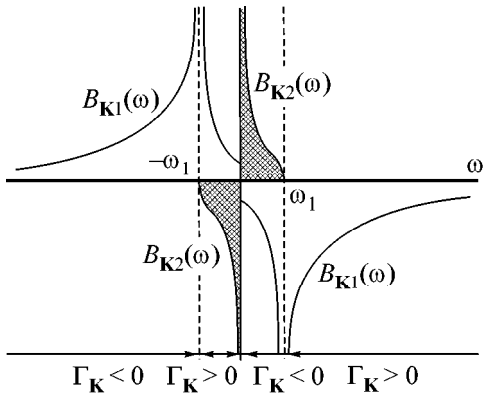

Fig. 2. Plots of the functions $B_{\mathbf{K}1}(\omega)$ and $B_{\mathbf{K}2}(\omega)$ (shaded).

because of the sharp decrease in the area of the corresponding region $\Xi_{\mathbf{K}}$; the Cooper effect proves to be impossible when $\hbar K \ge \Delta_0/\nu_F$, where Δ_0 is the superconducting energy gap at $\mathbf{K} = 0$ [9]. The exchange field existing in a weak ferromagnet pushes apart the Fermi surfaces corresponding to electrons with opposite spins, which provides the possibility for pairing when $\mathbf{K} \neq 0$ [10, 11]. Such a pairing is energetically advantageous when the Fermi surfaces are pushed apart by a distance of the order of the superconducting energy gap in the corresponding nonferromagnetic superconductor; the quasi-momentum of the pairs formed in this case is about $\Delta_0/\nu_F \ll \hbar k_F$.

In the case of pairing at $K \approx 2k_F$, the attenuation $\Gamma_{\mathbf{K}}$ is positive for $-\omega_{-1} \le \omega < 0$ and for $\omega \ge \omega_1$. Hence, if the solution to Eq. (6) falls within one of these energy intervals (the first interval, when the dominant type of hole–hole interaction is attraction, $w_{\mathbf{K}} < 0$, and the second interval in the case of repulsion, $w_{\mathbf{K}} > 0$), it will correspond to the QSS. When $\omega \ge \omega_1$, the QSS is characterized by a sufficiently long lifetime and, hence, can be considered as a special kind of elementary excitation of the electron subsystem of the crystal. For the energies $\omega < -\omega_{-1}$ and $0 < \omega < \omega_1$, the attenuation is $\Gamma_{\mathbf{K}} < 0$, which may testify to the instability of the electron subsystem with respect to the formation of the pair condensate; in this case, the position of the pole of the scattering amplitude is directly related to the energy-gap parameter [9]. Generally speaking, Eq. (6) has two solutions for both $w_{\mathbf{K}} < 0$ and $w_{\mathbf{K}} > 0$, as one can see from Fig. 2. In the first case, as in the case of the Cooper pairing, an unstable solution ($\Gamma_{\mathbf{K}} < 0$) occurs at any interaction intensity, and this solution corresponds to a greater (in magnitude) energy value. The solution in the form of the QSS appears only when the interaction is relatively weak, $|w_{\mathbf{K}}^{-1}| > B_{\mathbf{K}1}(-0)$; this solution is characterized by a fairly high attenuation. Therefore, in the case of attraction between the quasiparticles, the con-

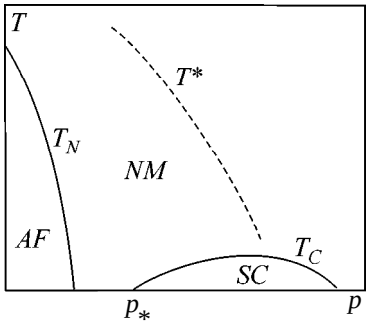

Fig. 3. Typical phase diagram of *p*-type doped high-T_C cuprates (schematic representation): *AF* is the region of antiferromagnetic ordering (T_N is the Néel temperature); *SC* corresponds to the superconducting phase (T_C is the superconducting transition temperature); *NM* is the normal metal phase (T^* is the temperature corresponding to the appearance of the pseudogap); and *p* is the hole concentration (the doping level).

densation of pairs should occur without the stage of QSS formation. By contrast, in the case of repulsion, a stable solution in the form of the QSS with a low attenuation [2] is obtained at any $w_{\mathbf{K}} > 0$, and the unstable solution appears only beginning at a certain value of the interaction intensity (in the course of its decrease, when $w_{\mathbf{K}}^{-1} > |B_{\mathbf{K}1}(+0)|$). The corresponding energy proves to be lower than the energy of the long-lived QSS, allowing the coexistence of the condensate and the QSS of the quasiparticle pairs. It should be noted that the energy interval $(-\omega_{-1}, \omega_1)$ belongs to the continuum spectrum; therefore, the solution with $\Gamma_{\mathbf{K}} < 0$ corresponding to the interval $0 < \omega < \omega_1$ must lead to a rearrangement of the continuum spectrum and, hence, to a decrease in the energy of the electron system as a result of the decrease in the kinetic energy [12] rather than due to the sign of the interaction energy, as in the BCS theory.

The possibility of the coexistence of the QSS and the condensate of quasiparticle pairs qualitatively agrees with the known phase diagram of high-T_C cuprates (Fig. 3), with the condition that both the condensate and the QSS are determined by the same repulsive interaction. In fact, $w_{\mathbf{K}}^{-1}(p)$ is an increasing function of hole concentration, because $w_{\mathbf{K}}^{-1} \sim k_0 \sim g_F^{1/2}$, and the 2D density of states has a logarithmic singularity in the vicinity of the saddle point. Therefore, we have $g_F \sim \ln(\omega_0/|\omega_{SP} - \omega_F|)$, where ω_F is the Fermi energy, ω_{SP} is the hole energy at the saddle point, and ω_0 is the cutoff parameter. As the doping level increases, the difference $\omega_{SP} - \omega_F$ decreases, leading to an increase in $w_{\mathbf{K}}^{-1}$ with increasing concentration.

Let us assume that, up to some concentration p_* determined from the condition $1 + w_{\mathbf{K}}(p_*) \times B_{\mathbf{K}1}(+0) = 0$, we only have the solution in the form of the QSS. The appearance of each QSS eliminates a pair of holes from the play and, hence, leads to a decrease in the density of states, which can be interpreted as the appearance of a pseudogap in the spectrum of single-particle excitations [2]. The energy of the QSS can be considered as the characteristic scale of the pseudogap width. When $p > p_*$ and $T = 0$, coexistence of the QSS and the hole pair condensate takes place (Fig. 3). From Fig. 2, one can see that, as the hole concentration increases, the stable and unstable solutions of Eq. (5) approach each other and, finally, become logarithmically close. In fact, this means the coincidence of the characteristic scales that determine the superconducting gap and the pseudogap. Thus, in the underdoped regime, coexistence of the condensate and the QSS of quasiparticle pairs takes place, whereas, with the transition to the superconducting state in the overdoped regime, the formation of a pair will be accompanied by its immediate precipitation into the condensate.

Experimental data [13–15] testify that, in underdoped high-T_C cuprates, the superconducting gap and the pseudogap are undoubtedly related to each other; they have the same symmetry and the same energy scale, and they exhibit a universal dependence on the doping level for different cuprates. These features of *p*-type doped high-T_C cuprates are interpreted [13] in the sense that the energy scale of the superconducting gap and the pseudogap represents the fundamental scale of the pairing interaction. Such an interaction can be a direct Coulomb repulsion between holes with a hyperbolic dispersion law [2].

One of the authors (Yu.V. Kopaev) acknowledges the support of the Federal Program “Integratsiya” (project nos. A0133 and A0155).

REFERENCES

1. Z.-X. Shen, W. E. Spicer, D. M. King, *et al.*, Science **267**, 343 (1995).
2. V. I. Belyavskiĭ, V. V. Kapaev, and Yu. V. Kopaev, Zh. Éksp. Teor. Fiz. **118**, 941 (2000) [JETP **91**, 817 (2000)].
3. E. F. Gross, V. I. Perel’, and R. I. Shekhmamet’ev, Pis’ma Zh. Éksp. Teor. Fiz. **13**, 320 (1971) [JETP Lett. **13**, 229 (1971)].
4. V. I. Belyavskiĭ, Yu. V. Kopaev, S. V. Shevtsov, and A. N. Zavarzin, Zh. Éksp. Teor. Fiz. **109**, 2179 (1996) [JETP **82**, 1175 (1996)].
5. J. R. Schrieffer, *Theory of Superconductivity* (Benjamin, New York, 1964; Nauka, Moscow, 1970).
6. A. I. Baz’, Ya. B. Zel’dovich, and A. M. Perelomov, *Scattering, Reactions, and Decays in Nonrelativistic Quan-*

tum Mechanics (Nauka, Moscow, 1971, 2nd ed.; Israel Program for Scientific Translations, Jerusalem, 1966).

7. L. D. Landau and E. M. Lifshitz, *Course of Theoretical Physics*, Vol. 3: *Quantum Mechanics: Non-Relativistic Theory* (Nauka, Moscow, 1989, 4th ed.; Pergamon, New York, 1977, 3rd ed.).
8. J. Bardeen, L. Cooper, and J. Schrieffer, Phys. Rev. **108**, 1175 (1957).
9. A. A. Abrikosov, L. P. Gor'kov, and I. E. Dzyaloshinskii, *Methods of Quantum Field Theory in Statistical Physics* (Fizmatgiz, Moscow, 1962; Prentice-Hall, Englewood Cliffs, 1963).
10. A. I. Larkin and Yu. N. Ovchinnikov, Zh. Éksp. Teor. Fiz. **47**, 1136 (1964) [Sov. Phys. JETP **20**, 762 (1964)].
11. P. Fulde and R. A. Ferrell, Phys. Rev. A **135**, 550 (1964).
12. M. R. Norman, M. Randeria, B. Janko, and J. C. Campuzano, Phys. Rev. B **61**, 14742 (2000).
13. G. V. M. Williams, J. L. Tallon, E. M. Haines, *et al.*, Phys. Rev. Lett. **78**, 721 (1997).
14. M. R. Norman, H. Ding, M. Randeria, *et al.*, Nature **392**, 157 (1998).
15. M. Opel, R. Nemetschek, C. Hoffmann, *et al.*, Phys. Rev. B **61**, 9752 (2000).

Translated by E. Golyamina

JETP Letters, Vol. 72, No. 10, 2000, pp. 516–520. Translated from Pis'ma v Zhurnal Éksperimental'noĭ i Teoreticheskoĭ Fiziki, Vol. 72, No. 10, 2000, pp. 740–745.

Direct Experimental Verification of the Isomorphism Hypothesis for Critical Phenomena

V. P. Voronov and E. E. Gorodetskiĭ

Institute of Oil and Gas Problems, Russian Academy of Sciences, Leninskiĭ pr. 65, Moscow, 117971 Russia

Received October 19, 2000

The heat capacity at constant volume of a mixture of methane and 0.0345 mole fractions of heptane is experimentally studied over a wide range of densities and temperatures. In the case when the transition from a three-phase state takes place in the presence of a noncritical liquid phase, it is found that the behavior of the heat capacity in the vicinity of the upper end critical point is fully isomorphic with the behavior of the heat capacity in the vicinity of the liquid–vapor critical point of one-component fluid. It is shown that the measured quantity in this experiment is the heat capacity at constant volume and constant chemical potential μ of the heavy impurity component $C_{v,\mu}$. Thus, it has been confirmed by direct measurements that the anomaly of this heat capacity completely coincides in character with the anomaly of the heat capacity at constant volume in the vicinity of the liquid–vapor critical point of one-component fluids. © *2000 MAIK "Nauka/Interperiodica".*

PACS numbers: 05.70.Jk; 65.20.+w

In accordance with the universality concept and the isomorphism hypothesis for critical phenomena, the singular part of the thermodynamic potential of solutions in the vicinity of their critical points written in terms of field variables (temperature and chemical potentials of solution components) coincides with the singular part of the thermodynamic potential of one-component fluids in the vicinity of the liquid–vapor critical point. In this case, the dependence of the singular part of the thermodynamic potential of a solution on the reduced chemical potential μ, equal to the difference of the chemical potentials of the components in the solution, is solely due to the dependence of the critical parameters on this variable. In particular, from here it follows that, in binary systems, the anomaly of the heat capacity at constant volume and constant chemical potential $C_{v,\mu}$ in the vicinity of the liquid–vapor critical point of the solution coincides in character with the anomaly of the heat capacity C_v in the vicinity of the liquid–vapor critical point of one-component fluids: $C_{v,\mu} \sim t(\mu)^{-\alpha}$. Here, $t(\mu) \equiv |(T - T_c(\mu))/T_c(\mu)|$, and the critical component α coincides with the component of the heat capacity at constant volume C_v of pure substances.

In the subsequent discussion, we will consider measurements of the heat capacity at fixed volume of the calorimetric cell and fixed average concentration of the solution. However, the nature of the heat capacity that is measured in this case depends on the phase diagram of the solution. In the case when a three-phase equilibrium in the system under study is absent, the constancy of the volume and the average concentration of the mixture means that the experimentally measured quantity is the heat capacity at constant volume $C_{v,x}$. It was shown in [1, 2] that the critical component of the heat capacity α in this path is renormalized: $\alpha \longrightarrow -\alpha/(1 - \alpha)$. Therefore, as the critical point is approached, a finite peak rather than infinite growth is observed experimentally in the heat capacity [3]. However, the renormalization of the critical component α is rather difficult to verify experimentally because of the complex crossover behavior of the heat capacity in the vicinity of the critical point of the solution. At the same time, the isomorphic heat capacity $C_{v,\mu}$ cannot be measured in such systems, since this would require the concentration of the sample to be varied during the experiment continuously and in a certain way.

In the case when a liquid–liquid–vapor three-phase equilibrium occurs in the system, the character of the measured heat capacity depends on which two of the three coexisting phases are in fact critical. If the liquids are the critical phases, that is, when the case in point is the critical demixing point (a large number of works are devoted to studying such systems [4]), the constancy of the volume and the average concentration of the solution nevertheless means that the heat capacity $C_{p,x}$ rather than $C_{v,x}$ is measured. This is due to the fact that, first, the variation of the saturation vapor pressure over the critical liquid phases within the temperature range under study is insignificant and, second, the amount of substance in the vapor phase is small and cannot

0021-3640/00/7210-0516$20.00 © 2000 MAIK "Nauka/Interperiodica"

change the concentration of the liquid phases to an appreciable degree.

A similar situation could take place when the critical phases are the vapor and one of the coexisting liquid phases. Actually, in this case, the chemical potential of the heavy component in the vicinity of the liquid–vapor critical point is determined by the noncritical liquid phase and varies insignificantly within the temperature range in which the critical phenomena are studied. That is, the heat capacity will be measured in the path for which μ = const. The volume of the calorimetric cell is constant; therefore, the volume of the critical phases will remain constant as well, because the variation of the volume of the noncritical liquid phase is insignificant. Hence, the measured heat capacity must be the isomorphic heat capacity $C_{v,\mu}$. That is, if the universality principle for critical phenomena and the isomorphism hypothesis are true, an anomaly should be observed experimentally that is fully analogous to the anomaly of the heat capacity at constant volume in the vicinity of the liquid–vapor critical point of one-component fluids.

In order to verify this statement, we selected a methane–heptane (C_1 + C_7) binary mixture. It is known [5] that there is a temperature region where three phases (liquid + liquid + vapor) coexist in this mixture. The heat capacity was measured at constant volume and constant average concentration of the mixture. It was found that the transition of the system from a three-phase state to a two-phase one is accompanied by infinite power growth of the heat capacity with an exponent that coincides with the critical component of the heat capacity at constant volume α for a one-component fluid. At the same time, the transition to a one-phase state is not accompanied by any appreciable growth of the heat capacity in the dew-bubble curve.

EXPERIMENTAL

The enthalpy and the heat capacity at constant volume were measured on an adiabatic scanning calorimeter with a cell volume of 14.6 cm^3. The cell was connected by a thin capillary with a strain sensor, which served to measure the pressure, and with a system for filling the cell with a mixture under investigation. The calorimeter design did not significantly differ from the microcalorimeter design described in [6]. In order to maintain the adiabatic measurement conditions, the cell was surrounded by two copper isothermal screens whose temperature strictly followed the cell temperature. In order to avoid heat supply through the capillary, the capillary was connected by a heating conduit with a copper isothermal ring whose temperature was kept equal to the cell temperature. The upper part of the capillary was kept ≈1 K higher to exclude the condensation of the mixture inside it. The temperature was measured by a platinum thermometer with a nominal resistance of 100 Ω placed inside the cell. The sample was stirred with a magnetic stirrer activated by a solenoid with a period of 10 s.

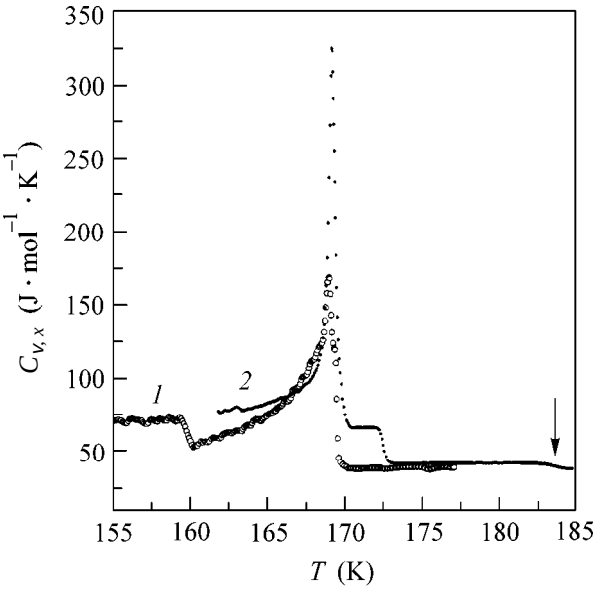

Fig. 1. Temperature dependence of the specific heat capacity at constant volume of a (C_1 + 0.0345 mole fractions of C_7) mixture for two densities: (*1*) ρ = 0.391 g/cm^3 and (*2*) ρ = 0.367 g/cm^3. The heat capacity peak at $T \approx 169$ K corresponds to the melting of the phase enriched with heptane. The jumps at $T \approx 159$ and $T \approx 172.5$ K correspond to the liquid–vapor transition between the phases enriched with methane in the presence of the phase enriched with heptane.

The measurement of the enthalpy (the amount of heat supplied to the cell) was described in detail in [7] and was performed and controlled by a computer system. Simultaneously with the enthalpy, the temperature and the pressure in the cell were measured. The heat capacity was calculated by numerically differentiating the enthalpy with respect to temperature. The measurements were performed for 20 isochores over the density range from 0.39 to 0.05 g/cm^3.

RESULTS AND DISCUSSION

The temperature dependence of the specific heat capacity at constant volume $C_{v,x}$ of a (C_1 + 0.0345 mole fractions of C_7) binary mixture is presented in Fig. 1 for two high densities ρ = 0.391 g/cm^3 (curve *1*) and ρ = 0.367 g/cm^3 (curve *2*). Two singularities are pronounced in both curves: a jump and a sharp peak. Each of these singularities in the heat capacity behavior corresponds to a phase transition. At temperatures below the temperature of the heat capacity jump at $T \approx 159$ K in curve *1*, three phases are in equilibrium: the solid phase s_1, the liquid phase l_2, and the vapor phase g_2 (subscript 1 corresponds to the phase enriched with heptane, and subscript 2 relates to the phases enriched with methane). The heat capacity jump corresponds to the liquid–vapor

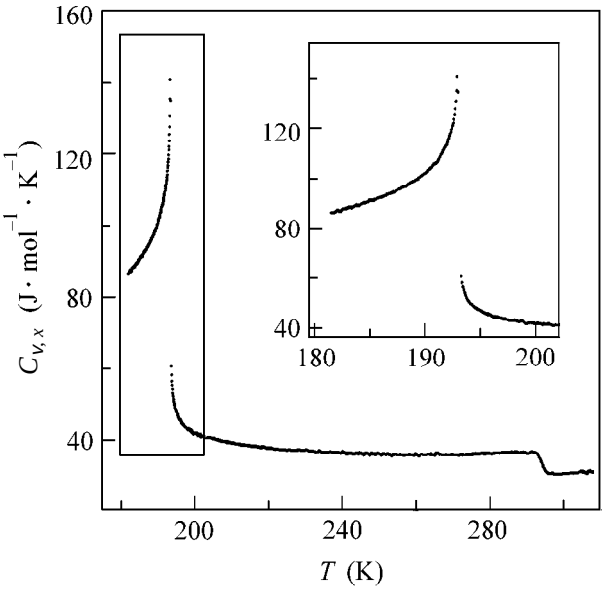

Fig. 2. Temperature dependence of the specific heat capacity at constant volume of a (C_1 + 0.0345 mole fractions of C_7) mixture in the isochore ρ* = 0.223 g/cm^3 passing through the end point of the three-phase equilibrium line. The heat capacity anomaly at T = 192.91 K corresponds to the upper end liquid–vapor critical point in the presence of the liquid phase enriched with heptane (inset shows the behavior of the heat capacity in the vicinity of the upper end critical point). The heat capacity jump at $T \approx 292$ K corresponds to the transition of the mixture to a one-phase state.

transition ($l_2 - g_2$) in the presence of the third solid phase (s_1) with the resulting formation of a two-phase solid–vapor ($s_1 + g_2$) equilibrium. The sharp peak of the heat capacity at $T \approx 169$ K corresponds to the melting of the solid phase (s_1) (melting point of pure heptane T_m = 182.54 K). Note that, when the solid phase melts, the mixture with this density transits directly from a two-phase equilibrium ($s_1 + g_2$) to a one-phase state.

For the density ρ = 0.367 g/cm^3 (curve *2*), the heat capacity peak corresponding to the melting of the solid phase is positioned at the same temperature as in curve *1*. This is quite natural, because the melting point of the solid phase depends only on the concentration. The liquid–vapor ($l_2 - g_2$) transition between the phases enriched with methane, which corresponds to the heat capacity jump at T = 172.5 K, takes place in this case only in the presence of the liquid phase l_1. At $T \approx 183$ K, the mixture transits to a one-phase state (this transition accompanied by a small jump of the heat capacity is designated by an arrow in Fig. 1). Thus, it may be argued that a three-phase liquid–liquid–vapor ($l_1 + l_2 + g_2$) equilibrium occurs at the density ρ = 0.367 g/cm^3 in the temperature range from the melting point ($T \approx$ 169 K) to the temperature of the heat capacity jump (T = 172.5 K).

As the average density of the mixture decreases, the heat capacity anomaly corresponding to the ($l_2 - g_2$) transition becomes larger and the three-phase equilibrium region extends, attaining its maximum value at the density ρ = ρ* = 0.223 g/cm^3. In the P–T coordinates, this isochore passes through the end point of the three-phase equilibrium line (P* = 4.855 ± 0.004 MPa, T* = 192.91 ± 0.02 K), which is the upper end critical point in the line of liquid–vapor critical points of the methane–heptane mixture. A specific feature of this experiment is that the liquid–vapor phase transition at the upper end critical point takes place in the presence of the noncritical liquid phase l_1.

The temperature dependence of the specific heat capacity at constant volume for the density ρ = ρ* = 0.223 g/cm^3 in the vicinity of the upper critical end point is shown in Fig. 2. It is evident that the λ-like behavior of the heat capacity is similar to the anomaly of the heat capacity at constant volume in the vicinity of the liquid–vapor critical point of a pure substance.

The temperature dependence of the $(\partial P/\partial T)_{V,x}$ derivative is presented in Fig. 3 for densities close to ρ*. For $\rho_1 > \rho^*$ and $\rho_2 < \rho^*$, the $(\partial P/\partial T)_{V,x}$ derivatives undergo jumps of opposite sign in going from the three-phase equilibrium to the two-phase ($l_1 + g_2$) one. At ρ = ρ*, a jump in the $(\partial P/\partial T)_{V,x}$ derivative is absent, as well as in the critical isochore of a one-component fluid.

As the mixture changes to the one-phase state, the heat capacity exhibits no anomaly in its behavior for any of the isochores studied (this transition corresponds to the jump at $T \approx 292$ K in Fig. 2). The jump of the heat capacity at constant volume grows smoothly with decreasing density.

In order to check that the anomaly of the heat capacity at constant volume in the vicinity of the upper critical end point found in this work actually behaves in the same way as at the liquid–vapor critical point of a pure substance, we compared experimental data for the enthalpy H with the enthalpy calculated by the equation

$$H_{cal} = \int_{t_0}^{t} C dt, \qquad (1)$$

where the limits of integration $t_0 = |T_0/T_c - 1|$ and t correspond to the temperature range of experimental data processing and the specific heat capacity at constant volume has the conventional scaling form

$$C = A^{\pm} t^{-\alpha} + B^{\pm} t^{\Delta - \alpha} + C^{\pm} + Dt + Et^2. \qquad (2)$$

The plus and minus superscripts in Eq. (2) designate the heat capacity branches for $T > T_c$ and $T < T_c$, respectively. The second term represents the nonasymptotic Wegner correction with the fixed value Δ = 0.5. The last three terms describe the regular part of the heat capac-

Coefficients for the specific heat capacity at constant volume ($\rho = \rho^* = 0.223$ g/cm^3) of a (C_1 + 0.0345 mole fractions of C_7) mixture in Eq. (2)

A^-	A^+	α	T_c	B^-	B^+	C^-	C^+	D	E
51.0	27.37	0.115	192.923	–8.86	(0)	22.87	(0)	54.3	–204
±0.5	±0.1	±0.002	±0.001	±2	–	±0.8	–	±0.9	±12

ity with equal coefficients for $T < T_c$ and $T > T_c$ in the linear and quadratic terms.

All the parameters in Eq. (2), the critical component α and the critical temperature T_c included, were determined by processing the experimental data using the least-squares method. In the case when all the parameters in Eq. (2) were adjustable, the coefficients B^+ and C^+ turned out to be insignificant and, therefore, were set equal to zero in the subsequent data treatment. The results of the simultaneous processing of enthalpy for $T < T_c$ and $T > T_c$ are given in the table. The values obtained for the critical component α and the universal ratio of the critical specific heat capacity amplitudes $A^-/A^+ = 1.86$ are in good agreement with the theoretical values for one-component fluids, which were confirmed by numerous experiments [4].

Thus, we may state that the behavior of the heat capacity at constant volume of the (C_1 + 0.0345 mole fractions of C_7) mixture measured in this work in the vicinity of the upper critical end point in the presence of the third liquid phase is isomorphic to the behavior of the heat capacity at constant volume in the vicinity of the liquid–vapor critical point of a pure substance. The noncritical liquid phase ensures the fulfillment of the condition μ = const, and, therefore, the heat capacity measured in this experiment in the vicinity of the upper end critical point is the heat capacity at constant volume and constant chemical potential $C_{v,\mu}$.

In conclusion, we will show that, if the noncritical liquid phase fixing the chemical potential of heptane in the phases enriched with methane were absent, the heat capacity at constant volume measured in the vicinity of the upper critical end point would be finite. As was already mentioned at the beginning of this work, the critical component of the heat capacity α in this path is renormalized: $\alpha \longrightarrow -\alpha/(1-\alpha)$. The temperature range τ in which the renormalization of the component α is observed is determined by the equation [1, 2]

$$\tau = X_A^{1/\alpha}, \quad X_A = A^- x(1-x)\left(\frac{1}{T_c}\frac{dT_c}{dx}\right)^2.$$

At $X_A \ll 1$, the renormalization region is very narrow, and the measured heat capacity must be close to the heat capacity at constant volume in the vicinity of the liquid–vapor critical point of a one-component fluid. However, it is easy to understand that the heat capacity anomaly observed in the methane–heptane mixture cannot be associated with this effect, because exactly the opposite condition $X_A > 1$ is fulfilled for this mixture. Though it is rather difficult to estimate the value of X_A for the methane–heptane mixture directly from our experiment, it is known [5] that this value ≈1.5 for a methane–hexane mixture and it can only increase in going to the methane–heptane system. Therefore, it would be impossible to observe the anomaly of the heat capacity at constant volume in the vicinity of the upper critical end point in the methane–heptane mixture if the noncritical liquid phase were absent. That is, fixing the chemical potential of the heavy component in the vicinity of the liquid–vapor critical point in the phases enriched with methane actually leads to singular behavior of the heat capacity similar to its behavior in one-component fluids.

Thus, we have carried out direct experimental verification of isomorphism between the heat capacity $C_{v,\mu}$ of a solution and the heat capacity at constant volume C_v of one-component fluids.

The authors are grateful to V. Kulikov and V. Podnek for useful discussions and critical comments. This work

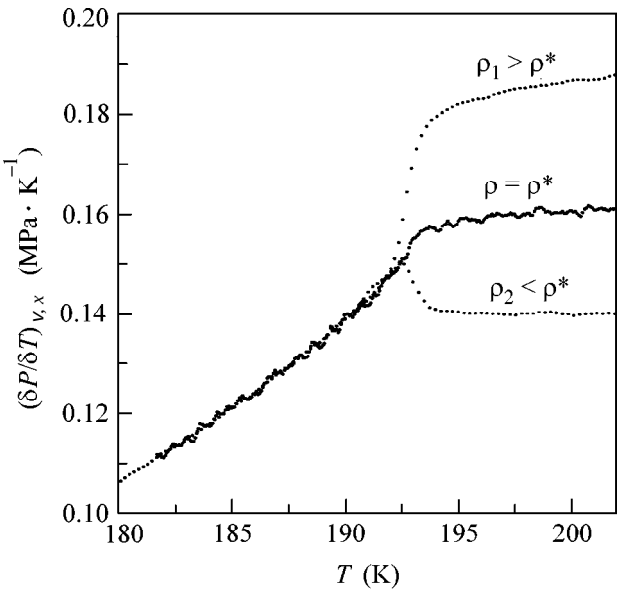

Fig. 3. Temperature dependence of the $(\partial P/\partial T)_{v,x}$ derivative of a (C_1 + 0.0345 mole fractions of C_7) mixture in the vicinity of the upper end liquid–vapor critical point for various densities: critical density $\rho^* = 0.223$ g/cm^3, $\rho_1 = 0.244$ g/cm^3, and $\rho_2 = 0.203$ g/cm^3.

was supported by the international oil and gas company Schlumberger Oilfield Services.

REFERENCES

1. M. Fisher, Phys. Rev. **176**, 257 (1968).
2. M. A. Anisimov, A. V. Voronel', and E. E. Gorodetskiĭ, Zh. Éksp. Teor. Fiz. **60**, 1117 (1971) [Sov. Phys. JETP **33**, 605 (1971)].
3. M. A. Anisimov, E. E. Gorodetskiĭ, and N. G. Shmakov, Zh. Éksp. Teor. Fiz. **63**, 2165 (1972) [Sov. Phys. JETP **36**, 1143 (1973)].
4. M. A. Anisimov, *Critical Phenomena in Liquids and Liquid Crystals* (Nauka, Moscow, 1987).
5. Y.-N. Lin, R. J. J. Chen, P. S. Chappelaer, and R. Kobayashi, J. Chem. Eng. Data **22**, 402 (1977).
6. L. V. Entov, V. A. Levchenko, and V. P. Voronov, Int. J. Thermophys. **14**, 221 (1993).
7. V. P. Voronov, Zh. Éksp. Teor. Fiz. **118**, 163 (2000) [JETP **91**, 144 (2000)].

Translated by A. Bagatur'yants

JETP Letters, Vol. 72, No. 10, 2000, pp. 521–526. From Pis'ma v Zhurnal Éksperimental'noĭ i Teoreticheskoĭ Fiziki, Vol. 72, No. 10, 2000, pp. 746–752.

Invariant Spin Coherent States and the Theory of the Quantum Antiferromagnet in a Paramagnetic Phase[1]

V. I. Belinicher*, and J. da Providencia****

** Institute of Semiconductor Physics Siberian Division, Russian Academy of Sciences, pr. Akademika Lavrent'eva 13, Novosibirsk, 630090 Russia*

e-mail: belin@isp.nsc.ru

*** University of Coimbra, 3000 Coimbra, Portugal*

Received September 29, 2000; in final form, October 23, 2000

A consistent theory of the Heisenberg quantum antiferromagnet in the disordered phase with short-range antiferromagnetic order was developed on the basis of the path integral for the spin coherent states. We presented the Lagrangian of the theory in the form that is explicitly invariant under rotations and found natural variables in terms of which one can construct a perturbation theory. The short-wavelength spin fluctuations are similar to the ones in spin-wave theory, and the long-wavelength spin fluctuations are governed by the nonlinear sigma model. We also demonstrated that the short-wavelength spin fluctuations should be considered accurately in the framework of the discrete version in time of the path integral. In the framework of our approach, we obtained the response function for the spin fluctuations for the whole region of the frequency ω and the wave vector $\mathbf{k}$ and calculated the free energy of the system. © *2000 MAIK "Nauka/Interperiodica".*

PACS numbers: 75.10.Jm; 75.50.Ee

The theory of the two-dimensional Heisenberg antiferromagnet (AF) has attracted great interest during the last several years in connection with the problem of AF fluctuations in copper oxides [1–3]. The approach of these papers was based on the sigma model, which describes the long-wavelength fluctuations of the Heisenberg AF in the paramagnetic phase with a short-range antiferromagnetic order. The sigma model is the continuum model for the unit vector $\mathbf{n}(t, \mathbf{r})$, $\mathbf{n}^2 = 1$ in the 1 + 2 time and space dimensions [4, 5]. As a long-wavelength theory, the sigma model can make a lot of physical predictions, such as the structure of the long-wavelength fluctuations and the magnitude of the correlation length [2, 3, 6]. But, up to now, a consistent theory of the spin fluctuations for the quantum AF (QAF) with short-range AF order was absent. This is just the topic of this paper.

Our approach to the description of the QAF is based on the functional integral for the generalized partition function in terms of spin coherent states. We introduce the concept of invariant spin coherent states and, on this basis, we formulate the theory.

We define the invariant spin coherent states (SCS) with the help of relation

$$|\mathbf{n}; \mathbf{m}\rangle = \exp(-i\varphi\hat{S}_z)\exp(-i\theta\hat{S}_y)\exp(-i\psi\hat{S}_z)|ss\rangle. \quad (1)$$

Here, the state $|ss\rangle$ is the state of spin s with the maximal spin projection s. The unit vectors $\mathbf{n}$ and $\mathbf{m}$ are orthogonal: $\mathbf{n}^2 = 1$, $\mathbf{m}^2 = 1$, $\mathbf{n} \cdot \mathbf{m} = 0$; θ, φ are the Euler angles of the unit vector $\mathbf{n} = (\cos\varphi\sin\theta, \sin\varphi\sin\theta, \cos\theta)$. The dependence on the vector $\mathbf{m}$ is included in the angle ψ only, which, in fact determines only the phase factor in the SCS (1). We can choose the angle ψ in some special manner, which distinguishes this definition from the standard one [7]: $\psi = -k_z/m_z$, where the vector $\mathbf{k} = [\mathbf{n} \times \mathbf{m}]$. This choice has a clear geometrical interpretation. The transformation (1) rotates the reference coherent state that is characterized by the vectors $\mathbf{n}_0 = (0, 0, 1)$ and $\mathbf{m}_0 = (1, 0, 0)$, into the SCS (1). From this geometric interpretation, it is obvious that, upon changing SCS by some rotation $\hat{a}$, we have $|\hat{a}\mathbf{n}; \hat{a}\mathbf{m}\rangle = \hat{U}(\hat{a})|\mathbf{n}; \mathbf{m}\rangle$ without the phase factor, which was introduced and discussed by Perelomov [8]. In this way, the scalar product $\langle\mathbf{n}'; \mathbf{m}'|\mathbf{n}; \mathbf{m}\rangle$ is an invariant, and the matrix element $\langle\mathbf{n}'; \mathbf{m}'|\hat{\mathbf{S}}|\mathbf{n}; \mathbf{m}\rangle$ is a vector under rotations. It seems that the vector $\mathbf{m}$ is an artificial one. However, for the problem of the QAF, it has some real meaning.

We consider the spin system which is described by the Heisenberg Hamiltonian with an interaction of nearest neighbors, $\hat{H}_{Hei}(l, l') = J\hat{\mathbf{S}}_l \cdot \hat{\mathbf{S}}_{l'}$, $\hat{\mathbf{S}}_l \cdot \hat{\mathbf{S}}_l = s(s + 1)$, where $\hat{\mathbf{S}}_l$ are the spin operators; the index l runs over a two-dimensional square lattice; the index l' runs over

[1] This article was submitted by the authors in English.

the nearest neighbors of the site l; $J > 0$ is the exchange constant which, since it is positive, corresponds to the AF spin interaction; and s is the spin magnitude. The most efficient method of dealing with a spin system is based on the representation of the generalized partition function Z or the generating functional of the spin Green functions $Z = Tr[\exp(-\beta\hat{H})]$ in the form of a functional integral over spin coherent states:

$$Z = \int_{-\infty}^{\infty} \dots \int_{-\infty}^{\infty} D\mu(\mathbf{n}_a, \mathbf{n}_b) \exp(A(\mathbf{n}_a, \mathbf{n}_b)), \tag{2}$$

$$D\mu(\mathbf{n}_a, \mathbf{n}_b) = \prod_{p=a,b;\,\tau,l} \frac{2s+1}{2\pi} \delta(\mathbf{n}_p^2(\tau, l) - 1) d\mathbf{n}_p(\tau, l), \tag{3}$$

where $T = 1/\beta$ is the temperature, τ is the imaginary time, and $A(\mathbf{n})$ is the action of the system. In the continuum approximation, which is valid in the leading order in $1/2s$, the expression of the action $A(\mathbf{n})$ is simplified:

$$A(\mathbf{n}_a, \mathbf{n}_b) = -\int_0^{\beta} \sum_l \mathcal{L}_{tot}(\tau, l) d\tau, \qquad \mathcal{L}_{tot}(\tau, l) = \mathcal{L}_{kin}(\tau, l) + \mathcal{H}(\tau, l), \tag{4}$$

$$\mathcal{H}(\tau, l) = Js^2 \sum_{l' = \langle l \rangle} \mathbf{n}_a(\tau, l) \cdot \mathbf{n}_b(\tau, l'), \qquad B_p(\tau, l) = \langle \mathbf{n}_p; \mathbf{m}_p | \frac{\partial}{\partial \tau} | \mathbf{n}_p; \mathbf{m}_p \rangle, \tag{5}$$

where $\mathcal{L}_{kin}(\tau, l) = B_a + B_b$ and $B_{a,b}$ are the Berry phases for the sublattice $p = a, b$. The idea of the short-range AF order was used in Eqs. (1)–(5), and we split our square lattice into two AF sublattices a and b. For the kinetic part of the action $\mathcal{L}_{kin}$ (which is highly nonlinear), we use the concept of invariant coherent states parametrized by arbitrary vectors $\mathbf{m}_{a,b}$.

In our case, we can define these vectors $\mathbf{m}_{a,b}$ in the following manner: $\mathbf{m}_{a,b} = (\mathbf{n}_{b,a} - x\mathbf{n}_{a,b})/(1 - x^2)^{1/2}$, $x = (\mathbf{n}_a \cdot \mathbf{n}_b)$. As a result, the invariant coherent states have a clear meaning. Substituting these expressions for $\mathbf{m}_{a,b}$ into Eq. (5), we have invariant forms for the Berry phases B_p, which depend on both vectors $\mathbf{n}_{a,b}$ for each sublattice a, b. For $\mathcal{L}_{kin}$, we have an invariant form under rotations:

$$\mathcal{L}_{kin} = \frac{is}{1 - \mathbf{n}_{a\tau l} \cdot \mathbf{n}_{b\tau l}} (\dot{\mathbf{n}}_{a\tau l} - \dot{\mathbf{n}}_{b\tau l}) \cdot [\mathbf{n}_{a\tau l} \times \mathbf{n}_{b\tau l}]. \tag{6}$$

Now we can introduce new, more convenient variables $\mathbf{\Omega}(\tau, l)$ and $\mathbf{M}(\tau, l)$, which realize the stereographic mapping of a sphere:

$$\mathbf{n}_{a,b} = \frac{\pm\mathbf{\Omega}(1 - \mathbf{M}^2/4) - [\mathbf{\Omega} \times \mathbf{M}]}{1 + \mathbf{M}^2/4}, \qquad \mathbf{\Omega}^2 = 1, \quad \mathbf{\Omega} \cdot \mathbf{M} = 0. \tag{7}$$

In terms of these variables, the total Lagrangian $\mathcal{L}_{\Omega M} = \mathcal{L}_{kin} + \mathcal{H}$ has the final form

$$\mathcal{L}_{kin} = \frac{2is\dot{\mathbf{\Omega}} \cdot \mathbf{M}}{1 + \mathbf{M}^2/4},$$

$$\mathcal{H} = Js^2 \times \sum_{l' = \langle l \rangle} \{\mathbf{\Omega} \cdot \mathbf{\Omega}'[(1 - \mathbf{M}^2/4)(1 - \mathbf{M}'^2/4) - \mathbf{M} \cdot \mathbf{M}'] + \mathbf{\Omega} \cdot \mathbf{M}'\mathbf{\Omega}' \cdot \mathbf{M}\}(1 + \mathbf{M}^2/4)^{-1}(1 + \mathbf{M}'^2/4)^{-1}, \tag{8}$$

where $\mathbf{\Omega} \equiv \mathbf{\Omega}_{\tau l}$, $\mathbf{\Omega}' \equiv \mathbf{\Omega}_{\tau l'}$, $\mathbf{M} \equiv \mathbf{M}_{\tau l}$, $\mathbf{M}' \equiv \mathbf{M}_{\tau l'}$. After this change of variables, the measure of integration $D\mu(\mathbf{n})$ (7) becomes

$$D\mu(\mathbf{n}) = \prod_{\tau l} \frac{(2s+1)^2(1 - \mathbf{M}^2/4)}{2\pi^2(1 + \mathbf{M}^2/4)^3} \times \delta(\mathbf{\Omega}^2 - 1)\delta(\mathbf{\Omega} \cdot \mathbf{M}) d\mathbf{\Omega} d\mathbf{M}, \tag{9}$$

where the product in Eq. (9) is performed over the AF (doubled) lattice cells.

The variable $\mathbf{\Omega}$ is responsible for the AF fluctuations, and the variable $\mathbf{M}$ for the ferromagnetic ones. The ferromagnetic fluctuations are small according to the parameter $1/2s$, and, therefore, one can expand the Lagrangian $\mathcal{L}_{\Omega M}$ (8) in $\mathbf{M}$. The vector of the ferromagnetic fluctuations $\mathbf{M}$ plays the role (to the factor $2s$) of the canonical momentum conjugate to the canonical coordinate $\mathbf{\Omega}$. The term of first order in $\mathbf{M}$ coincides (after a change of variables) with previous results [1, 3].

From Eq. (1) one can easily extract the quadratic part of the total Lagrangian in the variables $\mathbf{\Omega}$ and $\mathbf{M}$, $\mathcal{L}_{quad}$:

$$\mathcal{L}_{quad} = 2is(\mathbf{M} \cdot \dot{\mathbf{\Omega}}) + Js^2 \sum_{l' \in \langle l \rangle} [\mathbf{\Omega}^2 - \mathbf{\Omega} \cdot \mathbf{\Omega}' + \mathbf{M}^2 + \mathbf{M} \cdot \mathbf{M}']. \tag{10}$$

The Lagrangian $\mathcal{L}_{quad}$ (10) is very simple, but the measure $D\mu$ (9) is not simple due to the presence of two delta functions. Therefore, we cannot simply perform the Gaussian integration over the fields $\mathbf{\Omega}$ and $\mathbf{M}$. To solve this problem, we shall use the method of the Lagrange multiplier λ together with the saddle point approximation [4, 5] to eliminate $\delta(\mathbf{\Omega}^2 - 1)$. As a result, we shall have an additional integration over λ with the

additional Lagrangian $\mathcal{L}_\lambda(\tau, l) = [i\lambda(\tau, l) + \mu_0^2/2\mathcal{J}][\mathbf{\Omega}^2(\tau, l) - 1]$, where μ_0 is the primary mass of the Ω field and $\mathcal{J} = Jsz$.

To eliminate $\delta(\mathbf{\Omega} \cdot \mathbf{M})$, we shall use some kind of Faddev–Popov trick [5]. As a result of this trick, (*1*) the factor $\delta(\mathbf{\Omega} \cdot \mathbf{M})$ disappears from the measure (9); (*2*) $\mathbf{M} \longrightarrow \mathbf{M}_{tr} = \mathbf{M} - \mathbf{\Omega}(\mathbf{\Omega} \cdot \mathbf{M})$ in the Lagrangian (8); (*3*) an additional contribution to the action appears, the Lagrangian of which, $\mathcal{L}_{ga}$, can be chosen in the form $\mathcal{L}_{ga} = Js^2\sum_{l' \in \langle l \rangle}[(\mathbf{\Omega} \cdot \mathbf{M})^2 + (\mathbf{\Omega} \cdot \mathbf{M})((\mathbf{\Omega}' \cdot \mathbf{M}')]$, which kills the strongest interaction between the $\mathbf{\Omega}$ and $\mathbf{M}$ fields in the Lagrangian (10) that appears due to the substitution $\mathbf{M} \longrightarrow \mathbf{M}_{tr}$; and (*4*) in the measure of the integration in Eq. (9), the additional factor $(\det(\hat{B}_{ga}))^{1/2}$ arises, where the operator $\hat{B}_{ga}$ is just the operator in the quadratic form in the variable $(\mathbf{\Omega} \cdot \mathbf{M})$ for $\mathcal{L}_{ga}$. In this way, Eq. (10) for $\mathcal{L}_{quad}$ is valid in the leading order with respect to $1/2s$. The final expression for the total quadratic Lagrangian is $\mathcal{L}_{tqu} = \mathcal{L}_{quad} + \mathcal{L}_{ga} + \mathcal{L}_{\lambda quad}$.

Now, from the quadratic part of the total Lagrangian $\mathcal{L}_{tot}$ one can find the Green functions of the $\mathbf{\Omega}$ and $\mathbf{M}$ fields in $q = (\omega, \mathbf{k})$ representation:

$$\hat{G}_q\mathbf{X}_q^* \equiv \begin{pmatrix} G_q^\Omega, & G_q^d \\ G_q^u, & G_q^M \end{pmatrix}\begin{pmatrix} \mathbf{\Omega}_q^* \\ \mathbf{M}_q^* \end{pmatrix} = \frac{1}{2sL_q}\begin{pmatrix} Q_\mathbf{k}, & -\omega \\ \omega, & P_\mathbf{k}' \end{pmatrix},$$

$$L_q = \omega^2 + \omega_{0\mathbf{k}}^2,$$
$$\omega_{0\mathbf{k}}^2 = P_\mathbf{k}'Q_\mathbf{k} = (1 - \gamma_\mathbf{k}^2)\mathcal{J}^2 + (1 + \gamma_\mathbf{k})\mu_0^2/2, \quad (11)$$
$$(Q_\mathbf{k}, P_\mathbf{k}) = \mathcal{J}(1 \pm \gamma_\mathbf{k}),$$
$$\gamma_\mathbf{k} = (1/2)(\cos(k_x a) + \cos(k_y a)),$$

where the momentum $\mathbf{k}$ runs over the AF Brillouin zone, a is the lattice constant, $\omega = 2\pi jT$, and j is an integer number.

From Eq. (11), one can calculate the parameter of spin-wave nonlinearity of the theory, $\langle \mathbf{M}_{tr}^2 \rangle = (1/2s)C_M(T)$, where $C_M(T) = 0.65075$ for $T \ll \mathcal{J}$ and $C_M(T) = 1.48491T/\mathcal{J}$ for $T \geq \mathcal{J}$.

We also have the saddle point condition for the λ field $\langle \mathbf{\Omega}^2 \rangle = 1$, which is the most important constraint of the theory which determines its phase state:

$$1 = \langle \mathbf{\Omega}^2 \rangle = N\sum_q G_q^\Omega$$
$$= \frac{NT}{2s}\sum_{\omega, \mathbf{k}}\frac{Q_\mathbf{k}}{\omega^2 + \omega_{0\mathbf{k}}^2} = \frac{N}{2s}\sum_\mathbf{k}\frac{Q_\mathbf{k}}{2\omega_{0\mathbf{k}}}(1 + 2n_{0\mathbf{k}}), \quad (12)$$

where $N = 3$ and $n_{0\mathbf{k}} = (\exp(\omega_{0\mathbf{k}}/T) - 1)^{-1}$ is the Planck function. The right-hand side of Eq. (12) contains two terms. The first term $Q_\mathbf{k}/2\omega_{0\mathbf{k}}$ is responsible for the quantum fluctuations of the Ω fields. The second term $Q_\mathbf{k}n_{0\mathbf{k}}/\omega_{0\mathbf{k}}$ is responsible for the classical thermal fluctuations of the Ω fields. The role of these two terms is quite different. The quantum fluctuations are small according to the parameter of perturbation theory $1/2s$ and, for the basic approximation, they can be neglected. The thermal fluctuations can be considered in the continuum approximation, which leads to the well-known [1–3] zero-order expression for μ_0, $\mu_0 = T\exp[-2\pi Js^2/(TN)]$, and $\xi = \hbar c_s/\mu$, where ξ is the correlation length. From this expression for μ_0 an important conclusion follows: *in the regime of weak coupling the correlation length ξ is much larger than the lattice constant a.*

To close the theory, it is helpful to define the polarization operator $\Pi(q)$ of the $\mathbf{\Omega}$ field $A_{\lambda quad} = -\frac{1}{2}\sum_q \lambda^*(q)\Pi(q)\lambda(q)$, and the Green function of the λ field is $\Pi(q)^{-1}$. In the lowest approximation, $\Pi(q)$ is simply a loop from two Green functions $G^\Omega\Pi_0(q) = 2NT\sum_{q'} G^\Omega(q')\,G^\Omega(q - q')$. The main contribution in $1/2s$ for $\Pi_0(q)$ comes from the thermal fluctuations even at low temperatures T, because the integral strength of such fluctuations is fixed by the saddle point condition (12) and does not depend on the temperature. The explicit form for $\Pi_0(q)$ can be obtained in two limiting cases, $\hbar q \gg T$ and $\hbar q \ll T$, where $q^2 = w^2 + c_s^2 k^2$. In the first case, the momentum $q' \sim T/c_s \ll q$, and we can separate summation and integration over q' and put $q' = 0$ in $G^\Omega(q - q')$ in Eq. (14). The result is extremely simple:

$$\Pi_0(q) = 4G^\Omega(q) = \frac{2\mathcal{J}(1 + \gamma_\mathbf{k})}{s(\omega^2 + \omega_{0\mathbf{k}}^2)}, \quad (13)$$
$$q \gg k_T, \quad k_T = T/c_s.$$

Notice that it exceeds the quantum contribution in Eq. (14), $\Pi_0(q) = N/4q$, by a large parameter $16s\mathcal{J}/Nq$. For small $q \ll c_s/a$ and $q \ll k_T$, our results coincide with [3].

The dynamical spin susceptibility $\chi_{ij}(\omega, \mathbf{k})$ for all values of ω and $\mathbf{k}$ can be calculated. In the lowest order in $1/2s$, we can use the lowest order relation $\mathbf{n}(\mathbf{\Omega}(\tau, l), \mathbf{M}(\tau, l), \tau, l) \simeq \exp(ial) \cdot \mathbf{q}_{\mathbf{AF}}\mathbf{\Omega}(\tau, l) - [\mathbf{\Omega}(\tau, l) \times \mathbf{M}(\tau, l)]$, where $\mathbf{q}_{AF} = (\pi/a, \pi/a)$ is the AF vector (7). Calculating the average of two vectors $\mathbf{n}$, we get the dynamical spin susceptibility as a sum of two terms $\chi_{ij}(\omega, \mathbf{k}) = \delta_{ij}[\chi_A(\omega, \mathbf{k}) + \chi_F(\omega, \mathbf{k})]$. The spin susceptibility $\chi_A(\omega, \mathbf{k})$ is responsible for the AF fluctuations. It is proportional to the Green function G_q^Ω analytically continued to imaginary ω and shifted by the

AF vector $\mathbf{q}_{AF}$. For the ferromagnetic spin susceptibility $\chi_F(\omega, \mathbf{k})$, we have a loop expression which can be calculated on the basis of thermal fluctuation domination: $\chi_F(\omega, \mathbf{k}) \simeq -(2s^2/N)G^M(q)$ for $q \geq k_T$. As a result, we have

$$\chi_A(\omega, \mathbf{k}) = -\frac{Js^2 z(1+\gamma_{\mathbf{k}^*})}{2(\omega^2 - \omega_{0\mathbf{k}^*}^2 + i\omega\delta)},$$
$$\chi_F(\omega, \mathbf{k}) = -\frac{Js^2 z(1-\gamma_{\mathbf{k}})}{N(\omega^2 - \omega_{0\mathbf{k}}^2 + i\omega\delta)}, \quad (14)$$

where $\mathbf{k}^* = \mathbf{k} - \mathbf{q}_{AF}$.

The theory of spin fluctuations in the disordered QAF at sufficiently low temperature $T \ll \mathcal{J}$ allows one to perform the scale separation. In this case, $k_T \ll \pi/a$, the thermal fluctuations can be considered in a "renormalized classical" manner [2]. The magnitude of the quantum fluctuations at $q \leq k_T$ is small as compared with the classical fluctuations. In this situation, the parameters of the effective long-wavelength, low-frequency sigma model are renormalized by the quantum fluctuations. This renormalization is performed with respect to the parameter $1/2s$, but the interaction of the thermal fluctuations with the scales $|\mathbf{k}| \leq k_T$ and $\omega \leq T$ is over parameter $1/N$, where N is the number of components of the $\mathbf{n}$ field of the long-wavelength, low-frequency nonlinear sigma model. This picture follows directly from the approach of this paper.

Unfortunately, the continuum approximation in time does not work when we calculate corrections to the basic approximation. The reason for this observation is in the canonical structure of the Lagrangian (8) and the Green function (11): the sums over ω including this Green function are ambiguous and must be defined at the final time step Δ. Instead of Eq. (4) for the action $A(\mathbf{n})$, we shall use a more accurate expression for $A(\mathbf{n})$, in which the integral over τ is changed to the sum over $\tau = j\Delta$, $j = 0, 1, \ldots, N_\tau - 1$, where $\Delta N_\tau = \beta$. Now $\mathcal{L}_{kin}(j, l)$ is not Berry phase and consists of two parts, $\mathcal{L}_{kin} = \mathcal{L}_{mod} + \mathcal{L}_{pha}$. The first term is purely real and the second term is purely imaginary:

$$\mathcal{L}_{mod} = -\frac{s}{\Delta}\sum_{p=a,b} \ln[(1 + \underline{\mathbf{n}}_p \cdot \mathbf{n}_p)/2],$$
$$\mathcal{L}_{pha} = -\frac{s}{2\Delta}\sum_{p=a,b} \ln\left(\frac{R_p \underline{R}_p^*}{R_p^* \underline{R}_p}\right). \quad (15)$$

Here, the quantity $R_p = \underline{\mathbf{n}}_p \cdot (\mathbf{m}_p + i\mathbf{k}_p)$ for $p = a, b$; vectors $\mathbf{n}$, $\mathbf{m}$, $\mathbf{k}$ were defined in the introduction of the SCS; the underlined quantities $\mathbf{n}$, $\mathbf{m}$, $\mathbf{k}$ correspond to the time $\Delta(j+1)$, and the usual ones correspond to the time Δj. Notice that the Lagrangian $\mathcal{L}_{mod}$ can be expressed in terms of vectors $\mathbf{n}_{a,b}$ only, but $\mathcal{L}_{pha}$ cannot.

The Hamiltonian $\mathcal{H}(\mathbf{n})$ can be obtained on the basis of the following relation for the matrix element of the spin operator $\hat{\mathbf{S}}$: $\langle \underline{\mathbf{n}}|\hat{\mathbf{S}}|\mathbf{n}\rangle = \mathcal{S}(\underline{\mathbf{n}}, \mathbf{n})\langle \underline{\mathbf{n}}|\mathbf{n}\rangle$, where the vector $\mathcal{S}(\underline{\mathbf{n}}, \mathbf{n}) = (\underline{\mathbf{n}} + \mathbf{n} - i[\underline{\mathbf{n}} \times \mathbf{n}])/(1 + \underline{\mathbf{n}} \cdot \mathbf{n})$. If we substitute them into the matrix element of the Heisenberg Hamiltonian, we obtain

$$\mathcal{H}(\mathbf{n}) = Js^2 \sum_{l' \in \langle l \rangle} \mathcal{S}(\underline{\mathbf{n}}, \mathbf{n}) \cdot \mathcal{S}(\underline{\mathbf{n}}', \mathbf{n}'). \quad (16)$$

It was assumed that all vectors $\mathbf{n}_p$, $\mathbf{m}_a$, $\mathbf{k}_p$ for $p = a, b$ entering into Eqs. (15)–(16) are functions of the dynamical variables $\mathbf{\Omega}$ and $\mathbf{M}$ according to Eq. (7). For example, expansion of $\mathcal{L}_{pha}$ in the vector $\mathbf{M}$ has a rather complicated form, but one can prove that it is regular and contains only odd powers of $\mathbf{M}$.

By expanding the Lagrangians $\mathcal{L}_{mod}$, $\mathcal{L}_{pha}$ (15) and the Hamiltonian (16) in the vector $\mathbf{M}$ up to second order, we get $\mathcal{L}_{quad} = (\mathcal{L}_{kin} + \mathcal{H})|_{quad}$:

$$\Delta\mathcal{L}_{quad} = s[1 - \underline{\mathbf{\Omega}} \cdot \mathbf{\Omega} + \mathbf{M}^2 - \underline{\mathbf{M}} \cdot \mathbf{M}$$
$$+ i(\underline{\mathbf{\Omega}} \cdot \mathbf{M} - \mathbf{\Omega} \cdot \underline{\mathbf{M}})] + \Delta Js^2 \sum_{l' \in \langle l \rangle} [\underline{\mathbf{\Omega}} \cdot \mathbf{\Omega} - \mathbf{\Omega} \cdot \mathbf{\Omega}' \quad (17)$$
$$+ \underline{\mathbf{M}} \cdot \mathbf{M} + \mathbf{M} \cdot \mathbf{M}' - i(\underline{\mathbf{\Omega}} \cdot \mathbf{M} - \mathbf{\Omega} \cdot \underline{\mathbf{M}})].$$

According to the analysis performed above, it is necessary to add to the Lagrangian $\mathcal{L}_{quad}$ (17) the quadratic part of the Lagrangian $\mathcal{L}_\lambda$ and the gauge Lagrangian $\mathcal{L}_{ga}$ generalizing for the case of finite time step,

$$\mathcal{L}_{ga} = (s/\Delta)[(\mathbf{\Omega} \cdot \mathbf{M})^2 - (\underline{\mathbf{\Omega}} \cdot \underline{\mathbf{M}})(\mathbf{\Omega} \cdot \mathbf{M})]$$
$$+ Js^2 \sum_{l' \in \langle l \rangle} [(\underline{\mathbf{\Omega}} \cdot \underline{\mathbf{M}})(\mathbf{\Omega} \cdot \mathbf{M}) + (\mathbf{\Omega} \cdot \mathbf{M})(\mathbf{\Omega}' \cdot \mathbf{M}')],$$

which also kills the strongest interaction between the $\mathbf{\Omega}$ and $\mathbf{M}$ fields. The total quadratic Lagrangian is $\mathcal{L}_{tqu} = \mathcal{L}_{quad} + \mathcal{L}_{ga} + \mathcal{L}_{\lambda quad}$. The Green function for this case is

$$\hat{G}_q = \frac{1}{2s\bar{L}(q)}\begin{pmatrix} 1 - c_\omega + \Delta\mathcal{J}(c_\omega + \gamma_{\mathbf{k}}) & -s_\omega(1 - \Delta\mathcal{J}) \\ s_\omega(1 - \Delta\mathcal{J}) & 1 - c_\omega + \Delta\mathcal{J}(c_\omega - \gamma_{\mathbf{k}}) + \Delta\mu_0^2/2\mathcal{J} \end{pmatrix}, \quad (18)$$

$$\bar{L}(q) \simeq (1 - \Delta\mathcal{J} + \Delta\mu_0^2/4\mathcal{J})[2(1 - c_\omega) + \Delta^2\omega_{0\mathbf{k}}^2].$$

Here, $c_\omega = \cos(\omega\Delta)$ and $s_\omega = \sin(\omega\Delta)$; the quantities $Q_{\mathbf{k}}$, $P'_{\mathbf{k}}$, and the bare frequency $\omega_{0\mathbf{k}}$ were defined in Eq. (11). At $\Delta\omega \ll 1$, this Green function G_q transforms into Eq. (11), to the normalization factor $1/\Delta$. The Green function (18) is well defined in the sense that the summation over ω in the expressions including it must be performed in the limits $-\pi/\Delta \le \omega \le \pi/\Delta$. The result of such averaging depends crucially on the contribution at large $\omega \simeq \pi/\Delta$. For example, we have $\langle M_i M_j\rangle = (1/4s)\delta_{ij}(1 + c_0 - c_1)$, $\langle \underline{M}_i M_j\rangle = (1/4s)\delta_{ij}(c_0 - c_1)$. We see that the average $\langle \mathbf{M}^2\rangle$ discussed above, in fact, corresponds to the average $\langle \mathbf{M}\cdot\underline{\mathbf{M}}\rangle$ but the average $\langle \mathbf{M}^2\rangle$ is different.

The free energy of QAF in the paramagnetic state has three contributions, $F_{AF} = -T\ln(Z) = F_{\Omega M} + F_\lambda + F_{ga}$, $Z = Z_{\Omega M}Z_\lambda Z_{ga}$. In the lowest approximation in $1/2s$, $Z_{\Omega M}$, Z_λ, and Z_{ga} are powers of determinants. The explicit form of these determinants leads to

$$F_{\Omega M} = \frac{TNN_s}{2}\sum_{\omega\mathbf{k}} \ln[\bar{L}(q)],$$

$$F_{ga} = -\frac{TN_s}{2}\sum_{\omega\mathbf{k}} \ln[2s\bar{Q}(q)], \qquad (19)$$

$$F_\lambda = \frac{TN_s}{2}\sum_{\omega\mathbf{k}} \ln[s^2\Pi_0(q)].$$

One can verify that $F_{\Omega M}$ has a finite limit at $\Delta \longrightarrow 0$, $\Delta N_\tau = \beta$. F_{ga} and F_λ do not have a finite limit at $\Delta \longrightarrow 0$, $\Delta N_\tau = \beta$ separately, but their sum has a finite limit. After some transformation, the free energy F_{QAF} of QAF in the lowest order in $1/2s$ can be presented in the form $F_{QAF} = ((N-1)/N)F_{\Omega M} + F_{\lambda l}$, where

$$F_{\Omega M} = -N_s\mathcal{J} + 2N_s\sum_{\mathbf{k}}\{\omega_{0\mathbf{k}}/2 + T\ln[1 - \exp(-\omega_{0\mathbf{k}}/T)]\}, \qquad (20)$$

$$F_{\lambda l} = \frac{TN_s}{2}\sum_{\omega\mathbf{k}} \ln\left[\frac{s(\omega^2 + \omega_{0\mathbf{k}}^2)\Pi_0(q)}{2\mathcal{J}(1+\gamma_{\mathbf{k}})}\right].$$

Here, $2N_s$ is the number of lattice sites, and the polarization operator $\Pi_0(q)$was defined above. The temperature-dependent part of free energy (20) at low temperatures $T \ll \mathcal{J}$ is proportional to $F_{AF} \approx N_s T^3/\mathcal{J}$. Such a contribution has two origins: one from $F_{\Omega M}$ and another one from $F_{\lambda l}$.

Now, we present the result of the calculation of corrections to the mass operators of the $\mathbf{\Omega}$ and $\mathbf{M}$ fields. In the lowest order in $1/2s$, these corrections can be presented as renormalization of the initial quadratic Lagrangian (17). It is necessary to have the Lagrangian $\mathcal{L}_{mod}$ and the Hamiltonian $\mathcal{H}$ up to the fourth order in field $\mathbf{M}$, and the Lagrangian $\mathcal{L}_{pha}$ up to the third order.

The effective Lagrangian $\mathcal{L}_{eff}$ in the first $1/2s$ approximation is

$$\begin{aligned}\Delta\mathcal{L}_{eff} = s[&a_0(1 - \mathbf{\Omega}\cdot\underline{\mathbf{\Omega}}) + b_0(\mathbf{M}^2 - \mathbf{M}\cdot\underline{\mathbf{M}}) \\ &- ie_0(\mathbf{\Omega}\cdot\underline{\mathbf{M}} - \underline{\mathbf{\Omega}}\cdot\mathbf{M})] + \Delta Js^2\sum_{l'\in\langle l\rangle}[a_1(1 - \mathbf{\Omega}\cdot\underline{\mathbf{\Omega}}) \\ &+ a_2(1 - \mathbf{\Omega}\cdot\mathbf{\Omega}') + a_3(1 - \mathbf{\Omega}'\cdot\underline{\mathbf{\Omega}}) + b_1\mathbf{M}^2 \\ &+ b_2\mathbf{M}\cdot\underline{\mathbf{M}} + b_3\mathbf{M}\cdot\mathbf{M}' + b_4\mathbf{M}'\cdot\underline{\mathbf{M}} \\ &- ie_1(\mathbf{\Omega}\cdot\underline{\mathbf{M}} - \underline{\mathbf{\Omega}}\cdot\mathbf{M}) - ie_2(\mathbf{\Omega}'\cdot\underline{\mathbf{M}} - \underline{\mathbf{\Omega}}\cdot\mathbf{M}')],\end{aligned} \qquad (21)$$

where the constants $a_0, \ldots, e_2$ are $a_i = a_i^0 + g\alpha_i$, $b_i = b_i^0 + g\beta_i$, $e_i = e_i^0 + g\gamma_i$, where $g = (N-1)/4s$, $i = 0, 1, 2, 3$. The constants a_i^0, b_i^0, e_i^0 follow from Eq. (17). The explicit form of the constants α_i, β_i, γ_i will be presented in the complete version of this paper.

We shall give the explicit result for the correlation radius in this order in $1/2s$ on the basis of Eq. (12). The contribution of different frequencies ω and momenta $\mathbf{k}$ in this constraint relation can be separated into two parts. The first part is the high frequency and momentum part. To calculate this contribution it is sufficient to take the Green function $G^\Omega(q)$ in bare approximation (18), because this contribution, is of the order of $1/2s$. The second contribution, which is proportional to the distribution function $n_{\mathbf{k}}$, can be considered in the continuum approximation, but with $1/2s$ corrections taken into account: $G^\Omega(q) \simeq 1/[2a^2\chi_\perp\Delta(\omega^2 + \omega_{\mathbf{k}}^2)$, $\chi_\perp = \tilde{\rho}_s/c_s^2$, $\omega_{\mathbf{k}}^2 = c_s^2\mathbf{k}^2 + \mu^2$. Here, $\tilde{\rho}_s = Js^2a_{23}$; $c_s^2 = e_0^{-2}a_{23}b_{1234}\mathcal{J}^2a^2/z$, where $a_{23} = a_2 + a_3$, $b_{1234} = b_1 + b_2 + b_3 + b_4$. Now, instead of Eq. (12), we have $(N/4s\tilde{\rho}_s)\sum_{\mathbf{k}}[n_{\mathbf{k}}/\omega_{\mathbf{k}}] = R$, $R = 1 - g(1 + c_0 + c_1)$. The factor R includes in itself the direct short-wavelength renormalizations. Performing the integration, we have $\mu = T\exp[-2\pi\rho_s/TN]$, $\rho_s = \tilde{\rho}_s R$, $\xi = \hbar c_s/\mu$. The actual temperature dependence is changed in the preexponent factor ($T \longrightarrow \mathcal{J}$) if we take into account the long-wavelength fluctuations in the next order in $1/N$ approximation [3].

We are grateful to A.V. Chubukov, I.V. Kolokolov, and S. Sachdev for stimulating discussions; C. Providencia and V.R. Vieira for the accompanying discussions; and A.M. Finkelstein, and P. Woelfle for critical remarks. One of the authors (V.B.) is grateful to A.L. Chernyshev, L.V. Popovich, and V.A. Shubin for discussion and cooperation at an early step of this work. This work was supported in part by the Portuguese projects PRAXIS/2/2.1/FIS/451/94, V.B. was sup-

ported in part by the Portuguese program PRAXIS XXI/BCC/11952/97 and the Russian Foundation for Basic Research (project no. 97-02-18546).

REFERENCES

1. E. Manousakis, Rev. Mod. Phys. **63**, 1 (1991).
2. S. Chakravarty, B. I. Halperin, and D. R. Nelson, Phys. Rev. B **39**, 2344 (1989).
3. A. Chubukov, S. Sachdev, and J. Ye, Phys. Rev. B **49**, 11919 (1994).
4. A. M. Polyakov, *Gauge Fields and Strings* (Harwood Academic, New York, 1987).
5. J. Zinn-Justin, *Quantum Field Theory and Critical Phenomena* (Clarendon Press, Oxford, 1996).
6. P. Hasenfratz and F. Niedermayer, Phys. Lett. B **268**, 231 (1991); Phys. Lett. B **245**, 529 (1990); P. Hasenfratz, M. Maggiore, and F. Niedermayer, Phys. Lett. B **245**, 522 (1990).
7. J. R. Klauder and B. S. Skagerstam, *Coherent States* (World Scientific, Singapore, 1985).
8. A. M. Perelomov, Commun. Math. Phys. **26**, 222 (1972); A. M. Perelomov, *Generalized Coherent States and Their Applications* (Springer-Verlag, Berlin, 1986).

JETP Letters, Vol. 72, No. 10, 2000, pp. 527–529. Translated from Pis'ma v Zhurnal Éksperimental'noĭ i Teoreticheskoĭ Fiziki, Vol. 72, No. 10, 2000, pp. 753–757.

"Negative Heat Capacity" of Stratified Fluids

L. Kh. Ingel

Institute of Experimental Meteorology, NPO "Taifun," Obninsk, Kaluga region, 249038 Russia
e-mail: lingel@obninsk.com

Received October 12, 2000

In "doubly nonequilibrium" fluids (e.g., solutions with stratified temperature and impurity concentration in the gravitational field), situations are possible when the addition of heat decreases temperature and vice versa. This is demonstrated by the simple example of a convection problem. © *2000 MAIK "Nauka/Interperiodica".*

PACS numbers: 44.25.+f; 47.27.Te

In recent years, some paradoxical experimental facts were reported in the geophysical literature [1, 2]: "Readings of instruments lowered into a well (*in the Antarctic ice shelf*, L.I.) revealed an unexpected paradox: temperature of seawater under ice is higher in winter than in summer" [2]. In other words, one may speak, in a sense, about the negative heat capacity of this geophysical medium.

In this letter, the simplest example of convection in a nonequilibrium stratified medium is considered to demonstrate that such effects are possible when both the temperature and the impurity (salt) concentration make contributions (of opposite signs) to density stratification.

Let us consider an infinite volume of a solution whose density ρ, as it is customarily accepted [3–5], linearly depends on temperature T and impurity concentration s:

$$\rho = \rho_0[1 - \alpha(T - T_0) + \beta(s - s_0)]. \quad (1)$$

Here, α is the thermal expansion coefficient of the medium and β is the corresponding coefficient for the impurity concentration (in oceanology, it is called the coefficient of compression salinity). The zero index denotes constant ("reference") values of the corresponding quantities. In the simplest models of stratified media, it is assumed that the temperature, impurity concentration, and density linearly depend on the vertical coordinate z (the z axis is in opposition to the gravitational force):

$$\bar{\rho}(z) = \rho_0[1 + (-\alpha\gamma_T + \beta\gamma_s)z], \quad (2)$$

where the constant gradients[1] $\gamma_T = d\bar{T}/dz$ and $\gamma_s = d\bar{s}/dz$; the bars denote the corresponding "background" values (in order to differentiate them from the perturbations introduced by heat release; see below).

For simplicity, let us restrict ourselves to the situation where the density stratification is neutral (the temperature and the impurity concentration stratifications cancel each other in the density field):

$$-\alpha\gamma_T + \beta\gamma_s = 0; \quad \bar{\rho}(z) = \rho_0 = \text{const}. \quad (3)$$

In addition, it is sufficient to consider in this work the convection from a heat source of a certain simple form. Let us consider an instantaneous source uniformly distributed along the vertical z axis:

$$Q(r, t) = Q_0\delta(r)\delta(t)/2\pi r, \quad (4)$$

where δ symbolizes the delta function, r is the distance from the z axis, and Q_0 has the meaning of a source amplitude. Since the source does not depend on the z coordinate, the solution can also be sought in the z-independent form. The substantiation and the limits of applicability of such a "one-dimensional" convection regime are discussed, e.g., in [6, 7].

The set of equations of hydrodynamics and heat and impurity transport is written in the approximation that is ordinarily used in the convection problems, i.e., in the Boussinesq or free-convection approximation [3–5]. In this approximation, the compressibility of the medium is ignored but the dependence of its density on the temperature and impurity concentration is taken into account. The continuity equation in this approximation is written as $\mathrm{div}\mathbf{v} = 0$, where $\mathbf{v}$ is the velocity vector. It then follows, in conjunction with $\partial/\partial z = 0$, that the radial (perpendicular to the z axis) motion is absent. In this case, the above-mentioned set of equations takes the form (a more detailed deduction for the case of a single-component medium is given, e.g., in [7])

$$\frac{\partial w}{\partial t} = \nabla(\nu\nabla w) + g(\alpha T' - \beta s'), \quad (5)$$

$$\frac{\partial T'}{\partial t} + \gamma_T w = \nabla(\kappa\nabla T') + Q, \quad (6)$$

[1] If the γ_T and γ_s gradients are constant, then the problem may arise of unlimited increase or decrease in the temperature, impurity concentration, and density at $z \longrightarrow \pm\infty$. This formal difficulty is insignificant, because, in reality, one deals, of course, with layers of finite thickness.

0021-3640/00/7210-0527$20.00

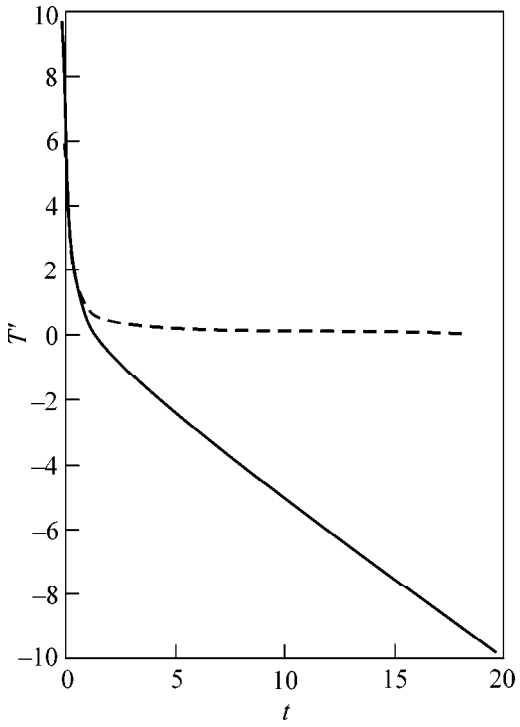

Time evolution of temperature perturbation on the $r = 0$ axis. Temperature is normalized to $Q_0(\alpha g\gamma_T)^{1/2}/4\pi K$ and time is normalized to $(\alpha g\gamma_T)^{-1/2}$. The dashed line illustrates a similar curve for a nonstratified medium.

$$\frac{\partial s'}{\partial t} + \gamma_s w = \nabla(\chi\nabla s'). \tag{7}$$

Here, w is the velocity z-component (the remaining components in this problem are zero), t is time, and the deviations from the background state are primed. It should be emphasized that the complete set of equations of hydrothermodynamics and impurity transport is reduced to a rather simple (linear, if the exchange coefficients ν, κ, and χ are independent of the velocity and other unknowns) set of Eqs. (5)–(7) owing solely to the symmetry of the problem, i.e., without any assumptions about the smallness of the perturbation amplitudes.

The boundary conditions are, first of all, formulated as a perturbation decay far from the source (at $r \longrightarrow \infty$). In addition, the symmetry considerations give for $t > 0$

$$\frac{\partial w}{\partial r} = \frac{\partial T'}{\partial r} = \frac{\partial s'}{\partial r} = 0, \quad r = 0. \tag{8}$$

The posed problem can easily be solved if the exchange coefficients are constant and equal to each other in different substances, i.e., if $\nu = \kappa = \chi = K =$ const (this simplification is commonly accepted in geophysical applications when dealing with the effective coefficients of turbulent exchange). Let us multiply Eq. (6) by α and Eq. (7) by β and subtract the latter from the former. Making use of Eq. (3), one obtains the following equation for the dimensionless buoyancy $b = \alpha T' - \beta s'$:

$$\frac{\partial b}{\partial t} = \frac{K}{r}\frac{\partial}{\partial r}r\frac{\partial b}{\partial r} + \alpha Q. \tag{9}$$

This is the standard diffusion (heat conduction) equation, whose solution for instantaneous source (4) has the form

$$b = \frac{\alpha Q_0}{4\pi K t}\exp(-r^2/4Kt). \tag{10}$$

To a constant multiplier, b has the meaning of a source in Eq. (5). One can readily verify that the solution of the latter can be expressed as

$$w = gtb = \frac{\alpha g Q_0}{4\pi K}\exp(-r^2/4Kt). \tag{11}$$

Let us now find the temperature perturbation. With regard to Eq. (11), Eq. (6) can be recast as

$$\frac{\partial T'}{\partial t} = \frac{K}{r}\frac{\partial}{\partial r}r\frac{\partial T'}{\partial r} - g\gamma_T tb + Q. \tag{12}$$

The solution of this equation can be represented as a sum of two terms corresponding to two sources on the right-hand side of Eq. (12). One of these terms corresponds to the source Q; this is the well-known Green function of the heat equation. It is straightforward to verify that the second source($-g\gamma_T tb = -\gamma_T w$) makes the $-\frac{1}{2}g\gamma_T t^2 b = -\frac{1}{2}\gamma_T t w$ contribution to the solution. As a result, the temperature perturbation caused by heat release has the form

$$T' = \frac{Q_0}{4\pi K t}\exp(-r^2/4Kt) - \frac{1}{2}\frac{\alpha g\gamma_T t Q_0}{4\pi K}\exp(-r^2/4Kt) = \frac{Q_0}{4\pi K t}\exp(-r^2/4Kt)\left(1 - \frac{1}{2}\alpha\gamma_T t^2\right). \tag{13}$$

The expression for the impurity concentration perturbation can be obtained in a similar manner [of the two terms in Eq. (13), the corresponding expression contains only an analogue of the second term].

The first term in Eq. (13) needs no comment because it allows for the diffusion of heat released on the z axis at $t = 0$. The second term describes the temperature changes induced by thermal advection, i.e., heat transfer caused by the vertical convective motions in the stratified medium. A peculiarity of the second term is, first, that its amplitude increases rather than decreases (as does the first term) with time. The presence of an increasing response to an infinitesimal initial perturbation is an indication of system instability. In this respect, one may speak about a new (apparently, not discussed before) type of instability.

Another specific feature of the second term in Eq. (13) is that it may be opposite in sign (at $\gamma_T > 0$) to the initial heat release.

The time evolution of the temperature perturbation on the z axis is displayed in the figure for $\gamma_T > 0$. For short times, the first term in Eq. (13) dominates; i.e., the usual "diffusional spreading" of the released heat takes place. However, subsequently, the perturbation temperature changes sign; i.e., in response to the released heat, the negative deviation of temperature increases in the system (a colder fluid is admitted from below). In this respect, one may speak about the effective negative heat capacity of the medium.

The example of the convection problem considered above (a heat source of infinite length in an infinite medium) may appear to be quite specific and artificial. Nevertheless, this example was taken only for simplicity and with the aim of obtaining an exact analytic solution. One can easily verify that, in "doubly nonequilibrium" media (e.g., media with stratified temperature and impurity concentration), a similar result can be obtained for the other well-known convection forms as well. For instance, the models of convective jets and "thermics" described in monograph [4] can readily be generalized to the case of a binary mixture, where, in addition to the temperature stratification, the density stratification is also governed by the vertical dependence of impurity concentration. In the simplest situation, where the overall density stratification is neutral while the temperature stratification is stable, results similar to the ones presented above can easily be obtained for jets and thermics. Indeed, after receiving extra heat, the corresponding volume of a medium, evidently, floats up. It is then quite possible that this volume becomes colder than the ambient medium (since it transfers up a colder fluid) but continues to float up (by virtue of the contribution from the negative impurity concentration perturbation to the buoyancy). Thus, in response to the extra heat received by the fluid, the negative deviation of temperature rises! This result is physically explicable but, at the same time, is, in a sense, unexpected.

REFERENCES

1. K. W. Nickolls, Nature **388**, 460 (1997).
2. B. I. Silkin, Meteorol. Hydrol., No. 4, 127 (1998).
3. G. Z. Gershuni and E. M. Zhukhovitskiĭ, *Convective Stability of Incompressible Fluids* (Nauka, Moscow, 1972).
4. J. S. Turner, *Buoyancy Effects in Fluids* (Cambridge Univ. Press, Cambridge, 1973; Mir, Mosow, 1977).
5. L. D. Landau and E. M. Lifshitz, *Course of Theoretical Physics*, Vol. 6: *Fluid Mechanics* (Nauka, Moscow, 1986; Pergamon, New York, 1987).
6. B. Gebhart, Y. Jaluria, R. Mahajan, and B. Sammakia, *Buoyancy-Induced Flows and Transport* (Springer-Verlag, Berlin, 1988; Mir, Moscow, 1991).
7. L. Kh. Ingel, Izv. Akad. Nauk SSSR, Fiz. Atmos. Okeana **26**, 794 (1990).

Translated by V. Sakun

JETP Letters, Vol. 72, No. 10, 2000, pp. 530–540. Translated from Pis'ma v Zhurnal Éksperimental'noĭ i Teoreticheskoĭ Fiziki, Vol. 72, No. 10, 2000, pp. 758–773.

Variational Approaches to the Problems of Plasma Stability and of Nonlinear Plasma Dynamics

V. I. Ilgisonis and V. P. Pastukhov

Institute of Nuclear Fusion, Russian Research Centre Kurchatov Institute, pl. Kurchatova 1, Moscow, 123182 Russia
e-mail: vil@nfi.kiae.ru; past@nfi.kiae.ru

Received October 26, 2000

A variational method is developed in order to investigate the nonlinear dynamics and stability of plasma using hydrodynamic plasma models, namely, the one-fluid, Hall, and electron MHD models. The key idea of the method is to adequately take into account variational symmetries and the associated conservation laws inherent in these hydrodynamic models. This approach is applied to derive variational criteria for the stability of a steadily moving plasma and to propose a variational method of the adiabatic separation of fast and slow motions, which makes it possible to simplify (reduce) the basic hydrodynamic models. © *2000 MAIK "Nauka/Interperiodica"*.

PACS numbers: 52.30.-q; 52.55.Dy

1. INTRODUCTION

Numerous processes in a magnetized plasma can be adequately described using various MHD models. Thus, the equations of an ideal one-fluid MHD model describe the steady states and the macroscopic dynamics of the plasma, as well as a wide variety of plasma oscillations and waves, among which fast ideal MHD instabilities are usually the most dangerous and destructive for both laboratory and space plasmas. In order to provide a more adequate description of the plasma dynamics, along with the one-fluid MHD model, one can use multifluid plasma models, in particular, the Hall MHD (HMHD) and electron MHD (EMHD) two-fluid models. Dynamic problems that involve a small parameter can often be solved using simpler (reduced) models.

Since there is a wide variety of MHD models describing numerous dynamic plasma processes, it is necessary to develop fairly general and efficient methods for their theoretical analysis. In this way, it should be kept in mind that, under the conditions prevailing in space plasmas and magnetically confined high-temperature plasmas, the dissipative processes associated with Coulomb collisions are much slower than the dynamic processes. In this case, the dynamic processes described by an ideal (dissipation-free) model should play a governing role, while the dissipative processes are responsible for the slow evolution of the invariants of the "ideal" motion (in particular, bifurcations of the dynamic state of the system).

Lagrangian methods used in the mechanics of continuous media (primarily, variational methods) seem to be most appropriate for the analysis of ideal MHD models. We emphasize that, in contrast to the widely held opinion, applying variational methods to ideal MHD systems does not reduce merely to the derivation of the integral criteria, such as the so-called "energy principle" [1], which makes it possible to investigate the linear stability of the steady equilibrium states. One of the most important steps in studying Lagrangian systems (to which all of the ideal MHD models are related) is a search for variational symmetries, because, according to Noether's theorem, any variational symmetry (i.e., such a transformation of independent variables in the Lagrangian under which the action is conserved) generates a certain dynamic conservation law. However, the form of the law and its very existence are far from being *a priori* clear. Of course, the existence of conservation laws imposes certain restrictions on variations of the physical quantities, which qualitatively affects the stability and nonlinear dynamics of the system. For example, a system possessing relabeling symmetry may have solutions corresponding not only to a static equilibrium state but also a dynamic state with steady flows. The method of the adiabatic separation of fast and slow motions in Lagrangian systems is conceptually very similar to the search for variational symmetries and makes it possible to construct the above-mentioned reduced MHD models without violating the variational symmetries of the basic model.

The effectiveness of variational methods is most strongly manifested when analyzing the stability of a complex continual system, in which case the powerful mathematical apparatus of the Lyapunov stability theory may be employed in full measure. Unlike the energy principle, the methods of the Lyapunov theory make it possible to derive sufficient conditions for both linear and nonlinear stabilities and can also be used to treat the problems inherent in multifluid models and investigate the stability of states with steady flows. In

0021-3640/00/7210-0530$20.00

the latter case, in constructing the Lyapunov functional, it is very important to take into account all of the conservation laws in order to minimize the freedom in the functions to be varied and to derive a sufficient stability condition that is as close to the necessary condition as possible (or even to arrive at the necessary and sufficient stability criterion).

In this paper, we briefly review recent results concerning the application of variational methods to the problems of the stability and nonlinear dynamics of plasmas described by different ideal MHD models. We focus on the original results obtained in studies supported by the Russian Foundation for Basic Research (under project nos. 97-02-17238 and 97-02-17730). In Section 2, we briefly describe the formalism for seeking the variational symmetries and relevant conservation laws. In Section 3, we consider the variational symmetries and conservation laws inherent in the most familiar MHD models. In Section 4, we outline the fundamentals of the variational method of the adiabatic separation of fast and slow motions in Lagrangian systems. As an illustration, we employ this method to derive an improved version of the reduced Kadomtsev–Pogutse–Strauss equations. In Section 5, we obtain variational criteria for the MHD models under analysis. In Section 6, we briefly discuss the results obtained.

2. VARIATIONAL SYMMETRIES

Here, we describe the formalism for seeking variational symmetries with the help of Noether's theorem. Only a brief and somewhat mathematized discussion of this issue is given here, because the variational formalism is described in detail in textbooks (see, e.g., [2, 3]). For brevity, we introduce the following notation, which will be used only in this section: x is a complete set of independent variables $\{x^i\}$ (including time and spatial coordinates in a certain volume Γ), $u = u(x)$ is a dependent vector function, and the subscripts denote differentiation with respect to x. When varying the Lagrangian density $L = L(x, u, u_i, u_{ij}\ldots)$, we use the symbol ∂ for the partial derivative with respect to the corresponding argument, while the symbol d_i stands for the total derivative with respect to the independent variable x^i.

Let us analyze the infinitesimal transformation $u(x) \longrightarrow u(x) + \delta u$, which leads to the following variation of the action integral:

$$\begin{aligned}\delta S &= \delta\int_\Gamma L dx = \int_\Gamma \delta L dx \\ &= \int_\Gamma\left(\frac{\partial L}{\partial u}\delta u + \frac{\partial L}{\partial u_i}\delta u_i + \ldots\right)dx \\ &= \int_\Gamma (E[L]\delta u + d_i(W^i[L]\delta u))dx.\end{aligned} \tag{1}$$

Here,

$$E[L] = \frac{\partial L}{\partial u} - d_i\frac{\partial L}{\partial u_i} + d_i d_j\frac{\partial L}{\partial u_{ij}} - \ldots \tag{2}$$

is the so-called Euler operator and the flux in Eq. (1) has the form

$$W^i[L] = \frac{\partial L}{\partial u_i} - d_j\frac{\partial L}{\partial u_{ij}} + \ldots .$$

Up to this point, we used no boundary conditions.

First, we consider variations that vanish at the boundary, $\delta u|_{\partial\Gamma} = 0$. Hamilton's principle, which implies that the action integral has an extremum at the real motion, yields the equations of motion in the form

$$E[L] = 0. \tag{3}$$

Note that, if the transformation at hand is a variational symmetry, or, in other words, ensures the equality

$$\delta S + \int_\Gamma d_i\Lambda^i dx = 0, \tag{4}$$

then the following conservation law holds for real motion:

$$d_i(W^i[L]\delta u + \Lambda^i) = 0 \tag{5}$$

(here, we took into account that $E[d_i\Lambda^i] \equiv 0\ \forall\Lambda^i$). This assertion, which follows directly from Eqs. (1) and (4), is the essence of Noether's theorem in Boyer's formulation. Note that, following Boyer [4], we varied only the dependent functions $u(x)$. It is also important to note that, for any conservation law, there exists at least one variational symmetry generating this law in the sense of Noether's theorem [5]. Since any variational symmetry maps a motion into a motion, it is, at the same time, the Lie–Bäcklund symmetry for the Euler–Lagrange equations $E[L] = 0$. The converse is not always true. Hence, the variational symmetries can be sought for only in the class of Lie–Bäcklund symmetries by applying the well-developed mathematical technique.

A transformation δu that depends on x, u, u_{i_1}, $u_{i_1 i_2}$, …, $u_{i_1\ldots i_n}$, generates the nth order Lie–Bäcklund symmetry if and only if the condition

$$U^{(m)}E[L] \equiv 0 \tag{6}$$

is valid for any u satisfying Eq. (3). Here, m is the largest order of the derivative of the function u in the Euler operator (2), which is regarded as a function of x, u, u_{i_1}, $u_{i_1 i_2}$, …, $u_{i_1\ldots i_n}$, and $U^{(m)}$ is the extended infinitesimal generator, which is equal, by definition, to

$$U^{(m)} = \delta u\frac{\partial}{\partial u} + \delta u_i\frac{\partial}{\partial u_i} + \ldots + \delta u_{i_1\ldots i_m}\frac{\partial}{\partial u_{i_1\ldots i_m}},$$

where $\delta u_i = d_i \delta u$, …, $\delta u_{i_1 \ldots i_m} = d_{i_m} \delta u_{i_1 \ldots i_{m-1}}$. The $\equiv$ sign in Eq. (6) indicates that all coefficients in front of x, u, u_{i_1}, $u_{i_1 i_2}$, … should vanish. In terms of the extended infinitesimal generator, the variational symmetries satisfy the equation

$$U^{(m)} L + d_i \Lambda^i \equiv 0. \tag{7}$$

They can be sought for only in the class of solutions to Eq. (6).

Note that Eq. (6) is the equation $E[L] = 0$ linearized in the vicinity of an *arbitrary motion*.

3. HYDRODYNAMIC MODELS AND THEIR SYMMETRIES

To construct a Lagrangian for a particular set of hydrodynamic equations is not a trivial matter. The main difficulty in this method usually lies in the choice of an adequate set of variables that could be regarded as being independent. The physical quantities entering the desired set of equations are not independent variables, because they are just related by these equations.

Below, we will follow the Euler method for introducing the labels of volume fluid elements (Lagrangian coordinates). The motivation for the use of this approach to constructing Lagrangians can be found in [6], where other approaches are also outlined. Here, we only note that the continuity equations, "frozen-in" equations, etc., which are usually exploited in hydrodynamic models and can be written as $\partial_t \hat{T} + L_{\mathbf{v}} \hat{T} = 0$ (where $\hat{T}$ is a frozen-in quantity and $L_{\mathbf{v}}$ is the Lie derivative relative to the vector field $\mathbf{v}$), are integrable in Lagrangian coordinates, so that the Lagrangian is constructed exclusively for the equation of motion. Of course, for a dissipative system, these equations are generally nonintegrable. However, if the dissipation is sufficiently low, the structure of the hydrodynamic motion is governed by the "ideal" Lagrangian, while the dissipation manifests itself merely in the evolution of both the quasi-equilibrium parameters of the system and the invariants of the ideal motion.

The Lagrangian coordinate grid is formally introduced by the three independent functions $\{\alpha^i(t, \mathbf{r})\}$ with a nonvanishing Jacobian $J = \nabla\alpha^1 \cdot [\nabla\alpha^2 \times \nabla\alpha^3] \neq 0$. The independent functions should be frozen in the fluid:

$$\partial_t \alpha^i + \mathbf{v}\nabla\alpha^i = 0, \quad i = 1, 2, 3. \tag{8}$$

The related covariant and contravariant bases are defined as

$$\mathbf{e}^i = \nabla\alpha^i, \quad \mathbf{e}_i = \frac{1}{2J}\epsilon_{imn}\mathbf{e}^m \times \mathbf{e}^n, \tag{9}$$

where ε_{imn} is a completely antisymmetric unit tensor. The Jacobian J satisfies the continuity equation $\partial_t J + \mathrm{div} J\mathbf{v} = 0$. Consequently, if the Jacobian J is everywhere nonzero at the initial instant, it does not vanish for any sufficiently smooth vector field $\mathbf{v}(t, \mathbf{r})$, $J(t, \mathbf{r}) \neq 0$, so that the Lagrangian grid is nondegenerate. An important point is that all of the components of the invariant tensor $\hat{T}$ in bases (9) are functions of the Lagrangian coordinates solely [6].

The dynamic equations for the basis vectors follow immediately from definitions (8) and (9):

$$\delta_t \mathbf{e}_i = (\mathbf{e}_i\nabla)\mathbf{v} - (\mathbf{v}\nabla)\mathbf{e}_i, \ \partial_t \mathbf{e}^i = -\nabla(\mathbf{v} \cdot \mathbf{e}^i). \tag{10}$$

The desired infinitesimal transformation $\boldsymbol{\xi}$ ($\boldsymbol{\xi} = \xi^i \mathbf{e}_i$) of the independent functions $\{\alpha^i(t, \mathbf{r})\}$ can be introduced by the relationships $\alpha^i \longrightarrow \alpha^i + \delta\alpha^i$, where $\delta\alpha^i = -\xi^i$. The variations of the density ρ and entropy η, which are described by the conventional continuity and adiabatic equations, and the variation of the velocity have the form

$$\begin{aligned} \delta\rho &= -\mathrm{div}(\rho\boldsymbol{\xi}), \quad \delta\eta = -\boldsymbol{\xi}\nabla\eta, \\ \delta\mathbf{v} &= \dot{\boldsymbol{\xi}} + (\mathbf{v}\nabla)\boldsymbol{\xi} - (\boldsymbol{\xi}\nabla)\mathbf{v}, \end{aligned} \tag{11}$$

where the superior dot denotes the partial derivative $(\partial_t)|_{\mathbf{r}}$. The expression for the variation of the electromagnetic field depends on the specific hydrodynamic models.

Below, we will find variational symmetries and the related explicit conservation laws inherent in the most widely used hydrodynamic model.

3.1. One-Fluid Magnetohydrodynamics

In the one-fluid MHD model, the magnetic field $\mathbf{B}$ is assumed to be frozen in the fluid:

$$\partial_t \mathbf{B} = \mathrm{curl}[\mathbf{v} \times \mathbf{B}] \quad (\mathrm{div}\mathbf{B} \equiv 0). \tag{12}$$

The variation of the magnetic field has the form

$$\delta\mathbf{B} = \mathrm{curl}[\boldsymbol{\xi} \times \mathbf{B}]. \tag{13}$$

The adiabatic equation $(\partial_t + (\mathbf{v}\nabla))\eta = 0$ is often written for the entropy function $s(\eta) = p/\rho^\gamma$, where γ is the adiabatic index, in which case the Lagrangian with the density

$$L = \frac{\rho\mathbf{v}^2}{2} - \frac{p}{\gamma - 1} - \frac{\mathbf{B}^2}{2} \tag{14}$$

yields the following MHD equation of motion [7]:

$$\rho\dot{\mathbf{v}} + \rho(\mathbf{v}\nabla)\mathbf{v} + \nabla p + [\mathbf{B} \times \mathrm{curl}\mathbf{B}] = 0. \tag{15}$$

We pass over from Λ^i to the temporal and spatial components Λ^0 and $\boldsymbol{\Lambda}$ in order to rewrite condition (7) for the existence of variational symmetry in explicit

form. Specifically, if there exist $\boldsymbol{\xi}$, Λ^0, and $\boldsymbol{\Lambda}$ satisfying the equation

$$\partial_t\Lambda^0 + \mathrm{div}\boldsymbol{\Lambda} - \frac{v^2}{2}\mathrm{div}(\rho\boldsymbol{\xi}) + \rho\mathbf{v}(\dot{\boldsymbol{\xi}} + (\mathbf{v}\nabla)\boldsymbol{\xi} - (\boldsymbol{\xi}\nabla)\mathbf{v}) - \mathbf{B}\mathrm{curl}[\boldsymbol{\xi}\times\mathbf{B}] + \frac{1}{\gamma-1}(\boldsymbol{\xi}\nabla p + \gamma p\mathrm{div}\boldsymbol{\xi}) = 0 \tag{16}$$

for any α^i satisfying Eq. (15), then the set of MHD equations possesses conservation law (5), which can be written as

$$\partial_t(\rho\boldsymbol{\xi}\mathbf{v} + \Lambda^0) + \mathrm{div}(\rho\mathbf{v}(\boldsymbol{\xi}\mathbf{v})) + \mathrm{div}\left(\boldsymbol{\xi}\left(\mathbf{B}^2 + \frac{\gamma p}{\gamma-1} - \frac{\rho\mathbf{v}^2}{2}\right) - \mathbf{B}(\boldsymbol{\xi}\mathbf{B}) + \boldsymbol{\Lambda}\right) = 0. \tag{17}$$

If, in addition, the last term on the right-hand side is equal to $\mathrm{div}(\mathbf{v}\Lambda^0)$, then the quantity $(\Lambda^0 + \rho\boldsymbol{\xi}\mathbf{v})$ is an Eulerian invariant (i.e., it is proportional to J, the proportionality coefficient being dependent only on the Lagrangian coordinates).

In the works reviewed here, a study was made, in particular, of all of the first-order Lie–Bäucklund symmetries for the equations of the one-fluid MHD model. Omitting a fairly involved procedure for seeking these symmetries, we present one of the final results: the permissible symmetries can only be linear functions of the derivatives of the coordinate functions $\{\alpha^i\}$; i.e., they are represented as

$$\boldsymbol{\xi} \equiv \xi^i\mathbf{e}_i = [c^i_k\dot{\alpha}^k + c^{ij}_k\boldsymbol{\nabla}_j\alpha^k + \xi^{*i}]\mathbf{e}_i, \tag{18}$$

where the scalars c^i_k, c^{ij}_k, and ξ^{*i} depend solely on $(t, \mathbf{r}, \{\alpha^j\})$.

As expected, the family of permissible symmetries contains variational symmetries and scale transformations (scalings). Discarding the scalings, we arrive at the following general variational symmetries for the one-fluid MHD equations:

$$\boldsymbol{\xi} = [b_0v^i + (\mathbf{b}_1 + \mathbf{b}_2\times\mathbf{r} + \mathbf{b}_3t)\boldsymbol{\nabla}\alpha^i + \xi^{*i}(\{\alpha^j\})]\mathbf{e}_i = b_0\mathbf{v} + \mathbf{b}_1 + \mathbf{b}_2\times\mathbf{r} + \mathbf{b}_3t + \boldsymbol{\xi}^{*i}. \tag{19}$$

where b_0 is a constant and $\mathbf{b}_1$–$\mathbf{b}_3$ are constant vectors. Special attention should be paid to the transformation $\boldsymbol{\xi} = \boldsymbol{\xi}^*$. The contravariant components ξ^{*i} depend only on the labels of fluid elements and thus describe the relabeling transformations [8]. These transformations are peculiar in that they do not change the velocity. We can readily show that if the relabeling transformations also do not change the magnetic field, density, and pressure, then they satisfy Eq. (16) and thus are variational symmetries. The conservation laws (17) that refer to the symmetries parameterized by the quantities b_0, $\mathbf{b}_1$, and $\mathbf{b}_2$ in expression (19) are the local conservation laws for the energy, momentum components, and angular momentum:

$$\partial_t\left(\frac{1}{2}\rho\mathbf{v}^2 + \frac{p}{\gamma-1} + \frac{1}{2}\mathbf{B}^2\right) + \mathrm{div}\left\{\mathbf{v}\left(\frac{1}{2}\rho\mathbf{v}^2 + \frac{\gamma p}{\gamma-1} + \mathbf{B}^2\right) - \mathbf{B}(\mathbf{v}\mathbf{B})\right\} = 0, \tag{20}$$

$$\partial_t[\rho(\mathbf{b}_1\mathbf{v})] + \mathrm{div}\left\{\rho\mathbf{v}(\mathbf{b}_1\mathbf{v}) + \mathbf{b}_1\left(p + \frac{1}{2}\mathbf{B}^2\right) - \mathbf{B}(\mathbf{b}_1\mathbf{B})\right\} = 0, \tag{21}$$

$$\partial_t[\rho([\mathbf{b}_2\times\mathbf{r}]\mathbf{v})] + \mathrm{div}\left\{\rho\mathbf{v}([\mathbf{b}_2\times\mathbf{r}]\mathbf{v}) + [\mathbf{b}_2\times\mathbf{r}]\left(p + \frac{1}{2}\mathbf{B}^2\right) - \mathbf{B}([\mathbf{b}_2\times\mathbf{r}]\mathbf{B})\right\} = 0. \tag{22}$$

The parameter $\mathbf{b}_3$ in expression (19) corresponds to the conservation law, which reduces to Eq. (21).

In contrast to the widely held opinion, the conservation law generated by the relabeling symmetry,

$$\partial_t(\rho\boldsymbol{\xi}^*\mathbf{v}) + \mathrm{div}\left\{\rho\mathbf{v}(\boldsymbol{\xi}^*\mathbf{v}) + \boldsymbol{\xi}^*\left(\mathbf{B}^2 + \frac{\gamma p}{\gamma-1} - \frac{\rho\mathbf{v}^2}{2}\right) - \mathbf{B}(\boldsymbol{\xi}^*\mathbf{B})\right\} = 0, \tag{23}$$

has a certain physical meaning: it determines additional [in comparison with the conservation laws (20)–(22)] relationships between the physical quantities and governs the structure of the steady motion and its very existence. The specific form of this conservation law is directly related to the magnetic field topology, which does not change with time in the ideal MHD model. For an arbitrary magnetic field, this law indicates conservation of the cross-helicity,

$$\partial_t(\mathbf{v}\mathbf{B}) + \mathrm{div}\left\{\mathbf{v}(\mathbf{v}\mathbf{B}) + \mathbf{B}\left(\frac{\gamma}{\gamma-1}\frac{p}{\rho} - \frac{1}{2}\mathbf{v}^2\right)\right\} = 0, \tag{24}$$

provided that the entropy is constant along the magnetic field lines. In the important case of magnetic configurations with an omnigenous topology of the toroidal magnetic flux surfaces ψ = const, we arrive at an additional conservation law:

$$\partial_t(\mathbf{v}\mathbf{D}) + \mathrm{div}\left\{\mathbf{v}(\mathbf{v}\mathbf{D}) + \mathbf{D}\left(\frac{\mathbf{B}^2}{\rho} + \frac{\gamma}{\gamma-1}\frac{p}{\rho} - \frac{1}{2}\mathbf{v}^2\right) - \frac{\mathbf{B}}{\rho}(\mathbf{D}\mathbf{B})\right\} = 0, \tag{25}$$

where the divergence-free vector **D** satisfies the frozen-in equation (12), is tangential to the flux surfaces ψ = const, and is linearly independent of **B**. The way to construct the vector **D** is described in detail in [9]. The conservation law (25) was first derived by Hameiri [10]. Later, we independently arrived at this law and used it to obtain the variational stability criterion [9].

We emphasize that, *by construction*, the variational relabeling symmetries determine the structure of the steady plasma motions (flows), because they are the only symmetry transformations that do not change the physical parameters of the system, which are therefore also invariant under finite relabeling transformations. In particular, for an omnigenous topology of the toroidal magnetic flux surfaces, the structure of the steady MHD flows has the form

$$\mathbf{V} = \kappa(\psi)\mathbf{B}/\rho + \eta(\psi)\mathbf{D}/\rho, \tag{26}$$

where κ and η are the flux-surface functions used to parameterize the flows (26).

In the one-fluid MHD model, Eqs. (20)–(23) exhaust the full family of conservation laws referring to first-order Lie–Bäucklund symmetries.

3.2. Hall Magnetohydrodynamics

In the HMHD model, the continuity and adiabatic equations, as well as the equation of motion, coincide with those in the one-fluid MHD model, while Eq. (12) for the magnetic field is replaced by the following equation, which implies that the magnetic field is frozen in the electron plasma component $\left(\mathbf{v}_e = \mathbf{v} - \frac{1}{a\rho}\operatorname{curl}\mathbf{B}\right)$:

$$\partial_t \mathbf{B} = \operatorname{curl}\left[\left(\mathbf{v} - \frac{1}{a\rho}\operatorname{curl}\mathbf{B}\right)\times\mathbf{B}\right], \tag{27}$$

where $a = e/m$ is the specific ion charge and the subscript e refers to the electron quantities. Although the HMHD equations are similar in form to one-fluid equations, the HMHD model is a particular case of the two-fluid hydrodynamic model with inertialess ($m_e \longrightarrow 0$) cold ($p_e \longrightarrow 0$) electrons, which serve merely as a neutralizing background for the ions. In the formal limit $a \longrightarrow \infty$, the HMHD equations transform into the one-fluid MHD equations.

In the HMHD model, the Lagrangian density can be written as [6]

$$L_{\mathrm{HMHD}} = \frac{\rho\mathbf{v}^2}{2} - \frac{p}{\gamma-1} + a\rho(\mathbf{v}-\mathbf{v}_e)\mathbf{A} - \frac{(\operatorname{curl}\mathbf{A})^2}{2}, \tag{28}$$

where ρ and η are specified on the ion Lagrangian grid (8) with bases (9) and the vector potential **A** defined by $\mathbf{B} = \operatorname{curl}\mathbf{A}$ is specified on the electron Lagrangian grid,

$$\mathbf{A} = A_i(\{\alpha_e^j\})\mathbf{e}_e^i. \tag{29}$$

Straightforward differentiation makes it possible to see that the curl of the vector potential (29) indeed satisfies Eq. (27).

The variations of the electron coordinates $\{\alpha_e^j\}$ are not completely independent, because the quasineutrality condition

$$a\rho + a_e\rho_e = 0 \tag{30}$$

relates the electron and ion displacements:

$$\begin{aligned} &a\operatorname{div}(\rho\boldsymbol{\xi}) + a_e\operatorname{div}(\rho_e\boldsymbol{\xi}_e) = 0 \\ &\Rightarrow \boldsymbol{\xi}_e = \boldsymbol{\xi} + \frac{1}{\rho}\operatorname{curl}\boldsymbol{\chi}, \end{aligned} \tag{31}$$

where $\boldsymbol{\chi}$ is an arbitrary vector.

Varying Lagrangian density (28) with respect to $\boldsymbol{\xi}$ and $\boldsymbol{\chi}$, we arrive at Eqs. (15) and (27), which serve as the Euler equations for the HMHD Lagrangian. If there exist $\boldsymbol{\xi}$, $\boldsymbol{\chi}$, Λ^0, and $\boldsymbol{\Lambda}$ satisfying the variational symmetry condition $d_t\Lambda^0 + \operatorname{div}\boldsymbol{\Lambda} + \delta L_{\mathrm{HMHD}} = 0$, then the related conservation law has the form

$$\begin{aligned} &\partial_t(\rho\mathbf{v}\boldsymbol{\xi} - a\mathbf{A}\cdot\operatorname{curl}\boldsymbol{\chi} + \Lambda^0) + \operatorname{div}\{\mathbf{v}(\rho\mathbf{v}\boldsymbol{\xi} - a\mathbf{A}\cdot\operatorname{curl}\boldsymbol{\chi}) \\ &\quad + \operatorname{curl}\mathbf{B}\left(\mathbf{A}\cdot\left(\boldsymbol{\xi} + \frac{\operatorname{curl}\boldsymbol{\chi}}{\rho}\right)\right) \\ &\quad - \boldsymbol{\xi}\left(\frac{\rho\mathbf{v}^2}{2} - \frac{\gamma p}{\gamma-1} + \mathbf{A}\cdot\operatorname{curl}\mathbf{B}\right) \\ &\quad + \mathbf{B}\times\left[\left(\boldsymbol{\xi} + \frac{\operatorname{curl}\boldsymbol{\chi}}{\rho}\right)\times\mathbf{B} - \nabla\left(\mathbf{A}\cdot\left(\boldsymbol{\xi} + \frac{\operatorname{curl}\boldsymbol{\chi}}{\rho}\right)\right)\right] + \boldsymbol{\Lambda}\Big\} = 0. \end{aligned} \tag{32}$$

Of course, the structure of the one-fluid MHD variational symmetries survives in the two-fluid HMHD model. However, in the HMHD model, additional freedom associated with the electron component can in principle lead to new variational symmetries. For example, under the transformation

$$\boldsymbol{\chi} = \boldsymbol{\chi}^* = \chi_i^*(\{\alpha_e^j\})\mathbf{e}_e^i, \quad \boldsymbol{\xi} = 0, \quad \Lambda^i = 0, \tag{33}$$

which determines the general relabeling symmetry of the electron fluid, the conservation law (32) passes over to

$$\partial_t(\mathbf{A}\cdot\operatorname{curl}\boldsymbol{\chi}^*) + \operatorname{div}\left(\left(\mathbf{v} - \frac{1}{a\rho}\operatorname{curl}\mathbf{B}\right)\mathbf{A}\cdot\operatorname{curl}\boldsymbol{\chi}^*\right) = 0. \tag{34}$$

In particular, the choice $\chi_i^* = A_i$ leads to the conservation law for the magnetic cross-helicity $\mathbf{A}\cdot\mathbf{B}$. For any relabeling transformation (33), conservation law (34) holds automatically and reflects the fact that, as is expected, the quantity $\mathbf{A}\cdot\operatorname{curl}\boldsymbol{\chi}^*/\rho$ is a passive scalar. Consequently, conservation law (34) does not introduce additional restrictions if the vector potential **A** is already written in the form (29). In contrast, the relabel-

ing of the ion fluid generates the nontrivial conservation law

$$\partial_t(\rho\boldsymbol{\xi}^*\cdot\mathbf{u}) + \mathrm{div}[\rho\mathbf{v}(\boldsymbol{\xi}^*\cdot\mathbf{u}) - \rho\boldsymbol{\xi}^*(\mathbf{v}\cdot\mathbf{u} - K)] = 0, \quad (35)$$

where $\mathbf{u} = \mathbf{v} + a\mathbf{A}$ and $K = \mathbf{v}^2/2 + \gamma p/\rho(\gamma - 1) + a\mathbf{A}\cdot\mathbf{v}_e$ is the Bernoulli function.

3.3. Electron Magnetohydrodynamics

The EMHD model describes another limiting case of motion, specifically, a quasineutral plasma motion on time scales short enough for the motion of the relatively heavy ions to be neglected in comparison with the fast electron motion [11]. The EMHD equations can be derived by varying the Lagrangian density

$$L_{\mathrm{EMHD}} = \frac{\rho_e\mathbf{v}_e^2}{2} - \frac{p_e}{\gamma_e - 1} + a_e\rho_e\mathbf{v}_e\cdot\mathbf{A} - \frac{(\mathrm{curl}\mathbf{A})^2}{2}$$

with respect to both the vector potential $\mathbf{A}$ of the magnetic field and the vector potential $\boldsymbol{\chi}$ of the electron fluid displacement, which is restricted by the quasineutrality condition (30): since the ions are immobile, we have $\partial_t\rho_e = 0$ and $\mathrm{div}\rho_e\boldsymbol{\xi}_e = 0$, so that

$$\boldsymbol{\xi}_e = \frac{1}{\rho_e}\mathrm{curl}\boldsymbol{\chi},$$

which agrees with Eq. (31) when $\boldsymbol{\xi} = 0$.

Following the above procedure, we can show that the EMHD equations

$$a_e\rho_e\mathbf{v}_e = \mathrm{curl}\mathbf{B}, \quad (36)$$

$$\partial_t\boldsymbol{\Omega} = \mathrm{curl}[\mathbf{v}_e\times\boldsymbol{\Omega}] + \nabla T_e\times\nabla\eta_e, \quad (37)$$

where, for brevity, we introduce the notation

$$\boldsymbol{\Omega} = \mathrm{curl}\mathbf{u}_e = \mathrm{curl}(\mathbf{v}_e + a_e\mathbf{A}),\ T_e = p_e/\rho_e, \quad (38)$$

possess the conservation law

$$\partial_t(\mathbf{u}_e\cdot\mathrm{curl}\boldsymbol{\chi}) + \mathrm{div}\{\mathbf{v}_e(\mathbf{u}_e\cdot\mathrm{curl}\boldsymbol{\chi}) + \mathbf{B}\times\delta\mathbf{A} + (\partial_t\mathbf{u}_e - \mathbf{v}_e\times\boldsymbol{\Omega} + \nabla(\mathbf{u}_e\mathbf{v}_e) - T_e\nabla\eta_e)\times\boldsymbol{\chi}\} = 0. \quad (39)$$

For the EMHD model, the class of general first-order Lie–Bäcklund symmetries and the variational symmetries for this class were investigated in [12]. It was found that the permissible displacements $\boldsymbol{\xi}_e$ and the associated conservation laws are similar in structure to those described by formulas (19) and (20)–(22) in the one-fluid MHD model. When $\boldsymbol{\xi}_e^*\nabla\eta = 0$, the relabeling transformation $\boldsymbol{\xi}_e = \boldsymbol{\xi}_e^*$ and $\delta\mathbf{A} = 0$ is the variational symmetry, which generates the conservation law

$$\partial_t(\mathbf{u}_e\cdot\mathrm{curl}\boldsymbol{\chi}_e^*) + \mathrm{div}(\mathbf{v}_e(\mathbf{u}_e\cdot\mathrm{curl}\boldsymbol{\chi}_e^*)) = 0. \quad (40)$$

Using this law, we can integrate two components of $\mathbf{u}_e$: $u_{2,3} = u_{2,3}^*(\{\alpha_e^i\})$, where the coordinate α_e^1 is chosen to be aligned with the gradient of the entropy η_e. This circumstance is important, in particular, because it makes the EMHD model simpler than the ideal MHD model, in which such local integration cannot be carried out [9].

We stress that all of the variational symmetries found in this section belong to the class of point and contact transformations, in which case we can anticipate that there will be no other symmetries of the same or higher orders, because, in the opposite case, the Olver theorem [13] implies an infinite family of nontrivial symmetries.

4. ADIABATIC SEPARATION OF MOTIONS AND REDUCED MHD MODELS

The method of the adiabatic separation of weakly coupled fast and slow motions is widely applied in classical mechanics. The method is based on revealing rapidly oscillating stable degrees of freedom in the dynamic system under analysis. The characteristic oscillation period T_f of the fast motion should satisfy the condition $T_f/\tau_s \sim \varepsilon \ll 1$, where τ_s is the characteristic time of slow motions. Further analysis of the fast degree of freedom involves the construction of an adiabatic invariant, i.e., an approximate integral of motion, which remains unchanged during a slow evolution (on a time scale of about τ_s) of the system. This slow evolution can be described by adiabatic equations of motion that are derived from the complete set of basic equations under the assumption that the adiabatic invariant is an exact integral of motion of the system.

For continuous media, the method of the adiabatic separation of motions was developed by Pastukhov [14, 15], who drew an analogy with the search for variational relabeling symmetries. The essence of the method can be briefly described as follows (the logical development of the method is described in detail in [15]). Let us consider a Lagrangian system with motions on significantly different characteristic time scales, whose ratio ε is small ($\varepsilon \ll 1$). In the case, the expression for the perturbed potential energy usually contains terms on the order of unity and ε^2, which correspond to structurally different classes of motions. Following the procedure of searching for a symmetry transformation (see Sections 2, 3), we seek an infinitesimal transformation $\delta_a\alpha^i(\mathbf{r}, t)$ that does not change the Lagrangian of the system through both the leading and first orders in ε. In other words, we are interested in the transformation satisfying the condition

$$\delta_a\int_\Gamma L(\{\alpha^i\}, \{\partial_t\alpha^i\}, \{\nabla\alpha^i\}, \varepsilon)d^3\mathbf{r} = O(\varepsilon^2). \quad (41)$$

If an "adiabatic" transformation of this sort does indeed exist, then, in accordance with Section 2, it plays a role of an approximate symmetry transformation for fast motion. The reason for this is that the equations describing the dynamics of fast motion on time scales

shorter than τ_s can be derived from Hamilton's principle by neglecting terms on the order of ε^2 in the variation of the Lagrangian.

If the functions $\delta_a\alpha^i$ satisfying condition (41) depend only on the generalized coordinates $\alpha^i(\mathbf{r}, t)$ and slow time (i.e., $\delta_a\alpha^i = f^i(\{\alpha^j\}, \varepsilon t)$), then the functions $\delta_a\alpha^i$ play the role of relabeling transformation for fast motion (see Section 3). To continue drawing an analogy with relabeling transformations, we introduce an adiabatic field of the generalized velocities that has the same functional structure as the transformation $\delta_a\alpha^i$. For fast motions, the adiabatic velocity field plays the role of the steady-state (neutral) flows discussed in Section 3.

Since the transformation $\delta_a\alpha^i$ is a subset of the initial set of arbitrary variations of the generalized coordinates, the functions $\delta_a\alpha^i$ depend on a smaller number of independent "adiabatic" generalized coordinates and can be obtained from a smaller number of equations, which can be derived from Hamilton's principle in the absence of fast motion by driving to zero the coefficients in front of the independent variations of the adiabatic generalized coordinates in the variation of the action integral (1) taken with $\delta\alpha^i = \delta_a\alpha^i$. The equations constructed in this fashion describe the dynamics of slow motion when no fast stable motions are excited. Since the symmetry transformations that do not change the Lagrangian are a subset of the set of the adiabatic transformations $\delta_a\alpha^i$ just due to the way in which the latter are constructed, the adiabatic equations of motion possess all of the symmetry properties of the basic equations. In particular, the adiabatic equations admit solutions describing states with steady plasma flows that are consistent with the basic equations of motion. We emphasize that, if no fast motions are excited at the initial state (this corresponds to a zero adiabatic invariant of fast motions) and if fast motions remain stable during the development of the adiabatic flows, then the evolution of the system is approximately described by the adiabatic equations on *arbitrarily long time scales*.

This procedure was applied by Pastukhov [14] to derive an improved (adiabatic) version of the reduced Kadomtsev–Pogutse–Strauss MHD equations [16–21], which describe the dynamics of a tokamak plasma. Under the condition $\beta \equiv 2p/B^2 \ll 1$, which is characteristic of tokamaks, the most interesting dynamic processes are associated with perturbations that are very stretched out along the magnetic field ($|\nabla_\parallel| \ll |\nabla_\perp|$) and have characteristic frequencies peculiar to Alfvén waves, $\omega \sim c_A |\nabla_\parallel|$ (where c_A is the Alfvén speed), or lower. Since, in such processes, fast stable magnetosonic (compressional Alfvén) waves with the characteristic frequencies $\omega \sim c_A |\nabla_\perp|$ remain essentially unperturbed, we can exclude them from consideration with the help of the procedure proposed for the adiabatic separation of motions. In this case, the role of the small parameter is played by the inverse aspect ratio $\varepsilon = B_p/B_T \sim a/R$, where a and R are the minor and major radii of the toroidal plasma column. We also assume that the transverse and longitudinal gradients of the perturbed quantities satisfy the condition $|\nabla_\parallel| \le \varepsilon |\nabla_\perp|$ and that $\beta \sim \varepsilon^2 a |\nabla_\perp|$.

We consider the variation of the standard Lagrangian density (14) in the one-fluid MHD model. According to [14, 15], the transformation under which the dominant terms $\mathbf{B}\cdot\delta\mathbf{B}$ and $\rho\mathbf{v}\cdot\delta\mathbf{v}$ in the Lagrangian density variation become as small as ε^2 can be represented in the form of the infinitesimal adiabatic displacement

$$\boldsymbol{\xi}_a = \frac{1}{(\mathbf{B}\cdot\nabla\zeta)}([\nabla\zeta\times\nabla\delta_a\alpha] - \mathbf{B}\delta_a\zeta), \qquad (42)$$

where $\delta_a\alpha$ and $\delta_a\zeta$ are arbitrary functions of the pseudo-Lagrangian coordinates and slow time and ζ is a pseudo-Lagrangian function, which, by definition, satisfies the equation $\partial_t\zeta + (\mathbf{v} - \mathbf{V})\cdot\nabla\zeta = 0$ and, in a steady state, coincides with the traditional toroidal angle φ. The remaining terms in the Lagrangian density variation are also equal in order of magnitude to ε^2. Consequently, adiabatic transformation (42) can be, roughly speaking, regarded as the relabeling transformation for magnetosonic waves. The adiabatic velocity field corresponding to transformation (42) can be represented as

$$\mathbf{v}_a = \frac{1}{B^2}\left[\mathbf{B}\times\left(\nabla\phi - \nabla\zeta\frac{(\mathbf{B}\cdot\nabla\phi)}{(\mathbf{B}\cdot\nabla\zeta)}\right)\right] + \mathbf{B}\frac{h_v}{B^2}, \qquad (43)$$

where ϕ has the meaning of the electric potential and h_v is the cross-helicity. We can readily see that the velocity field $\mathbf{v}_a$ describes, in particular, steady flows (26), because, for $\phi = \phi_0(\psi)$ and $h_v = \mathbf{V}\cdot\mathbf{B}$, we have $\mathbf{v}_a = \mathbf{V}$.

In order to switch from the basic one-fluid MHD model to the adiabatic MHD model, we must use the adiabatic (rather than arbitrary) velocity field (43). In this case, the structure of the frozen-in, continuity, and adiabatic equations, which are valid for an arbitrary velocity field, remains unchanged correct to the replacement of $\mathbf{v}$ by $\mathbf{v}_a$. This replacement is most strongly manifested in the frozen-in equation

$$\partial_t\mathbf{B} = \left[\nabla\zeta\times\nabla\frac{(\mathbf{B}\cdot\nabla\phi)}{(\mathbf{B}\cdot\nabla\zeta)}\right]. \qquad (44)$$

In velocity field (43), the functions ϕ and h_v are determined from the adiabatic equations of motion, which follow from Hamilton's principle. Driving to zero the coefficient of $\delta\zeta$ in the variation of the action integral and taking into account the pseudo-Lagrangian character of the functions $\rho/(\mathbf{B}\cdot\nabla\zeta)$ and $p/\rho^\gamma = s(\psi)$, we arrive

at the following differential conservation law for the cross-helicity:

$$\partial_t h_v + \mathrm{div}\left\{\mathbf{v}_a h_v - \mathbf{B}\left(\frac{v_a^2}{2} - \frac{\gamma}{\gamma-1}\frac{p}{\rho}\right)\right\} = 0, \qquad (45)$$

which is also valid for the basic (unreduced) MHD equations [see Eq. (24)]. Equating the coefficient of $\delta\alpha$ to zero, we arrive at the second dynamic equation of the adiabatic MHD model in the form of the conservation law for the generalized momentum P_α, which is canonically conjugate to the adiabatic coordinate α:

$$\partial_t P_\alpha + \mathrm{div}\left\{\mathbf{v}_a P_\alpha - \mathbf{B}\frac{\mathrm{div}[\mathbf{B}\times\nabla\zeta]}{(\mathbf{B}\cdot\nabla\zeta)} - \frac{[\nabla\zeta\times\nabla p]}{(\mathbf{B}\cdot\nabla\zeta)}\right.$$

$$+ \frac{\rho}{(\mathbf{B}\cdot\nabla\zeta)}\left[\nabla\zeta\times\nabla\frac{v_a^2}{2}\right] - \frac{\rho}{(\mathbf{B}\cdot\nabla\zeta)}$$

$$\left.\times[\mathbf{v}_a\times\nabla(\mathbf{V}\cdot\nabla\zeta)]\right\} = 0, \qquad (46)$$

$$P_\alpha = \mathrm{div}\left\{\frac{1}{c_A^2}\left(\nabla\phi - \nabla\zeta\frac{(\mathbf{B}\cdot\nabla\phi)}{(\mathbf{B}\cdot\nabla\zeta)}\right.\right.$$

$$\left.\left. - \mathbf{B}\frac{(\nabla\zeta\cdot\nabla\phi)}{(\mathbf{B}\cdot\nabla\zeta)} + \mathbf{B}\frac{(\nabla\zeta)^2(\mathbf{B}\cdot\nabla\phi)}{(\mathbf{B}\cdot\nabla\zeta)^2}\right)\right\}.$$

This equation can also be derived directly from the unreduced vector equation of motion.

When solving particular problems associated with the processes occurring on relatively short time scales, some of the higher order terms in Eqs. (43)–(46) can be omitted. It should be noted, however, that special care is needed in doing this in order not to break the self-consistent character of the resulting set of equations and their symmetry properties. An example of such simplification was considered in [15]. Along with relatively universal small parameters, such as the ratio B_p/B_T in tokamaks and β, many plasma-related problems may contain additional small parameters associated, e.g., with the closeness to the instability threshold for MHD modes. The additional parameters also provide the possibility of separating the motions adiabatically, in which case the role of slow motions is played by the most dangerous modes, for which the stability condition can be violated. As an example, we can mention the adiabatic equations that were derived in [15] for modeling two-dimensional MHD plasma convection near the threshold for flute instability in systems of the compact torus type.

5. VARIATIONAL PRINCIPLES FOR STABILITY

The standard variational method for stability studies is based on the Lyapunov theory. The main difficulties in applying the Lyapunov theory to continual systems are associated not only with the construction of the Lyapunov functional itself, but also with the choice of an adequate set of independent variables with respect to which the variations should be made. In isolated systems, the "natural candidate" for the Lyapunov functional is the total energy (the Hamiltonian). On the other hand, how to choose a correct set of independent variables is less obvious, because the physical quantities contained in the Hamiltonian can be interdependent due to the system dynamics. Such a dependence can be reflected by the corresponding conservation laws. Of course, even with an unjustifiably large set of physical quantities to be varied, we will arrive at a sufficient Lyapunov stability condition. However, this sufficient condition seems to be of little physical importance, because neglecting (partially or wholly) the relationships between the physical quantities substantially reduces the class of steady states admitted by the basic equations and makes the stability criterion more stringent compared to the expected one (i.e., far wider than the necessity criterion) and even impossible to satisfy.

In connection with this, we can mention the following well-known example. In ideal magnetohydrodynamics, the stability of static ($\mathbf{V} = 0$) plasma equilibria can be studied using the energy principle [1], which gives necessary and sufficient conditions (the criterion) for MHD stability. (A proof of necessity of the criterion is given in, e.g., [22]. In [23], it was proved that this criterion is valid in the nonlinear case.) However, this approach turned out to be inapplicable for describing steady states with plasma flows. Even the linear stability criterion derived by Frieman and Rotenberg [24] is too stringent: it always fails to hold for plasma flows whose equilibrium velocity $\mathbf{V}$ is not parallel to the magnetic field $\mathbf{B}$. The reason is that, in [24], the functions to be varied have an excessive freedom, i.e., without allowance for certain conservation laws that characterize the real dynamics of the system.

There is a widespread opinion that an adequate Lyapunov functional can be constructed using the "Hamiltonian + family of Casimirs" scheme, i.e., the Hamiltonian and the full family of kinematic invariants of motion (see, e.g., [25]). Since a hydrodynamic system is characterized by an infinite family of Casimirs and the Casimirs can be nontrivially multiplied, only a small family of Casimirs is usually utilized in practice. However, as was mentioned above, the results obtained with this approach are often of minor physical importance (see, e.g., [26], where even an equilibrium configuration is subject to restrictions). On the other hand, choosing the Lagrangian coordinates as independent functions automatically enables us to cover the full infinite family of Casimirs [6] and the only meaningful

conservation laws are those that reflect the dynamics of the system and, in particular, are consistent with relabeling symmetries. It is this point in which the "Hamiltonian + family of Casimirs" scheme differs from the approach developed by Arnold [27], who took into account the conservation of helicity in conventional hydrodynamics, in which this conservation law is dynamic in character. In ideal magnetohydrodynamics, conservation laws (24) and (25) are also dynamic in character; in [9, 28], these laws were taken into account, which made it possible to substantially improve the criterion derived in [24].

5.1. Variational Stability Criterion in Hall Magnetohydrodynamics

Based on the above considerations, we derive the variational stability criterion for the HMHD model. Conservation law (35) implies the invariance of the integral

$$I = -\int d^3x\, \rho \mathbf{u}\cdot\mathbf{V}, \tag{47}$$

where the velocity $\mathbf{V}$ of the steady ion flow is to be determined and $\mathbf{u} = \mathbf{v} + a\mathbf{A}$. Taking the Legendre transformation of Lagrangian (28) and using integral (47), we construct the Lyapunov functional

$$\mathcal{H} = \int d^3x\left(\frac{(\mathbf{P}+\mathbf{P}_e)^2}{2\rho} + \frac{1}{2}\mathrm{curl}^2\frac{\mathbf{P}_e}{a\rho} + \frac{p}{\gamma-1}\right) + I, \tag{48}$$

where the velocities are expressed in terms of the canonical momenta $\mathbf{P} = -\rho\mathbf{u}$ and $\mathbf{P}_e = a\rho\mathbf{A}$.

We can easily see that the first variation of (48) determines the general equilibria for the HMHD model and the second variation can be minimized by the choice $\delta\mathbf{P} = -\rho\delta(\mathbf{V} + a\mathbf{A}) + \mathbf{P}(\delta\rho/\rho) + \delta\mathbf{P}_1$, where the term $\delta\mathbf{P}_1(\boldsymbol{\xi})$ should ensure that conservation law (35) holds for the first and second variations. As a result, we arrive at the stability criterion [29]

$$\delta^2\mathcal{H} = \delta^2\mathcal{H}_{\mathrm{MHD}} + \delta^2\mathcal{H}_1, \tag{49}$$

where

$$\delta^2\mathcal{H}_{\mathrm{MHD}} = \int d^3x\left\{\delta\mathbf{B}^2 + \delta\mathbf{B}\cdot[\mathrm{curl}\mathbf{B}\times\boldsymbol{\xi}]\right.$$
$$+\frac{\delta\mathbf{P}_1^2}{\rho} - \rho(\delta\mathbf{V})^2 + [\delta(\rho\mathbf{V})\times\boldsymbol{\xi}]\cdot\mathrm{curl}\mathbf{V} \tag{50}$$
$$\left.+\boldsymbol{\xi}\cdot\nabla\frac{V^2}{2}\delta\rho + (\boldsymbol{\xi}\nabla p)\mathrm{div}\boldsymbol{\xi} + \gamma p\,\mathrm{div}^2\boldsymbol{\xi}\right\},$$

$$\delta^2\mathcal{H}_1 = \int d^3x\left\{\delta\mathbf{B}\cdot[\mathrm{curl}\boldsymbol{\chi}\times\mathbf{V}]\right.$$
$$\left.-\frac{\mathrm{curl}\boldsymbol{\chi}\times\mathbf{B}}{\rho}\cdot\delta(\rho\mathbf{V}) + \mathbf{V}_e\cdot[\mathrm{curl}\boldsymbol{\chi}\times\mathbf{B}]\frac{\delta\rho}{\rho}\right\}. \tag{51}$$

Recall that $\delta\rho = -\mathrm{div}\rho\boldsymbol{\xi}$, $\delta\mathbf{V} = (\mathbf{V}\nabla)\boldsymbol{\xi} - (\boldsymbol{\xi}\nabla)\mathbf{V}$, and $\delta\mathbf{B} = \mathrm{curl}\,\delta\mathbf{A} = \mathrm{curl}\,\delta(\mathbf{P}_e/a\rho)$ and that the variations are made with respect to the independent variables $\boldsymbol{\xi}$ and $\boldsymbol{\chi}$. For simplicity, we have omitted the total spatial divergences in order to illustrate the most important "volume" part of the criterion.

The only difference between expression (50) and the related expression obtained in [9] from the ideal MHD model is that the magnetic field has the form $\mathbf{B} = \mathrm{curl}[\boldsymbol{\xi}_e\times\mathbf{B}]$ and, accordingly, also depends on $\boldsymbol{\chi}$. The one-fluid MHD model corresponds to the limiting transition $\mathbf{V}_e \longrightarrow \mathbf{V}$, $\mathrm{curl}\boldsymbol{\chi} \longrightarrow 0$, and $\delta^2\mathcal{H}_1 \longrightarrow 0$. The question of how to choose the term $\delta\mathbf{P}_1$ was discussed in detail in [9]; the choice $\delta\mathbf{P}_1 = 0$ refers to the criterion derived in [24].

5.2. Variational Stability Criterion in Electron Magnetohydrodynamics

For simplicity, we restrict ourselves to considering a barotropic electron fluid $T_e = T_e(\eta)$, in which case we can integrate the three components of $\mathbf{u}_e$, because the last term drops out of Eq. (36). The stability criterion can be derived by varying the Lyapunov functional

$$H_e = \int d^3x\left\{\frac{\rho\mathbf{v}_e^2}{2} + \frac{\mathbf{B}^2}{2}\right\}$$
$$= \int d^3x\left\{\frac{\rho a_e^2}{2}(\mathbf{A}_u - \mathbf{A})^2 + \frac{(\mathrm{curl}^2\mathbf{A})}{2}\right\} \tag{52}$$

with respect to the independent variables $\mathbf{A}$ and $\boldsymbol{\chi}$:

$$\delta\mathbf{B} = \mathrm{curl}\delta\mathbf{A},$$
$$\delta\mathbf{B}_u = \mathrm{curl}\delta\mathbf{A}_u = \mathrm{curl}\left(\frac{1}{a_e\rho}\mathrm{curl}\boldsymbol{\chi}\times\mathbf{B}_u\right). \tag{53}$$

For convenience, we have introduced the notation $\mathbf{B}_u = \boldsymbol{\Omega}/a_e$ and $\mathbf{A}_u = \mathbf{u}/a_e$. Making the first variation of functional (52) leads to Eqs. (36) and (37), and minimizing the second variation with respect to $\delta\mathbf{A}$ yields the desired criterion:

$$\delta^2 H_e = \int d^3x(\delta\mathbf{B} + \mathrm{curl}\mathbf{B}\times\xi_e)\cdot\delta\mathbf{B}_u > 0, \tag{54}$$

where $\delta\mathbf{B}_u$ is defined in (53) and

$$\delta\mathbf{B} + \mathrm{curl}\left(\frac{\mathrm{curl}\delta\mathbf{B}}{a_e^2\rho}\right) = \delta\mathbf{B}_u. \tag{55}$$

Criterion (54) was obtained and discussed in [30]. In the limit $a_e \longrightarrow \infty$, we have $\delta\mathbf{B}_u \longrightarrow \delta\mathbf{B}$, so that criterion (54) passes over to the familiar energy principle [1], in which either the plasma pressure or the plasma compressibility is neglected (the immobile ion approximation).

In our previous studies, the approach described in this section was also applied to derive variational stability criteria for an anisotropic plasma (in the Chew–Goldberger–Low approximation) [31] and for the case of an "adiabatic" version [32] of the familiar energy principle [1].

However, we must keep in mind that all of the above stability criteria, being derived with allowance for the corresponding conservation laws, are merely sufficient conditions and, in particular situations, can be far wider than the necessity criteria. This may stem from several reasons.

(i) The necessary constraints that eliminate excessive freedom in the variations of the momenta and displacements are nonlocal and can, e.g., depend explicitly on time. Thus, it may be that the necessary and sufficient variational stability criterion is in principle impossible to derive.

(ii) The required constraints stem from nonlocal conservation laws, which requires to take into account, along with Lie–Bäucklund symmetries, nonlocal variational symmetries.

(iii) In Section 5, the stability criteria were indeed derived using the *integral consequences* [like integral (47)] of the conservation laws [like Eqs. (24) and (25)], which are *local* in nature and, accordingly, should be accounted for more accurately.

We think that taking into account the known conservation laws (see Section 3) in more detail would be fruitful to further improve the variational stability criteria.

6. CONCLUSION

We have shown that variational methods can be successfully used to analyze various problems of nonlinear plasma dynamics described by different MHD models. We mean, first of all, searching for variational symmetries and the related conservation laws, the construction of variational stability criteria, the adiabatic separation of motions, and the development of reduced MHD models. In applying variational methods, we have demonstrated that knowing the Lagrangian structure of hydrodynamic plasma models allows us to derive general expressions for the conservation laws inherent in these models.

For the hydrodynamic models under investigation, we have derived the equations for variational symmetries and the explicit conservation laws. An analysis of the one-fluid MHD model and the EMHD model has revealed the complete set of variational symmetries in the class of the first-order Lie–Bäucklund symmetries. An important feature of all MHD models is that, along with the well-known symmetries generating the conservation laws for energy, momentum, and total angular momentum, they admit the relabeling symmetries of the volume fluid elements in three-dimensional geometry. The relabeling symmetries, in turn, generate the conservation laws that provide more detailed information about the invariance of the generalized momentum components of the system under consideration. Therefore, contrary to the previously accepted views, these conservation laws are meaningful. Moreover, since these symmetries (and the related conservation laws) are very sensitive to the topology of the system and/or to the particular initial distributions of plasma parameters, it is the symmetries themselves (rather than an infinite family of Casimirs, which is covered by introducing the Lagrangian coordinate grid) that lead to the most important constraints on the permissible variations of the dynamic variables.

In our opinion, another important and promising approach to investigating nonlinear MHD system is to construct adiabatic MHD models, which make it possible to discard fast stable collective degrees of freedom and thus to substantially simplify a description of the dynamics of the system under analysis. The variational method proposed here for the adiabatic separation of fast and slow motions in Lagrangian systems is based on the search for approximate relabeling symmetry transformations for fast motion and provides a fairly systematic and efficient approach to constructing adiabatic MHD models. It is important to note that the method of adiabatic separation preserves the symmetry properties of the original dynamic system. The method not only serves to derive the adiabatic version of the reduced Kadomtsev–Pogutse–Strauss equations (which has been done here for illustration), but can also find many other applications.

This work was supported in large part by the Russian Foundation for Basic Research, project nos. 97-02-17730 and 97-02-17238. V.I. Ilgisonis is grateful to V.P. Lakhin for his collaboration in obtaining the results on the full groups of symmetries for the one-fluid MHD equations and EMHD equations.

REFERENCES

1. I. B. Bernstein, E. A. Frieman, M. D. Kruskal, and R. M. Kulsrud, Proc. R. Soc. London, Ser. A **244**, 17 (1958).
2. R. Courant and D. Hilbert, *Methoden der mathematischen Physik* (Springer-Verlag, Berlin, 1931; Gostekhizdat, Moscow, 1951).
3. J. Serrin, *Handbuch der Physik*, Ed. by S. Flügge (Springer-Verlag, Berlin, 1959), Bd. VIII/1.
4. T. H. Boyer, Ann. Phys. **42**, 445 (1967).
5. V. Rosenhaus and G. H. Katzin, J. Math. Phys. **35**, 1998 (1994).
6. V. I. Ilgisonis and V. P. Lakhin, Fiz. Plazmy **25**, 64 (1999) [Plasma Phys. Rep. **25**, 58 (1999)].

7. W. Newcomb, Nucl. Fusion Suppl. **2**, 451 (1962).
8. N. Padhye and P. Morrison, Fiz. Plazmy **22**, 960 (1996) [Plasma Phys. Rep. **22**, 869 (1996)].
9. V. I. Ilgisonis and V. P. Pastukhov, Fiz. Plazmy **22**, 228 (1996) [Plasma Phys. Rep. **22**, 208 (1996)].
10. E. Hameiri, J. Math. Phys. **22**, 2080 (1981).
11. A. S. Kingsep, K. V. Chukbar, and V. V. Yan'kov, in *Reviews of Plasma Physics*, Ed. by B. B. Kadomtsev (Énergoizdat, Moscow, 1987; Consultants Bureau, New York, 1990), Vol. 16.
12. V. I. Ilgisonis and V. P. Lakhin, Electromagn. Waves Electron. Syst. **3** (2–3) (1998).
13. P. J. Olver, *Applications of Lie Groups to Differential Equations* (Springer-Verlag, Berlin, 1986).
14. V. P. Pastukhov, Pis'ma Zh. Éksp. Teor. Fiz. **67**, 892 (1998) [JETP Lett. **67**, 940 (1998)].
15. V. P. Pastukhov, Fiz. Plazmy **26**, 566 (2000) [Plasma Phys. Rep. **26**, 529 (2000)].
16. B. B. Kadomtsev and O. P. Pogutse, Zh. Éksp. Teor. Fiz. **65**, 575 (1973) [Sov. Phys. JETP **38**, 283 (1974)].
17. B. B. Kadomtsev and O. P. Pogutse, Zh. Éksp. Teor. Fiz. **66**, 2067 (1974).
18. R. White, D. Monticello, *et al.*, in *Proceedings of the 5th International Conference on Plasma Physics and Controlled Nuclear Fusion Research, Tokyo, 1974* (IAEA, Vienna, 1975), Vol. 1, p. 495.
19. H. Strauss, Phys. Fluids **19**, 134 (1976).
20. H. Strauss, Nucl. Fusion **23**, 649 (1983).
21. R. D. Hazeltine, M. Kotschenreuther, and P. J. Morrison, Phys. Fluids **28**, 2466 (1985).
22. A. Bernstein, in *Basic Plasma Physics*, Ed. by A. A. Galeev and R. N. Sudan (Énergoatomizdat, Moscow, 1983; North-Holland, Amsterdam, 1983), Vol. 1.
23. V. I. Ilgisonis and V. P. Pastukhov, Pis'ma Zh. Éksp. Teor. Fiz. **61**, 186 (1995) [JETP Lett. **61**, 189 (1995)].
24. E. Frieman and M. Rotenberg, Rev. Mod. Phys. **32**, 898 (1960).
25. D. D. Holm, J. E. Marsden, T. Ratiu, and A. Weinstein, Phys. Rep. **123** (1–2), 1 (1985).
26. V. A. Gordin and V. I. Petviashvili, Zh. Éksp. Teor. Fiz. **95**, 1711 (1989) [Sov. Phys. JETP **68**, 988 (1989)].
27. V. I. Arnold, J. Appl. Math. Mech. **29**, 1002 (1965).
28. E. Hameiri and H. A. Holties, Phys. Plasmas **1**, 3807 (1994).
29. V. I. Ilgisonis, Trans. Fusion Technol. **35**, 170 (1999).
30. V. I. Ilgisonis, in *Proceedings of the 26th EPS Conference on Controlled Fusion and Plasma Physics, Maastricht, 1999* [ESA **23J**, 861 (1999)].
31. V. I. Ilgisonis, Phys. Plasmas **3**, 4577 (1996).
32. V. P. Pastukhov, in *Proceedings of the Joint Varenna–Lausanne International Workshop on Theory of Fusion Plasmas, Varenna, 1998*, Ed. by J. W. Connor, E. Sindoni, and J. Vaclavik (Bologna, Compositori, 1998), p. 449.

Translated by O. Khadin